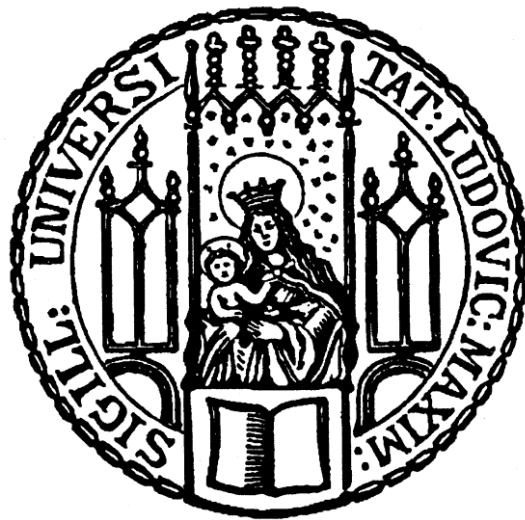


Dissertation zur Erlangung des Doktorgrades
der Fakultät für Chemie und Pharmazie
der Ludwig-Maximilians-Universität München



Epigenetic gene regulation by TET3
and 5-hydroxymethylcytosine
during retinal maturation

Arshan Perera
aus Wiesbaden
2015

Erklärung

Diese Dissertation wurde im Sinne von § 7 der Promotionsordnung vom 28. November 2011 von Prof. Dr. Martin Biel betreut.

Eidesstattliche Versicherung

Diese Dissertation wurde eigenständig und ohne unerlaubte Hilfe erarbeitet.

München, den 04.05.2015

.....

(Arshan Perera)

Dissertation eingereicht am

04.05.2015

1. Gutachter:

Prof. Dr. Martin Biel

2. Gutachter:

PD Dr. Stylianos Michalakis

Mündliche Prüfung am

02.06.2015

*“Let us try to teach generosity and altruism, because we are born selfish.
Let us understand what our own selfish genes are up to, because we may then at least have the
chance to upset their designs, something that no other species has ever aspired to.”*

(Richard Dawkins)

Table of contents

Erklärung	II
Eidesstattliche Versicherung	II
Table of contents	4
Abbreviations	7
Index of figures	10
Index of tables	12
1. Introduction	13
1.1 Background	13
1.2 The nucleosome	15
1.3 The epigenetic code	17
1.4 DNA methylation.....	20
1.5 TET-mediated 5mC oxidation	22
1.6 The 6 th DNA base 5-hydroxymethylcytosine	25
1.7 Retinal maturation.....	27
1.8 The aims of this thesis.....	28
2. Material and Methods	29
2.1 Animals	29
2.2 Chemicals, solutions and buffers	29
2.3 Cell culture and plasmid transfection	29
2.4 siRNA experiments.....	31
2.5 Lentiviral plasmids.....	31
2.6 Lentiviral production	32
2.7 <i>In vitro</i> retinal explant cultures	33
2.8 Metabolic feeding with [methyl- ¹³ CD ₃]-methionine	34
2.9 LV transduction of retinal explant cultures	36
2.10 Genomic DNA isolation	37
2.11 DNA immunoprecipitation	38
2.12 hMeDIP qPCR validation	40
2.13 Origin of mouse embryonic stem cells	41
2.14 RNA extraction	41
2.15 cDNA synthesis	42
2.16 quantitative PCR (qPCR).....	42

2.17	Retina preparation	43
2.18	Retinal cryosections	44
2.19	Immunohistochemistry	44
2.20	Proximity ligation assay	45
2.21	Nuclear extract preparation	47
2.22	Co-immunoprecipitation (Co-IP)	49
2.23	Protein isolation for GFP-immunoprecipitation	50
2.24	TMT-labeling for protein quantification	50
2.25	Acid extraction of histones	51
2.26	Quantification of histone modifications	52
2.27	Bioinformatics	53
2.28	Statistics	54
3.	Results	55
3.1	Transcriptional changes during retinal maturation	55
3.2	Epigenetic changes during retinal maturation	56
3.3	Dynamics of 5hmC localization	57
3.4	Subnuclear localization of 5hmC	58
3.5	[methyl- ¹³ CD ₃]-L-methionine feeding	59
3.6	Dnmt Expression levels	60
3.7	Genomic distribution of 5hmC during retinal maturation	61
3.8	Tet expression levels during retinal maturation	62
3.9	Identification of neuronal TET3 interactors	63
3.10	Identification of endogenous TET3 interactors	65
3.11	Functional characterization of TET3 binders	67
3.12	TET3 induced changes in gene expression	68
3.13	siRNA knockdown of REST and TET3 overexpression	69
3.14	5hmC and REST co-localize in euchromatin	70
3.15	5hmC co-localizes with the active histone mark H3K36me3	72
3.16	TET3 stimulates NSD3 for H3K36 trimethylation	74
3.17	Effects of TET3 overexpression in retinal explants	76
4.	Discussion	77
4.1	Active DNA demethylation during retinal maturation	77
4.2	Epigenetic role of 5hmC	78
4.3	TET-mediated 5hmC formation	79
5.	Summary	82
6.1	Primers	85
6.2	Lists of identified interaction partners	87
6.	Appendix	94

7.1	List of Publications	94
7.1.1	Publications.....	94
7.1.2	Meeting Abstracts	95
7.2	Curriculum vitae	96
7.3	Curriculum vitae (German).....	98
7.4	References.....	100
7.5	Acknowledgments.....	109

Abbreviations

5caC	5-carboxymethylcytosine
5fC	5-formylmethylcytosine
5hmC	5-hydroxymethylcytosine
5hmU	5-hydroxymethyluridine
5mC	5-methylcytosine
AD	Alzheimer's disease
AID	activation induced cytidine deaminase
ALS	Amyotrophic lateral sclerosis
APOBEC	apolipoprotein B mRNA editing enzyme, catalytic
APS	Ammonium persulfate
BER	base excision repair
BHT	2, 6-di-tert-butyl-4-methyl-hydroxytoluene
bp	base pairs
BRD	bromodomain
C	cytosine
CARM1	co-activator arginine methyltransferase
CD	chromodomain
ddH ₂ O	double deionized water
desferal	deferoxamine mesylate salt
DNA	desoxyribonucleic acid
DNMT	DNA methyltransferase
<i>e.g.</i>	<i>exempli gratia</i>
ESC	embryonic stem cells
ENCODE	Encyclopedia of DNA Elements
<i>et al.</i>	<i>et alii</i>
GCL	ganglion cell layer
GFP	green fluorescent protein
h	hour
H1-4	histone 1-4
HAT	histone acetyltransferase
HCl	hydrochloric acid

HDAC	histone deactylase
HDM	histone demethylase
HEK293T	human embryonic kidney cells
HGP	Human Genome Project
HMT	histone methyltransferase
<i>i.e.</i>	<i>id est</i>
INL	inner nuclear layer
IP	immunoprecipitation
K	lysine
kDa	kilodalton
LC	liquid-chromatography
LFQ	label-free quantification
me	monomethylation
me ₂	dimethylation
me ₃	trimethylation
mg	milligram
min	minute
ml	milliliter
MBD	methyl-CpG binding protein
MS	mass spectrometry
NHGRI	National Human Genome Research Institute
NIH	National Institutes of Health
nm	nanometer
O-GlcNAc	O-glucosyl-N-acetylation
OGT	O-GlcNAc transferase
ONL	outer nuclear layer
p	postnatal day
PAGE	polyacrylamide gel electrophoresis
PB	phosphate buffer
PBS	phosphate buffer saline
PCR	polymerase chain reaction
PHD	plant homodomain
PLA	proximity ligation assay

Pol II	polymerase II
PRC2	polycomb repressive complex 2
PRMT	protein arginine N-methyltransferase
ptm	posttranslational modification
R	arginine
RNA	ribonucleic acid
s	seconds
SAM	S-adenosyl-methionine
SD	standard deviation
SDS	sodium dodecyl sulfate
SEM	standard error of the mean
SET	su(var)3-9, Enhancer-of-zeste and Trithorax
SMUG1	single-strand selective monofunctional uracil-DNA glycosylase
T	thymine
TDG	thymine DNA glycosylase
TET	ten-eleven translocation
TEMED	tetramethylethylenediamine
THU	deaminase inhibitor tetrahydrouridine
TSS	transcriptional start site
TTS	transcriptional termination site
µg	microgram
µm	micrometer
WHSC1L1/NSD3	Wolf-Hirschhorn syndrome candidate 1-like 1

Index of figures

Figure 1. The epigenetic landscape by Conrad Waddington.....	14
Figure 2. The nucleosome core structure.....	15
Figure 3. Schematic view of a nucleosome.	16
Figure 4. Most common histone modifications of core histones.....	17
Figure 5. Epigenetic readers, writers and erasers.	19
Figure 6. DNA methylation by maintenance and <i>de novo</i> DNMT enzymes.....	20
Figure 7. Model pathways of active DNA demethylation via oxidation.....	23
Figure 8. Model pathways of active DNA demethylation via deamination.	24
Figure 9. Synaptic wiring and terminal differentiation of neurons in mouse retina.....	27
Figure 10. <i>De novo</i> methylation tracing experiments.....	35
Figure 11. Schematic overview of metabolic tracing experiments.	36
Figure 12. Schematic overview of the hMeDIP experiment.	39
Figure 13. Schematic workflow of PLA experiment.....	47
Figure 14. Transcriptional changes during retinal maturation.	55
Figure 15. Cytosine derivative levels during retinal maturation.	56
Figure 16. Immunosignal of 5hmC during retinal maturation.....	57
Figure 17. Subnuclear localization of 5mC and 5hmC.	58
Figure 18. Isotope tracing in mouse retinal explant cultures.....	59
Figure 19. Time course of Dnmt expression levels.	60
Figure 20. Differentially hydroxymethylated regions during retinal maturation.	61
Figure 21. Genomic localization of 5hmC and its effect on gene expression.	62
Figure 22. Tet expression levels during retinal maturation.	63
Figure 23. Schematic view of TET3 recruitment.	64
Figure 24. Neuronal TET3 interacting proteins.....	65
Figure 25. Endogenous TET3-interacting proteins.	66
Figure 26. Functional analysis of the interaction of REST and neuronal TET3	67
Figure 27. Neuronal TET3 induced expression changes in HEK293T cells.....	69
Figure 28. Gene expression of three TET3-induced REST-target genes	70
Figure 29. PLA staining of 5mC / 5hmC and REST.....	71
Figure 30. Accumulation of 5hmC is associated with chromatin remodeling	72
Figure 31. PLA staining of 5hmC and H3K36me3.....	73

Figure 32. Quantification of PLA signal (5hmC/ H3K36me3).....	73
Figure 33. Effect of TET3-mediated hydroxylation on chromatin structure.....	75
Figure 34. TET3 overexpression leads to activation of neuronal genes.....	76
Figure 35. Potential role of 5hmC in retinal neurons.	79
Figure 36. Model for neuronal TET3 mediated transcriptional activation.....	83

Index of tables

Table 1. Neurological disorders associated with alterations of 5hmC levels.....	26
Table 2. Parameters for RT-qPCR.....	43
Table 3. Primers used for RT-qPCR in mouse retina.....	85
Table 4. Primers used for hMeDIP qPCR validation.	85
Table 5. Primers used for RT-qPCR in HEK293T cells.	86
Table 6. TET3 interaction partners identified after TET3 overexpression.	88
Table 7. Endogenous TET3 interaction partners.....	90
Table 8. Endogenous REST interaction partners.....	93

1. Introduction

1.1 Background

“So that I may perceive whatever holds, the world together in its inmost folds. See all its seeds, its working power, and cease word-threshing from this hour.” is a quote by the German poet Johannes Wolfgang Goethe describing his protagonist’s desire of gaining more knowledge. Echoing these sentiments the US government announced their research plan "The Human Genome Project" in 1990 to understand our genetic inheritance. Several years later the Human Genome Project (HGP) declared that the human genome containing 3.2 billion DNA base pairs was fully sequenced and all human genes had been identified (Lander et al., 2001). Importantly, the HGP revealed that people are 99.9 % identical at the DNA level. Although this was a scientific breakthrough, the difference of 0.1 % in DNA sequence alone was not able to explain the inter-individual differences.

Moreover, the human body contains more than 200 different cell types *i.e.* heart cells or liver cells that share an identical DNA sequence, display different phenotypes (Surani, 2001). These different phenotypes include a unique cellular identity formed by tissue-and stage-specific gene expression. The changes in gene expression must be controlled and interpreted by mechanisms independent of the genetic code due to the identical DNA sequence.

Conrad Hal Waddington explained this discrepancy by introducing the term epigenotype referring to it as a complex interplay of genes and environment that modulate a genotype to a particular phenotype (Waddington, 2012). Waddington used the analogy of a marble on a hill to describe the epigenetic landscape. During the process of differentiation from a germ cell to a specialized cell type the epigenetic landscape decides which specific cell type is formed by ridges and valleys that branch at different points. As the marble rolls downhill, the possible paths are progressively narrowed, and by the time it reaches the valley, it becomes a differentiated cell (Figure 1).

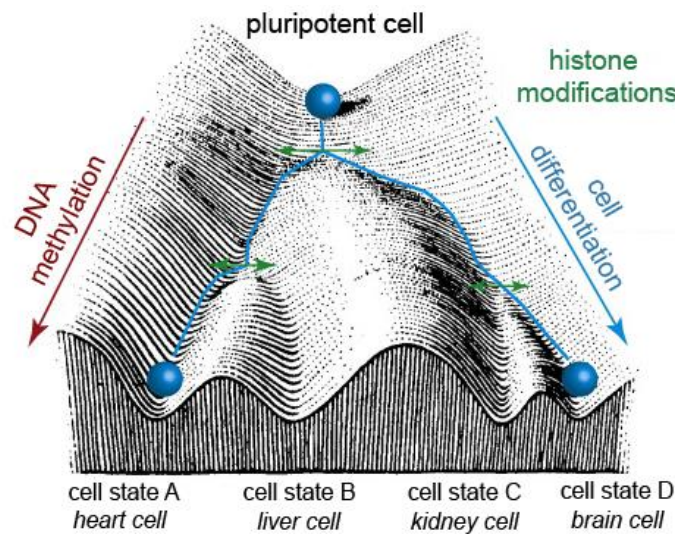


Figure 1. The epigenetic landscape by Conrad Waddington.

The process of cellular differentiation can be compared to a marble on a hill that represents a pluripotent cell state. The hill contains different paths that the marble can roll down and each path will eventually lead to a distinct final differentiated cell type i.e. a heart cell, liver cell, kidney cell and brain cell. During the process of differentiation the amount of alternative paths are limited by epigenetic modifications resulting in a loss of pluripotency and terminal differentiation. Adapted from (Barth and Imhof, 2010).

The main components of this epigenetic landscape involve modifications of histone proteins, ribonucleic acid (RNA), mediated gene silencing and the covalent modification of DNA bases. All of these modifications can alter the accessibility of genes and subsequently control gene expression (Jaenisch and Bird, 2003). Epigenetic mechanisms are important key regulators in development and disease. Defects in epigenetic regulation are involved in different diseases including neurodegenerative disorders i.e. Autism, Alzheimer's disease, cancer, obesity and mental retardation (Egger et al., 2004; Portela and Esteller, 2010). In reference to the genetic code the concept of a histone or epigenetic code was established (Jenuwein and Allis, 2001; Turner, 2000). Based on the HGP the Encyclopedia of DNA Elements (ENCODE) project was launched to study functional elements *i.e.* mapping epigenetic modifications within the human genome by the National Human Genome Research Institute (NHGRI) in 2003. Although, this project had significant impact for human genetics studies, a major drawback was that most of the findings relied on a limited amount of cultured human cell lines. Thus, a new project called the Roadmap Epigenomics Project launched by the US National Institutes of Health (NIH)

investigates epigenomic data directly from different human cells, e.g. stem cells and differentiated cells derived from healthy and diseased people.

1.2 The nucleosome

The nucleosome is a basic repetitive structuring unit of DNA that is present in all eukaryotic chromosomes and an important factor for DNA accessibility (Jiang and Pugh, 2009) (Figure 2). It consists of 200 ± 40 base pairs of DNA and a highly conserved basic protein octamer that consists of two copies of the core histone (H) protein dimers H2A/H2B and H3/H4 forming a negative supercoiling and has a molecular weight of 206 kilo Dalton (kDa) (Richmond and Davey, 2003). The core histone proteins consist of an N-terminal- a globular- and a C-terminal domain. The protruding histone N-terminal tails (histone tails), and to a lower degree the C-terminal regions, can be altered by a variety of enzyme-catalyzed, posttranslational modifications known as histone modifications (Richmond and Davey, 2003). These modifications are necessary for higher order chromatin structure and intranucleosomal and internucleosomal interactions.

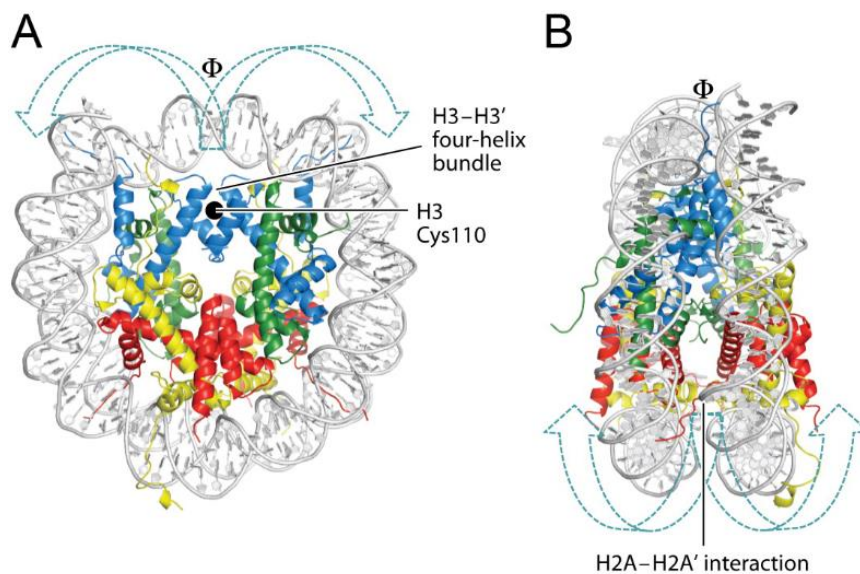


Figure 2. The nucleosome core structure.

(A) The nucleosome viewed down the superhelical axis. Histones H2A, H2B, H3, and H4 are shown in yellow, red, blue, and green, respectively. (B) Viewed as in panel (A) but rotated around the y axis by 90° . Adapted from (Andrews and Luger, 2011).

The nucleosome contains two different DNA components. The nucleosomal core particle consists of 146 base pairs of DNA that are wrapped in 1.67 superhelical turns around the histone octamer (Luger et al., 1997). The nucleosomal DNA is present in a "beads-on-a-string"-like structure, a 10 nm fiber, where the nucleosomes represent the beads and the DNA the string (Olins and Olins, 1974; van Holde and Zlatanova, 1996). The "linker DNA" is linear DNA present between histone octamers. It varies in a tissue- and species-specific manner from 20 – 90 base pairs.

Due to the presence of a linker histone H1 the nucleosome can be further compacted to a 30 nm fiber (Richmond and Davey, 2003) (Figure 3A-B). Further compaction of the chromatin is triggered by scaffold proteins that result in the formation of chromosomes (Arold et al., 2010).

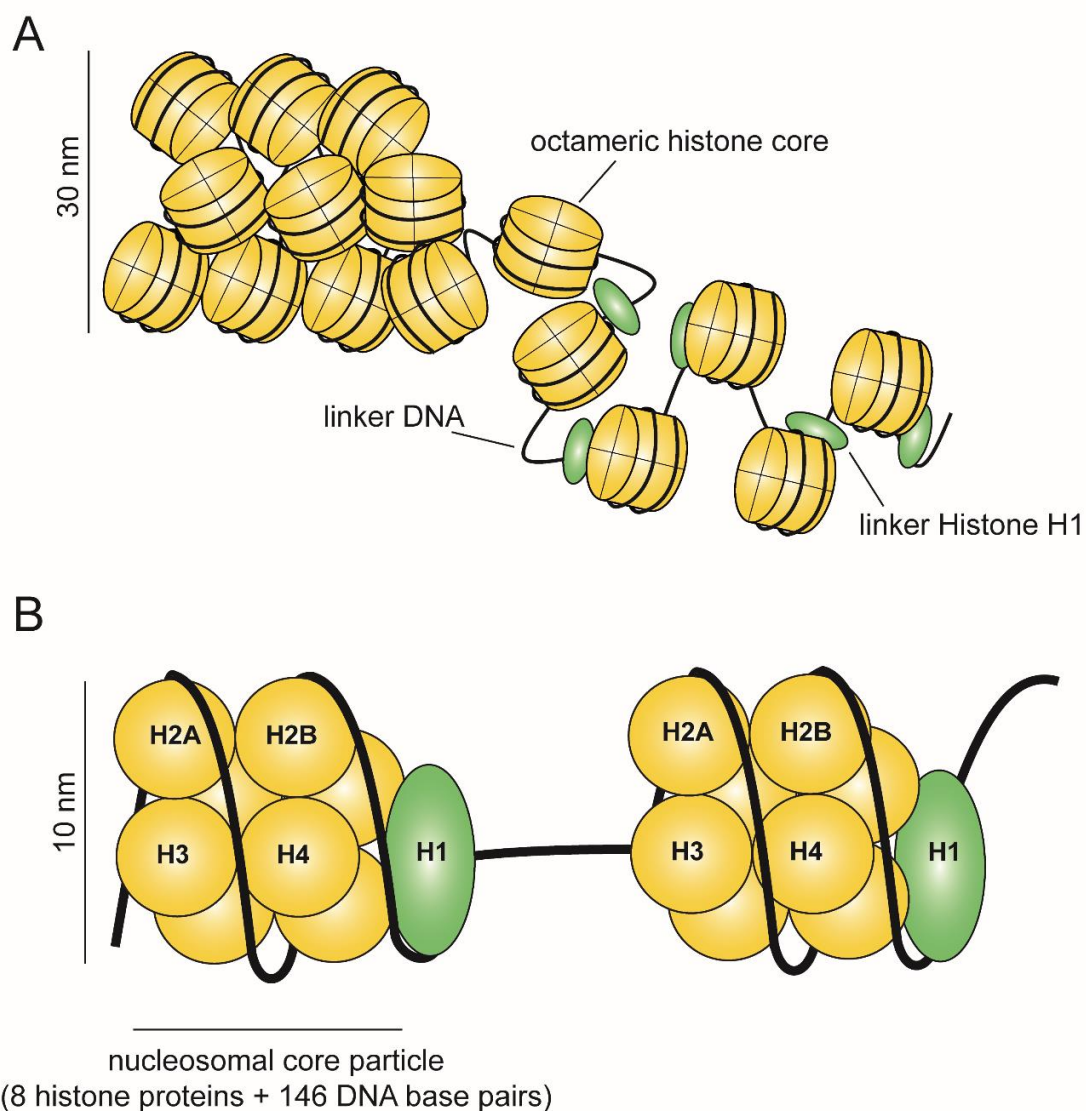


Figure 3. Schematic view of a nucleosome.

1.3 The epigenetic code

The nucleosome that encrypts the epigenetic code has divergent functions. On the one hand, it has to stabilize, package and protect the DNA. On the other hand, the nucleosome has to be flexible and dynamic in order to allow access for polymerases to transcribe and replicate. One of the main mechanisms to modify nucleosomes are epigenetic modifications such as the covalent deposition of a methyl group to the DNA base cytosine for transcriptional silencing (Razin, 1998). Another mechanism to allow changes in DNA accessibility is the replacement of canonical histones with specialized histone variants. The incorporation of these histone variants leads to major changes in chromatin structure, thus influencing transcription and genome stability (Ahmad and Henikoff, 2002). Furthermore, the establishment of posttranslational modifications on the histone tails of core histone proteins is essential for transcriptional regulation (Allfrey et al., 1964). Among the best-characterized histone modifications are small chemical moieties such as methylation, phosphorylation and acetylation of specific amino acid residues (Figure 4). These modifications are established, respectively, by specific enzymes called histone writers, *i.e.* histone methyltransferases (HMT), kinases and histone acetyltransferases (HAT) at specific amino acid residues. Furthermore, ADP-ribosylation, biotinylation, O-Glucose-N-Acylation (O-GlcNAc), SUMOylation, and ubiquitinylation can occur on histone tails to modify the nucleosomal architecture (Zhou et al., 2011).

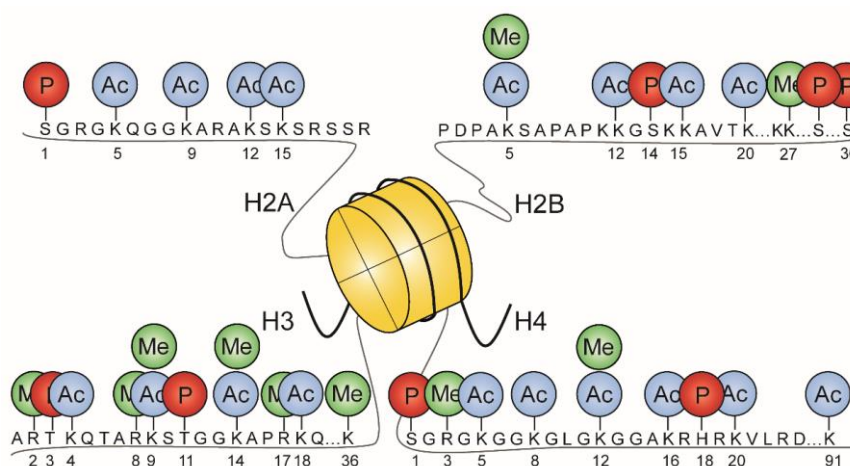


Figure 4. Most common histone modifications of core histones.

Schematic view of N-terminal histone modifications on the four canonical histones H2A, H2B, H3, H4. The covalent posttranslational modifications such as methylation (Me), acetylation (Ac), phosphorylation (P) of distinct amino acid residues are highlighted on the N-terminal tails of each histone.

The methylation of histones was discovered more than 40 years ago. It involves the activity of histone methyltransferases and requires S-adenosyl-methionine (SAM) for its catalytic activity (Murray, 1964). Histone methylation is essential for transcriptional regulation and can occur in different forms such as mono-, di-, and trimethylation of lysine (K) or mono- and dimethylation of arginine (R) residues. Histone 3 (H3) can be methylated at various K residues *i.e.* K4, K9, K27, K36, K79 and R residues *i.e.* R2, R8, R17 and R26. K methylation is mainly generated by SET domain containing proteins such as EZH1-2, SET1 and NSD3, whereas R methylation is carried out by co-activator arginine methyltransferase (CARM1) and protein arginine methyl transferases (PRMT) (Bannister et al., 2002; Chen et al., 2011; Dillon et al., 2005).

Histone methylation leads to transcriptional activation or repression depending on the position of the amino acid residue and the degree of methylation. In eukaryotes the methylation of K at position 4 and 36 of the histone 3 (H3) is associated with transcriptional initiation and elongation leading to active gene transcription. Di (me₂)- and trimethylation (me₃) of H3K4 is predominantly present around transcriptional start site (TSS) of promoter regions and is formed by HMTs such as SETD1A/B and MLL, whereas H3K36me_{2/3} is established within gene bodies by HMTs such as SETD2 and NSD1-3 (Ruthenburg et al., 2007; Schmidt and Jackson, 2013; Wysocka et al., 2005). In contrast to this "activating" histone methylation marks, the di- and trimethylation of H3K27 or H3K9 is associated with transcriptional repression (Mikkelsen et al., 2007). H3K27 trimethylation is generated in promoter regions by EZH2, a member of the polycomb repressive complex 2 (PRC2) (Cao and Zhang, 2004). Interestingly, H3K27me₃ can co-exist with H3K4me₃ leading to poised gene transcription of developmental genes (Bernstein et al., 2006).

Histone methylation was thought to be irreversible until the first histone demethylase (HDM) KDM1A was discovered that demethylates H3K4 and H3K9 mono- and demethylation (Shi et al., 2004). Two different mechanisms for demethylation exist: a flavin adenine dinucleotide (FAD)-dependent amine oxidation by HDMs such as KDM1A, and an Fe(II) and α -ketoglutarate-dependent dioxygenation by KDM4A and similar HDMs (Hino et al., 2012; Tsukada et al., 2006).

Most of the histone modifications are reversible and can be removed by enzymes known as histone erasers, *e.g.* histone deacetylases (HDACs) that remove histone acetylations

(Jakovcevski and Akbarian, 2012). Around 240 amino acid residues within a nucleosome are available for histone modifications. This allows a vast combination of different histone modifications leading to changes in DNA accessibility and recruitment of non-histone proteins known as histone readers. These histone readers contain binding domains that allow for specific binding to distinct histone modifications (Figure 5). For example histone methylation is recognized by chromodomains (CD) and non-related plant homeo domains (PHDs), whereas acetylation is recognized by bromodomains (BRD) (Nielsen et al., 2002; Zeng et al., 2010). There are different mechanisms allowing histone readers to act on histone modifications. First they can bind their target histone modification and directly condense or decondense the underlying chromatin (Verdin and Ott, 2015). Furthermore, a reader can associate with histone writers to form a multiprotein complex and introduce additional modifications to the nucleosome (Musselman et al., 2012). In conclusion the interplay of histone readers, writers and erasers enable a complex coding machinery of the nucleosomal environment (Figure 5).

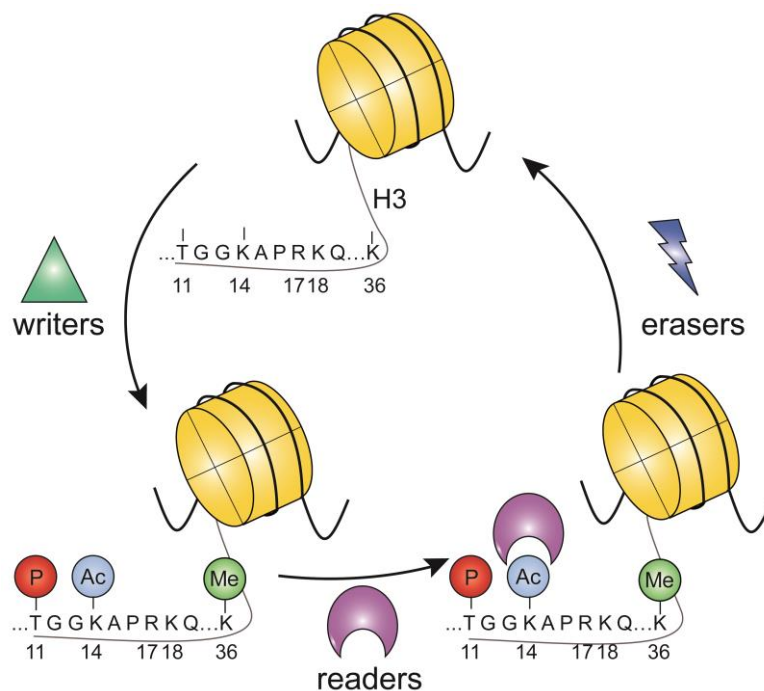


Figure 5. Epigenetic readers, writers and erasers.

Epigenetic writers *e.g.* histone acetyltransferases (HATs), histone methyltransferases (HMTs), protein arginine methyltransferases (PRMTs) and kinases establish defined modifications on specific histone tail amino acid residues. Epigenetic readers *e.g.* bromodomain or chromodomain containing enzymes recognize and bind specific histone modifications. Epigenetic erasers *e.g.* histone deacetylases (HDACs), lysine demethylases (KDMs) and phosphatases remove histone modifications.

1.4 DNA methylation

DNA methylation usually refers to the covalent addition of a methyl group at the 5-carbon of the cytosine base yielding 5-methylcytosine (5mC) (Figure 6A). The deposition of methyl groups on cytosines is an important epigenetic mechanism for repression of gene expression that is involved in processes such as embryonic development, genomic imprinting, X-chromosome inactivation and preservation of chromosome stability (Boyes and Bird, 1991). DNA methylation is controlled by a family of enzymes known as DNA methyltransferases (DNMTs). Three different DNMTs (DNMT1, DNMT3A and DNMT3B) are involved in the maintenance and establishment of DNA methylation patterns. Another member of this family called DNMT3L, lacking methyltransferase activity, stimulates methylation by recruitment of DNMT3A and DNMT3B (Chedin et al., 2002; Pacaud et al., 2014). In contrast, DNMT1 is recruited by its obligate partner UHRF1 for the maintenance of DNA methylation during cell division. UHRF1 binds to hemimethylated CG sites and recruits DNMT1 leading to methylation of the nascent DNA strand to maintain DNA methylation patterns through cell division (Liu et al., 2013b) (Figure 6B). In contrast to DNMT1, DNMT3A and DNMT3B are involved in *de novo* methylation of DNA (Okano et al., 1999) (Figure 6C). However, the mechanisms directing *de novo* DNMT enzymes to their respective sites are not well understood.

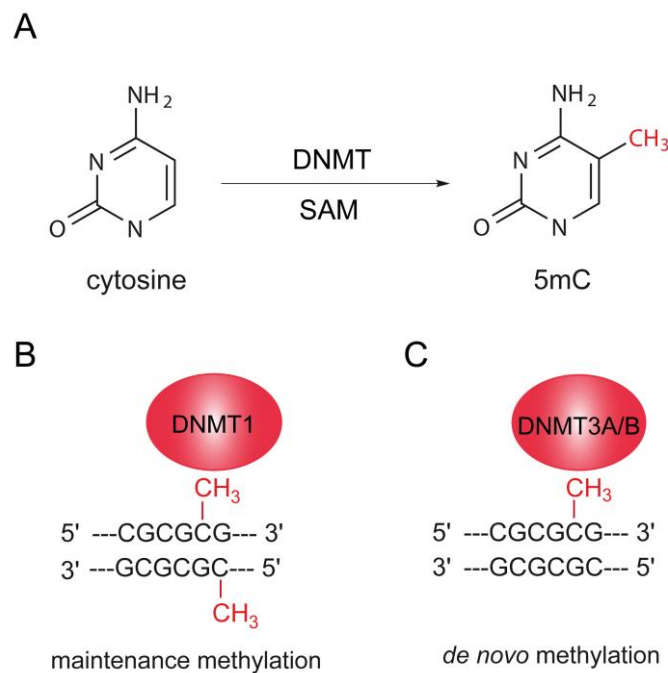


Figure 6. DNA methylation by maintenance and *de novo* DNMT enzymes.

(A) DNA methylation occurs at cytosine bases when a methyl group (-CH₃) from the co-factor S-adenosyl methionine (SAM) transferred to the position 5 of the pyrimidine ring by DNMT1 and DNMT3A/B. (B) The maintenance methyltransferase DNMT1 methylates hemi-methylated DNA at the complementary strand. (C) The *de novo* methyltransferases DNMT3A and DNMT3B initiate *de novo* methylation of previously nonmethylated cytosines.

Several studies have shown that methylation within a promoter region is able to recruit methyl-CpG-binding domain proteins (MBPs), which then prevent binding of transcription factors and, thus, inhibit gene transcription (Boyes and Bird, 1991; Gu et al., 2011). Subsequently, these MBPs are able to recruit histone modifying enzymes (Tan and Nakielny, 2006). These ATP-dependent enzymes lead to chromatin compaction and further transcriptional repression by altering chromatin accessibility.

Vertebrates and plants have conserved DNA methylation machinery. However, the DNA demethylation machinery is different. Plants possess the DNA glycosylases repressor of silencing (ROS1) and Demeter (DME). These glycosylases can excise 5mC and the abasic site is replaced by an unmethylated cytosine via base excision repair (BER) (Choi et al., 2002; Gong et al., 2002). However, such enzymes are not present in vertebrates. A potential mechanism to remove the 5mC mark in vertebrates is passive DNA demethylation, also known as replication-dependent demethylation. Passive 5mC removal can occur by dilution of symmetrically-methylated regions by inactivation or absence of the maintenance methyltransferase DNMT1 after DNA replication leading to hemimethylation in the daughter cells. Subsequent cell division would lead to subsequent 5mC dilution by generating two unmethylated and two hemimethylated daughter cells (Kagiwada et al., 2013).

1.5 TET-mediated 5mC oxidation

A potential candidate for active DNA demethylation is the ten-eleven translocation (TET) family of 5mC hydroxylases that can convert 5mC to 5-hydroxymethylcytosine (5hmC) (Kriaucionis and Heintz, 2009; Tahiliani et al., 2009). TET proteins belong to the family of 2-oxoglutarate and Fe(II)-dependent enzymes and are able to further oxidize 5hmC to 5-formylcytosine (5fC) and 5-carboxycytosine (5caC) (Tahiliani et al., 2009).

At least four pathways are imaginable for oxidative DNA demethylation by TET enzymes (Figure 7). 5hmC could facilitate passive DNA demethylation by interfering with the maintenance methylation. In line with this hypothesis it was shown *in vitro* that UHRF1 that recruits DNMT1, binds tenfold less efficient hemi-5hmC DNA compared to hemi-5mC DNA. This results in a 50-fold reduction of recombinant DNMT1 activity at hemi-5hmC sites (Hashimoto et al., 2012). Another mechanism of demethylation involves further oxidation of 5hmC to 5fC and 5caC by TET enzymes. It was shown that 5fC and 5caC can be removed by thymidine DNA glycosylase (TDG) leading to replacement of the abasic site by BER machinery (He et al., 2011; Maiti and Drohat, 2011). The third putative mechanism is the direct decarboxylation of 5caC. It was shown in embryonic stem cells (ESC) that direct conversion of 5caC to cytosine can occur without BER (Schiesser et al., 2013). However, the enzyme catalyzing this reaction is not yet identified. The fourth mechanism is the removal of 5hmC to cytosine by DNMT enzymes under oxidizing conditions that was shown to be the case in *in vitro* experiments (Chen et al., 2012). However, it is not known if this reaction occurs *in vivo*.

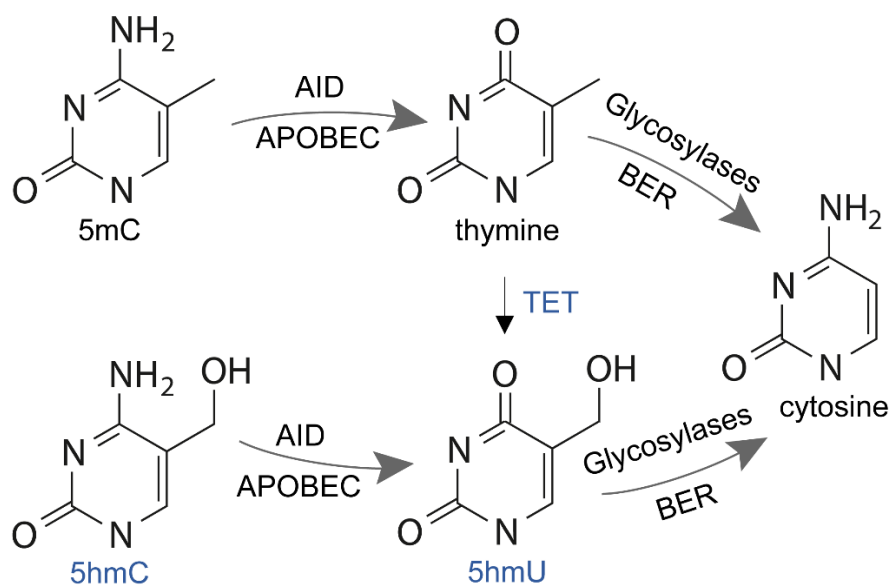


Figure 8. Model pathways of active DNA demethylation via deamination.

5mC and 5hmC can be deaminated by AID/APOBEC deaminases resulting in thymine (T) and 5-hydroxymethyluracil (5hmU). Furthermore, T can be oxidized by TETs to produce 5hmU and both T and 5hmU can be excised by glycosylases coupled to BER.

In summary, TET induced DNA demethylation could occur by facilitation of passive demethylation, DNA repair, enzymatic deformylation/decarboxylation and deamination.

1.6 The 6th DNA base 5-hydroxymethylcytosine

5hmC is not only a degradation intermediate during active DNA demethylation but is also actively involved in gene expression regulation (Hahn et al., 2013; Mellen et al., 2012). Thus, in reference to 5mC that is called the 5th DNA base, 5hmC was coined the 6th DNA base (Münzel et al., 2010).

5hmC is abundant in most mammalian tissues, but high levels are present in embryonic stem (ES) cells (5-10% relative to 5mC) and the highest levels are found in neurons (Globisch et al., 2010; Szulwach et al., 2011). The high abundance of 5hmC in neurons suggested that 5hmC is a stable epigenetic DNA base and not a transient DNA demethylation intermediate in a sequential demethylation process. In line with this, it was shown that 5hmC accumulates during neurogenesis (Hahn et al., 2013; Szulwach et al., 2011). Interestingly, 5hmC was mainly acquired in promoters and gene bodies of neuronal differentiation-related genes and the increase in 5hmC was associated with transcriptional activation. Furthermore, a study by Hahn et al. (Hahn et al., 2013) showed that TET3 is the most highly expressed TET isoform in the developing mouse brain. This suggests that TET3 may play a major role in 5hmC formation. However, how Tet-mediated 5hmC formation is controlled and directed to specific sites is not well understood.

Mapping experiments have shown that all three TET proteins are strongly enriched at CpG-rich promoters (Kohli and Zhang, 2013). It was shown that TET1 and TET3 bind unmethylated CpG sequences due to the presence of a CXXC domain (Allen et al., 2006; Xu et al., 2012). In line with this finding the distribution of TET proteins and oxidized 5mC species only overlap partially (Pastor et al., 2013). TET2 lacks such a CXXC domain, but was shown to functionally interact with the CXXC domain containing protein IDAX (Ko et al., 2013). TET3, the major Tet isoform in neurons (Colquitt et al., 2013; Hahn et al., 2013), exists in various isoforms generated by alternative splicing (Liu et al., 2013a), two isoforms containing a CXXC domain and one shorter isoform lacking such a domain. The TET3 isoform lacking a CXXC domain (neuronal TET3) was shown to be particularly enriched in neuronal tissue (Liu et al., 2013a). However, the preferential binding sites of neuronal TET3 and the recruitment to the DNA are not known. It was suggested that transcriptional regulators might bind directly to TET3 thereby facilitating its specific targeting to genomic positions and, hence, controlling 5hmC levels (Xu et al.,

2012). If such a regulation mechanism exists, transcription factor-dependent control of TET3 activity could potentially contribute to epigenetic regulation of gene expression in neurons. However, transcriptional regulators that functionally interact with TET3 have not been identified so far. Different mechanisms of action are possible for 5hmC to act as an epigenetic regulator with specific biochemical coding properties. First, 5hmC could block or alter binding of 5mC specific binding proteins (readers) such as the family of MBD proteins (Pastor et al., 2013). In a reciprocal manner 5hmC could recruit novel specific readers such as transcriptional regulators. Recent studies have shown that UHRF1, MECP2, MBD3 and the CHTOP-methylosome complex interact with 5hmC *in vitro* (Hashimoto et al., 2012; Mellen et al., 2012; Takai et al., 2014; Yildirim et al., 2011). Moreover, a proteomic approach identified several tissue-specific 5hmC readers in ESC, neuronal progenitor cells (NPC) and brain (Spruijt et al., 2013). Thus, suggesting that 5hmC is able to recruit different sets of readers in a tissue-specific manner and thereby increasing its spectrum of epigenetic regulation. Interestingly, several studies strongly suggest that dysregulation of 5hmC or altered 5hmC binding are implicated in neurological disorders (Table 1).

diseases	alteration of 5hmC	Reference
Angelman syndrome	global increase	(Szulwach et al., 2011)
Amyotrophic lateral sclerosis (ALS)	global increase	(Figuroa-Romero et al., 2012)
Alzheimer's disease (AD)	decrease or increase	(Chouliaras et al., 2013; Condliffe et al., 2014; Coppieters et al., 2014)
Autism	enrichment on autism related genes	(Khare et al., 2012; Wang et al., 2012; Zhubi et al., 2014)
Fragile X syndrome (FXS)	enrichment in FXS related genes	(Wang et al., 2012)
Huntington's disease (HD)	global decrease	(Villar-Menendez et al., 2013; Wang et al., 2013)
Rett syndrome	global decrease	(Szulwach et al., 2011)

Table 1. Neurological disorders associated with alterations of 5hmC levels.

1.7 Retinal maturation

The retina is a complex neural network that is necessary for detection, processing and transfer of visual information to higher brain regions. It consists of five major classes of neurons that are arranged in three cellular layers (Figure 9). Light detection occurs in the outer nuclear layer (ONL) that contains rod and cone photoreceptors. Synaptic wiring of bipolar cells, horizontal cells and photoreceptors occurs in the outer plexiform layer (OPL). The nuclei of bipolar cells, amacrine cells and horizontal cells are in the adjacent inner nuclear layer (INL). Next to the INL is the inner plexiform layer (IPL) that harbors the synapses of bipolar cells and ganglion cells. The cell bodies of ganglion cells are present in the ganglion cell layer (GCL) (Figure 9). It is known that this complex retinal network is established in a precisely timed and organized fashion during development (Heavner and Pevny, 2012; Kuhrt et al., 2012). However, the molecular mechanisms underlying these morphological and functional changes are only partly understood (Gregory-Evans et al., 2013; Xiang, 2013). In mouse retina this terminal maturation process involves major morphological and functional changes largely occurring within a week after eye opening (Hoon et al., 2014; Okawa et al., 2014). The exact mechanisms that orchestrate retinal maturation are not known. Potential pathways may involve the *de novo* remodeling of epigenetic marks to facilitate silencing and/or activation of specific genes via DNA methylation and histone modifications.

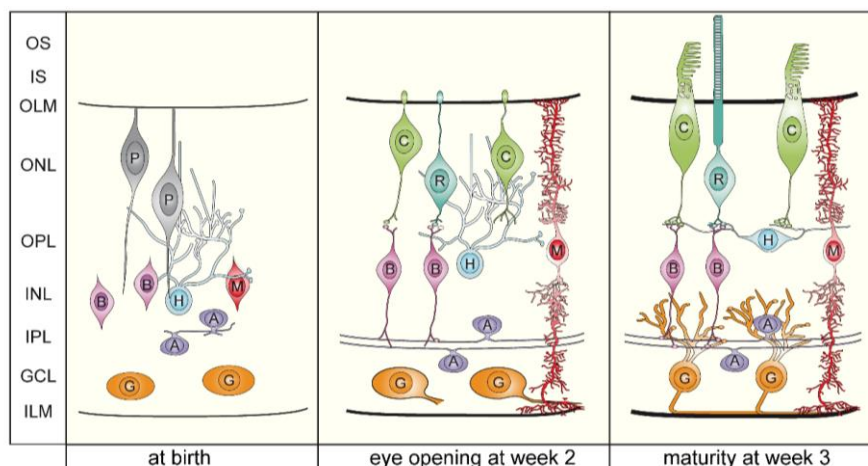


Figure 9. Synaptic wiring and terminal differentiation of neurons in mouse retina.

Cartoon illustrating the sequence of postnatal maturation of the vertebrate retina, exemplified for the mouse. OS = outer segment, IS = inner segment, OLM = outer limiting membrane, ONL = outer nuclear layer, OPL = outer plexiform layer, INL = inner nuclear layer, IPL = inner plexiform layer, GCL = ganglion cell layer, ILM = inner limiting membrane.

1.8 The aims of this thesis

The mechanisms controlling transcriptional changes during neuronal maturation are poorly understood. However rising evidence suggests that epigenetic events are crucial for proper transcriptional control and differentiation during this critical period. In this thesis particular interest was paid to unravel the role of 5hmC and TET3 during neuronal maturation in mouse retina. The rationale of the thesis is to address the following subjects:

1.) Epigenetic role of 5-hydroxymethylcytosine

5hmC is suggested to be an intermediate during DNA demethylation. However, several studies suggest that 5hmC can function as a stable epigenetic DNA base (Bachman et al., 2014; Globisch et al., 2010; Szulwach et al., 2011). The aim of this study was to unravel the role of 5hmC during retinal maturation. Therefore, genomic distribution of 5hmC should be studied in immature retina (postnatal week 2) and adult retina (postnatal week 3). Moreover, the effects of 5hmC accumulation on gene expression levels should be investigated.

2.) Functional role of neuronal TET3

The exact mechanisms on how 5hmC marks are established by TET enzymes are not known. It was suggested that the CXXC domain present in TET1 and TET3 is responsible for DNA binding. However, the predominant neuronal TET3 isoform is lacking a CXXC domain or any other DNA binding. Hypothesizing that neuronal TET3 interacts with transcriptional regulators that mediate DNA binding and promote TET3 hydroxylase activity a screen for putative interaction partners should be performed.

2. Material and Methods

2.1 Animals

All mice used were on the C57BL/6 genetic background. All procedures concerning animals were performed with permission of the local authority (Regierung von Oberbayern). Day of birth was considered as postnatal day 1 (p1). All mice were given *ad libitum* access to food (Ssniff; regular feed: R/M-H, breeding feed: M-Z Extrudat) and water. Mice were maintained on a 12 h light/dark cycle.

2.2 Chemicals, solutions and buffers

All chemicals used were obtained by Bio-Rad, Fluka, Merck, Roth and Sigma-Aldrich if not mentioned otherwise. The quality was "pro analysi" or "for molecular biological use". For all solutions high pure and deionised water was used (Milli-Q Plus System, Millipore). In experiments that required a high purity all solutions were autoclaved (Sterlisator, Münchener Medizin Mechanik).

2.3 Cell culture and plasmid transfection

Human embryonic kidney (HEK293) cells are a well-established over-expression system to investigate proteins and their function *in vitro*. For this purpose, HEK293T cells were transfected with plasmid DNA containing the protein of interest. All cell culture work was performed under a laminar flow (Hera Safe, Thermo Scientific) and aseptic conditions.

The following plasmids were used in this study:

LV-CMV-TET3ΔCXXC-eGFP (see also chapter 2.5)

LV-CMV-eGFP (see also chapter 2.5)

p6351-MSCV-CMV-CMV-Flag-HA-NSD3 (Plasmid #31357, Addgene)

pHR'-NRSF-CITE-GFP (Plasmid #21310, Addgene)

HEK293T cells (DMSZ) were cultivated in DMEM + GlutaMAX medium (+ 4.5 g/l glucose, - pyruvate + 10 % FBS) + 1 % penicillin/streptomycin (Biochrom) at 37 °C with 10 % CO₂ in an incubator (Heraeus Cells, Thermo Scientific). Transient transfections of HEK293T cells were performed using the calcium phosphate technique.

The calcium phosphate based transfection was performed by adding following solutions to a 15 ml falcon tube (Sarstedt):

DNA	20 µg
2.5 M CaCl ₂	100 µl
ddH ₂ O	ad 1 ml

While vortexing this mixture, 1 ml 2 x BBS solution was added in a drop-wise manner. Then, the mixture was incubated for max. 5 min. at room temperature. This mixture was added drop-wise to the 50-70 % confluent cells and the cells were incubated at 37 °C with 5 % CO₂ in an incubator (Hera Cell, Thermo Scientific). 24 h after transfection, the medium was replaced and the cells were incubated at 37 °C for 24 h with 10 % CO₂ in an incubator (Hera Cell, Thermo Scientific).

2 x BBS Solution

BES	10.65g
NaCl	16.35g
Na ₂ HPO ₄ · 2H ₂ O	0.21g
H ₂ O	ad 950 ml

adjust to pH 6.95 with NaOH and sterile filtrate using a 25mm syringe filter (VWR).

2.4 siRNA experiments

For RNAi experiments, REST-specific siRNA duplexes or control siRNA duplexes (OriGene, SR304036) and plasmid-expressing mouse TET3 were transfected using siTRAN (OriGene) in Opti-MEM I reduced serum medium (Invitrogen) according to the manufacturer's instructions. Cells were incubated at 37 °C and 10% CO₂ for 48 h in an incubator (Hera Cell, Thermo Scientific) and subsequently harvested for genomic DNA isolation using a cell scraper (VWR). Subsequently, the cells were centrifuged at 500 g for 5 min and the supernatant was removed by pipetting. Samples were snap-frozen in liquid nitrogen and stored at -80 °C until use. Knockdown efficiency of gene expression was verified using RT-qPCR as described in chapter 2.16. Primers used for siRNA studies are listed in Table 5.

2.5 Lentiviral plasmids

The original lentivirus plasmids were provided by the lab of Inder Verma (The Salk Institute for Biological Studies, Laboratory of Genetics, La Jolla, CA, USA).

Mouse TET3 was PCR cloned from mouse retinal cDNA using the following primers:

5'-CTATCTAGAACCGCCATGGACTCAGGGCCAGTGTAC-3' (forward)

5'-TCACCGGTAAGATCCAGCGGCTGTAGGG-3' (reverse)

Tet3 was ligated into a lentiviral vector containing a cytomegalovirus (CMV) promoter (Mistrik et al., 2005), yielding LV-CMV-TET3 Δ CXXC-eGFP. LV-CMV-eGFP was used for control experiments.

2.6 Lentiviral production

Lentiviral particles were produced in HEK293T cells (DSMZ). The following protocol refers to the production of two different LV constructs:

A 14.5 cm plate (Greiner Bio-One) with 90-100 % confluent HEK293T cells was re-suspended in 2 ml trypsin (0.05 % trypsin/EDTA) (Life Technologies) 16 ml DMEM + GlutaMAX medium (+ 4.5 g/l glucose, - pyruvate + 10 % FBS (Biochrom)) + 1 % penicillin/streptomycin (Biochrom) and was split to 2 x 14.5 cm plates (Greiner Bio-One) in an 1:9 dilution. Cells were incubated at 37 °C with 10 % CO₂ in an incubator (Hera Cell, Thermo Scientific) for 96 h. Each plate was split in a 1:7 dilution to 6 x 14.5 cm in 20 ml DMEM + GlutaMAX medium (+ 4.5 g/l glucose, - pyruvate + 10 % FBS + 1 % penicillin/streptomycin) and was incubated at 37 °C with 10 % CO₂ for 24 h or until they were 80 % confluent. The cells were transfected with the following transfection mixture:

6 x 14.5 cm plates

plasmid construct	108 µg
pMDL	70 µg
RsvRe	32 µg
pMD2.G	29 µg
CaCl ₂ (2.5 M) (drop-wise)	0.7 ml
polybrene (8 mg/ml) (hexadimethrin bromid, Sigma)	7 µl
dextran (10 mg/ml) (Fluka)	700 µl
H ₂ O (Sigma)	ad 12 ml

In 50 ml falcon tubes (Sigma), vortex and add 6 ml 2x BBS (see also chapter 2.3) in a drop-wise manner, vortexed and incubated for 12 min at room temperature.

2 ml of the transfection mixture was added to each plate. Subsequently cells were placed at 37 °C with 5 % CO₂ for 24 h in an incubator (Hera Cell, Thermo Scientific). The medium was replaced with 16 ml fresh DMEM + GlutaMAX medium (+ 4.5 g/l glucose, - pyruvate + 10 % FBS) + 1 % penicillin/streptomycin (Biochrom) and placed at 37 °C with 10 % CO₂ in an incubator (Hera Cells, Thermo Scientific). The virus containing

supernatant was harvested from the plates by filtration (0.45µm, Nalgene). 16 ml of fresh DMEM + GlutaMAX medium (+ 4.5 g/l glucose, - pyruvate + 10 % FBS) + 1 % penicillin/streptomycin (Biochrom) was added to the cells and they were placed back at 37 °C for 10 % CO₂. The filtrated medium was transferred in centrifugation tubes (Open-Top Thinwall Polypropylene, Konical Tube, Beckman & Coulter) and centrifuged for 2 h at 19.400 rpm at 17 °C (SW 28 Rotor, Beckman & Coulter). The supernatant was removed using a vacuum pump (Vacusafe, Integra Biosciences). The pellet was resuspended in 200 µl HBSS (Gibco) and was collected in a sterile 1.5 ml screw cap (Sarstedt). The samples were vortexed briefly and stored at 4 °C. On the following day the supernatant from the plates was again collected and filtered as mentioned above.

The re-suspended pellets in HBSS were washed and concentrated by a second centrifugation step in sucrose. Therefore, the samples were transferred to centrifugation tubes (Tube, Polypropylene, Thinwall, 5.0 ml, 13 x 51 mm, Beckman & Coulter) with 2 ml 20 % sucrose (Applichem) in ddH₂O (Sigma) and centrifuged for 2 h at 21.000 rpm 17 °C (SW55 Rotor, Beckman Coulter). The supernatant was carefully aspirated using a vacuum pump (Vacusafe, Integra Biosciences). The pellet was resuspended in 70 µl HBSS, collected in a new 1.5 ml screw cap, vortexed and incubated for 45 min in a thermocycler at room temperature and 1400 rpm (Thermomix, Eppendorf). After short centrifugation the supernatant was aliquoted in 1.5 ml screw caps containing 5 µl virus solution. Samples were stored at -80 °C until use.

2.7 *In vitro* retinal explant cultures

Retinal explant cultures were prepared following a protocol from Reidel et al (Reidel et al., 2006). Retina explant cultures were prepared under a laminar flow (Hera Guard, Thermo Scientific) and all media had been sterile filtered using a 25mm syringe filter (VWR).

Retinas from wildtype animals (C57BL/6) were used to generate retinal explants. Animals were euthanized and the eyes enucleated in DMEM Nutrient Mixture F12-HAM medium (GIBCO® Dulbecco's Modified Eagle Medium, Life Technologies), containing 10 % fetal bovine serum (FBS) (Biochrom) and 1 % antibiotics (penicillin/ streptomycin)

(Biochrom). Afterwards, the entire eyes were incubated in DMEM-F-12 (Sigma) serum free medium containing 0.12 % proteinase K (Sigma) for 15 min at 37 °C with 5 % CO₂ in an incubator (Hera Cell, Thermo Scientific). Next, proteinase K was inactivated using 10 % fetal bovine serum (Biochrom) in DMEM Nutrient Mixture F12-HAM medium (Sigma) for 5 min at 37 °C with 5 % CO₂ in an incubator (Hera Cell, Thermo Scientific). After rinsing the eyes three times in DMEM Nutrient Mixture F12-HAM medium (Life Technologies) without serum, the eyes were dissected aseptically using a stereoscopic microscope (Stemi 2000, Zeiss) in a 35 mm Petri dish (Cellstar, Greiner Bio-One GmbH). First the optic nerve was cut under slight tension using forceps and a micro-eye spring scissor (Mini Vanas, blade 3 mm, Frohnhäuser). Next, an incision was placed by gently inserting the scissor between the retinal pigment epithelium and the sclera. Afterwards the sclera was incised along the eyeball towards the cornea. Finally, the lens, vitreous, sclera, and choroids were carefully removed under preservation of retinal pigment epithelium. Next, the retina was cut perpendicularly to its edges, resulting in a cloverleaf-like shape. Subsequently, the retina was transferred to a Millicell culture dish filter insert (Millicell, Merck Millipore) with the retinal pigment epithelium layer facing the membrane. The insert was put into a six-well culture plate (Cellstar, Greiner Bio-One) and incubated in DMEM-F12 nutrient medium containing 10 % fetal bovine serum (FBS) (Biochrom) and 1 % antibiotics (penicillin/streptomycin) (Biochrom) at 37 °C with 5 % CO₂ in an incubator (Hera Cell, Thermo Scientific). Every second day, the full volume of the nutrient medium, 1.2 ml per well, was replaced with fresh DMEM Nutrient Mixture F12-HAM medium (Life Technologies), containing 10 % fetal bovine serum (FBS) (Biochrom) and 1 % antibiotics (penicillin/streptomycin) (Biochrom).

2.8 Metabolic feeding with [methyl-¹³C_D₃]-methionine

De novo methylation tracing experiment was performed using [methyl-¹³C_D₃]-methionine (heavy methionine) that was incorporated to the DNA as [¹³C, D₃] 5mC by DNA methyltransferases (DNMT) (Figure 10A) (Bachman et al., 2014; Pfaffeneder et al., 2014). Further oxidation of [¹³C, D₃] 5mC by TET enzymes led to the formation of [hydroxymethyl-¹³C, D₂] 5hmC (*de novo* 5hmC), [formyl-¹³C, D] 5fC (*de novo* 5fC) and [carboxy-¹³C] 5caC (*de novo* 5caC) (Figure 10B) (Pfaffeneder et al., 2014).

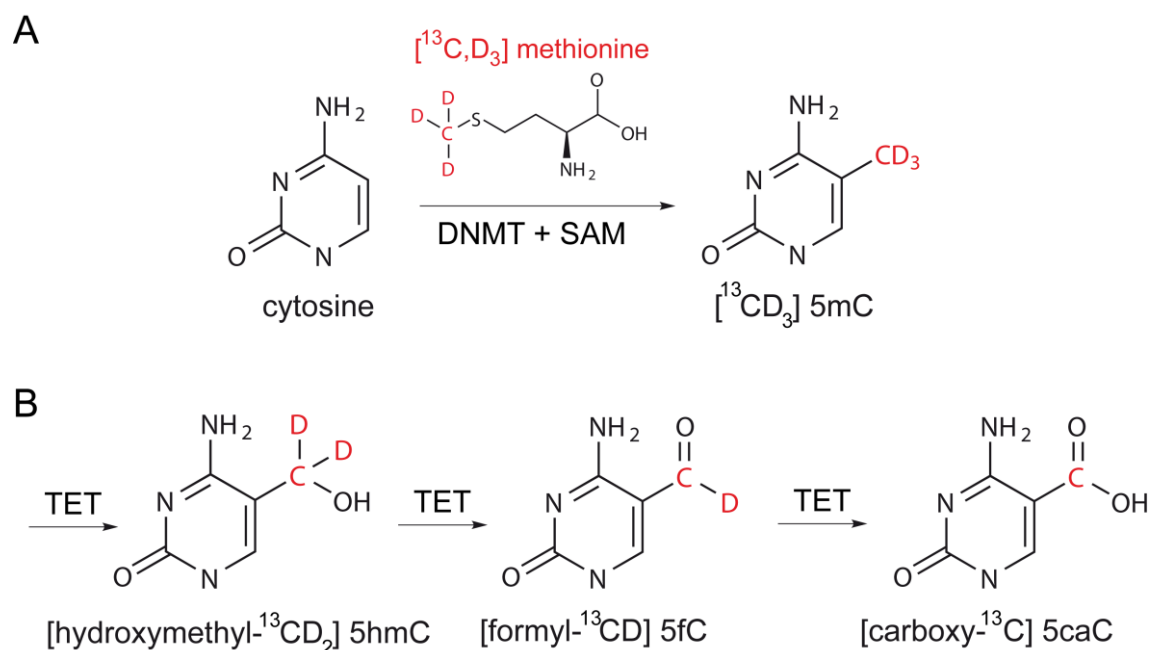


Figure 10. *De novo* methylation tracing experiments.

(A) *De novo* metabolic tracing experiments were performed in methionine free medium supplemented with $[^{13}\text{C}, \text{D}_3]$ -labeled L-methionine that is incorporated as $[^{13}\text{C}, \text{D}_3]$ 5mC. (*de novo* 5mC). (B) *de novo* 5mC can be further oxidized by TET enzymes to [hydroxymethyl- $^{13}\text{C}, \text{D}_2$] 5hmC (*de novo* 5hmC), [formyl- $^{13}\text{C}, \text{D}$] 5fC (*de novo* 5fC) and [carboxy- ^{13}C] 5caC (*de novo* 5caC).

To investigate *de novo* methylation and potential *de novo* 5mC oxidation in mouse retina, feeding experiments were performed in 11-day-old (p11) retinal explant cultures (Figure 11). Retinal explant cultures were prepared as described in chapter 2.3 except that DMEM Nutrient Mixture F12-HAM medium (Life Technologies) was replaced with custom L-methionine-free DMEM-KO (Invitrogen).

Retinal explant cultures were maintained in custom L-methionine-free DMEM-KO (Invitrogen) containing 10% FBS (Biocrom) and supplemented with 2 mM of [methyl- $^{13}\text{CD}_3$]-methionine (Sigma) for 9 days (after three days of incubation media was renewed) at 37 °C and 5 % CO_2 in an incubator (Hera Cell, Thermo Scientific) (Figure 11). Four retinal cultures were collected each three days after feeding and pooled for subsequent HPLC-MS/MS quantification that was conducted by Mirko Wagner (Carell group, LMU Munich).

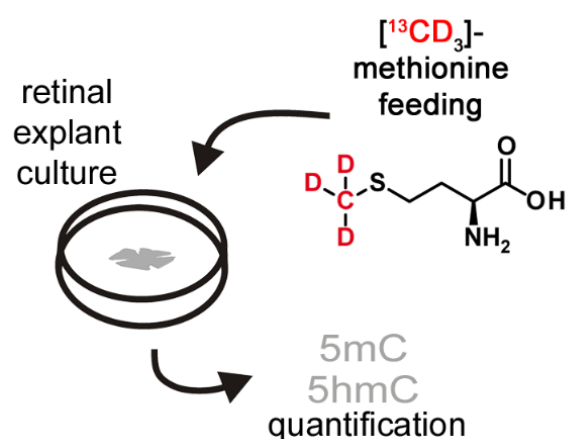


Figure 11. Schematic overview of metabolic tracing experiments.

De novo metabolic tracing experiments were performed using $[^{13}\text{C}, \text{D}_3]$ -labeled L-methionine in p11 retinal explants. 5mC and 5hmC levels were quantified after 3, 6 and 9 days of culturing using HPLC-MS/MS.

2.9 LV transduction of retinal explant cultures

Retinal explant cultures from 11-day-old mice were used for transduction experiments using LV-CMV-TET3 Δ CXXC-eGFP (neuronal TET3) or LV-CMV-eGFP (control). Twelve retinæ were used for each experiment. The LV particles were added to the scleral and vitreal part of retinal explants directly after preparation of the explant cultures. Every second day, the full volume of DMEM-F12 (Life Technologies), 1.2 ml per well (Cellstar, Greiner Bio-One), was replaced with fresh DMEM-F12 medium. Retinal explants were harvested after 12 days *in vitro* culturing. The retinal explants were snap frozen in liquid nitrogen and stored at $-80\text{ }^\circ\text{C}$ for nuclear protein extraction.

2.10 Genomic DNA isolation

The Blood and Cell Culture DNA Midi Kit (Qiagen) was used to extract genomic DNA (gDNA), following the manufacturer's instruction for cell culture samples or tissue samples, respectively. Additionally, all buffers until loading of the sample on *Genomic-tip 100/G* were supplemented with the antioxidants 2, 6-di-*tert*-butyl-4-methyl-hydroxytoluene (BHT, 200 μ M) (Sigma), deferoxamine mesylate salt (desferal, 200 μ M) (Sigma) and deaminase inhibitor tetrahydrouridine (THU, 200 μ M) (Sigma). Moreover, the elution buffer QF was supplemented with 200 μ M BHT. The following protocol was optimized for 25 mg tissue weight.

Tissue samples were homogenized with 2 ml Q2 buffer and a stainless steel bead in a TissueLyser (Qiagen) at 30 Hertz (Hz) for 2 min. Buffer G2 lyses the nuclei and denatures proteins such as nucleases, histones, and viral particles. The excess QIAGEN Protease digests the denatured proteins into smaller fragments. Next, 20 μ l proteinase K (Qiagen) were added and the solution was incubated for 3 h at 56 °C. Subsequently, DNase-free RNase A (4 ml, 100 mg/ml, Qiagen) was added and incubated for 5 min under shaking (600 rpm, Thermomixer, Eppendorf) at room temperature. Buffer G2 and QIAGEN Protease, in combination, were used to strip the genomic DNA of all bound proteins, facilitating efficient removal during purification. The sample was vortexed and transferred onto a QIAGEN Genomic-tip. The samples were allowed to enter the resin by gravity flow. The samples were washed 3 times using 1 ml Buffer QC and eluted using 1 ml Buffer QF.

After elution, all steps were performed at 4 °C or on ice. The genomic DNA samples were precipitated with NaOAc (0.3 M final) and 0.7 volumes isopropanol. The samples were mixed and centrifuged immediately at 5.000 x g for 15 min at 4 °C using a micro centrifuge (Fresco 17, Thermo Scientific). The supernatant was carefully removed by pipetting. Samples were resuspended in ddH₂O containing 200 μ M BHT. HPLC-MS/MS quantification were performed by Mirko Wagner (Carell group, LMU Munich) and Jessica Steinbacher (Carell group, LMU Munich).

2.11 DNA immunoprecipitation

DNA fragmentation was performed as described in Mohn et al (Mohn et al., 2009). First, 15 µg of isolated retinal gDNA ad 300 µl TE-Buffer was fragmented to an average size of 500 bp by sonication (Branson) applying 5 consecutive fragmentation steps each with an amplitude of 20 % for 10 s and 1 min pause after each pulse. hMeDIP was performed according to manufacturer's manual (Active Motif) (Figure 12). 3 µg of DNA and 4 µl of rabbit 5-hmC pAB (Active Motif, #39770) were incubated at 4 °C with end-to-end rotation overnight. To perform DNA capture the antibody-bound DNA was incubated with 25 µl Protein G magnetic beads (Active Motif) for 2 h at 4 °C with end-to-end rotation. After removal of the supernatant the beads were washed three times with wash buffers that contain nonionic surfactants and salts. In the first washing step 200 µl ice-cold washing buffer (buffer C, Active Motif) was used and for the second and third washing step 200 µl ice-cold washing buffer (buffer D, Active Motif) were used. The beads were re-suspended using 50 µl acidic elution buffer (buffer AM2, Active Motif). After 15 min incubation at room temperature with end-to-end rotation 50 µl TRIS-HCl based buffer was added to increase the pH (Neutralization Buffer, Active Motif).

The enriched 5hmC-containing DNA was purified using the Chromatin IP DNA Purification Kit (Active Motif). First, 500 µl binding buffer (Active Motif) was added to 100 µl of each sample DNA and 5 µl 3 M sodium acetate (Active Motif) was added and mixed by pipetting. The color of the DNA sample / DNA Purification Binding Buffer mixture should be bright yellow, not light orange or violet. If the color was light orange or violet the pH was above 7.5. Thus, if necessary more 3 M sodium acetate was added (5 µl steps) and mixed until the pH was below 7.5. The correct pH was important for successful binding and purification of the DNA due to the fact that the elution buffer had a basic pH. A DNA purification column (Active Motif) was placed in the collection tube (Active Motif) and the sample was added on the column. Subsequently, the samples were centrifuged at 14.000 rpm for 1 min in a micro centrifuge (Fresco 17, Thermo Scientific). The flow through was discarded and 750 µl of wash buffer (Active Motif) was added. Next, the samples were centrifuged again at 14.000 rpm for 1 min. After removal of the flow through the samples were centrifuged at 14.000 rpm for 2 minutes in a microcentrifuge to remove any residual wash buffer from the column. The columns were transferred to clean 1.5 ml tubes (Eppendorf tube, Eppendorf) and 50 µl of DNA Purification Elution

Buffer (Active Motif) was added to the center of the column matrix and incubated for 1 min. Next, the sample was centrifuged at 14.000 rpm for 1 min and the DNA concentration of the eluted DNA was measured using Nanodrop 2000c (Thermo Scientific). The samples were stored at -20 °C until use. Paired-end libraries were prepared using the paired-end TruSeq DNA sample prep kit (Illumina inc.) and performed by HiSeq 2000 instruments (Illumina inc.).

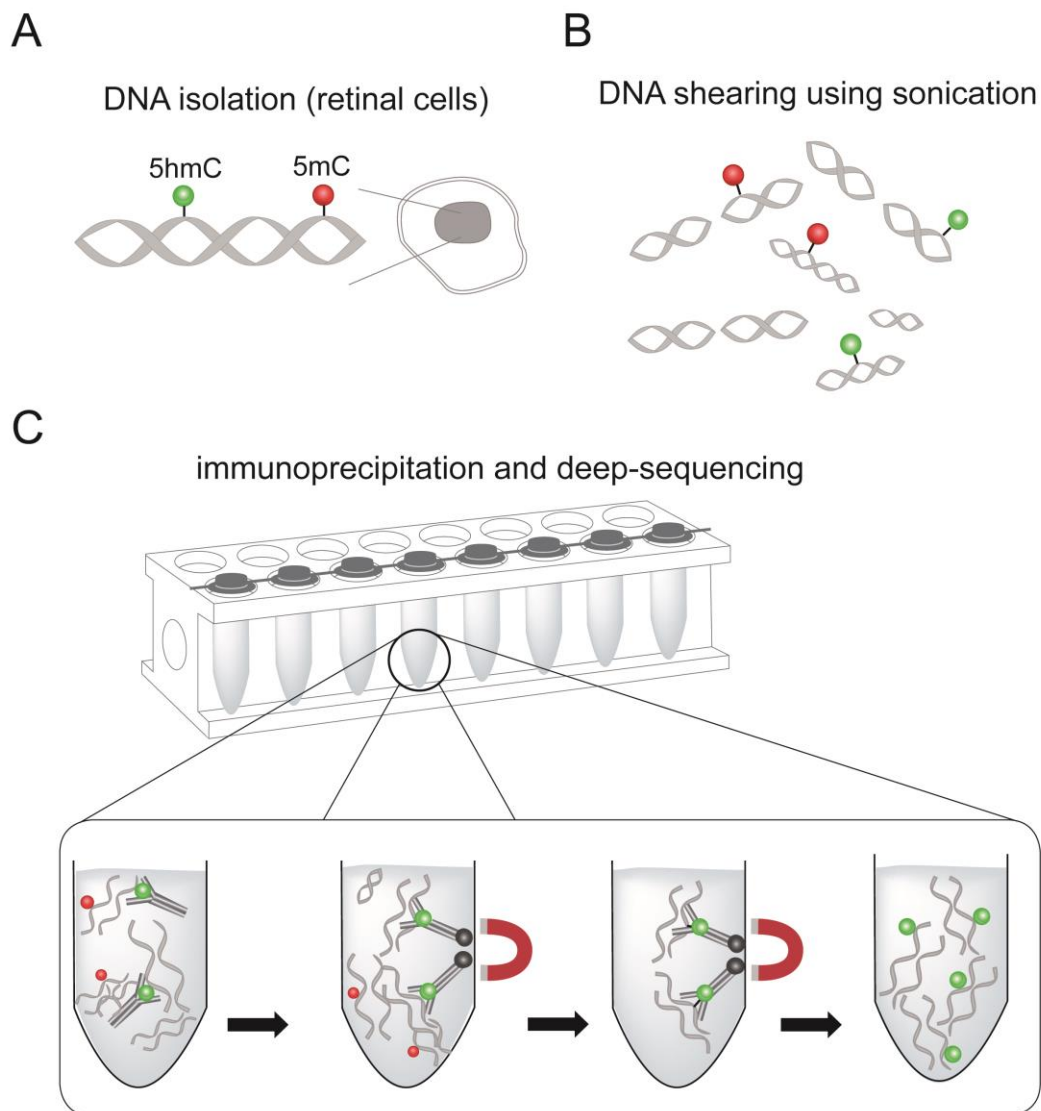


Figure 12. Schematic overview of the hMeDIP experiment.

(A) First DNA is isolated from mouse retinal tissue as described in chapter 2.7. (B) After that the DNA is sheared using a sonicator. (C) The DNA fragments are incubated with the primary antibody (rabbit anti-5hmC antibody). Next Protein G magnetic beads are added to the solution. The

magnetic beads – DNA complex is captured using a magnetic rack and washing steps are performed. After acidic elution and subsequent neutralization the DNA is purified and stored at -20 °C for further use. Adapted from http://www.diagenode.com/media/catalog/file/hMeDIP-_kit-manual.

2.12 hMeDIP qPCR validation

To validate the hMeDIP sequencing results, specific genomic regions were chosen that showed higher levels of 5hmC at postnatal week 3 compared to week 2 (gained 5hmC), lower levels of 5hmC at postnatal week 3 compared to week 2 (lost 5hmC) and stable regions that did not display alterations of 5hmC levels during retinal. First hMeDIP was performed and the 5hmC enriched DNA was purified as described in chapter 2.11. qPCR validation of selected 5hmC regions was performed using 200 ng of eluted DNA in duplicate 10 µl qPCR reactions (n=3).

10 µl PCR reactions

Fast SYBR Green master mix	5 µl
Forward primer* (5 pmol/µl)	0.5 µl
Reverse primer* (5 pmol/µl)	0.5 µl
Sterile water	1 µl
DNA sample (eluted DNA)	3 µl
Total volume	10 µl

Fold enrichment was calculated as 2^{-dC_T} , where $dC_T = C_T$ (5hmC week 2) – C_T (5hmC week 3). Primers used in hMeDIP-qPCR are listed in Table 4.

2.13 Origin of mouse embryonic stem cells

Mouse embryonic stem cells (mESC) for gene expression studies were kindly provided by Markus Moser (Max-Planck-Institute for Biochemistry).

2.14 RNA extraction

Total RNA extraction was performed using the RNeasy-Mini Kit (Qiagen) according to the manufacturer's protocol. Briefly, 350 μ l RLT Buffer was added to each retina (approximately 15 mg tissue). The tissue was disrupted and homogenized using a 27G needle (Sterican) and a 1 ml syringe (Terumo). The lysates were pipetted directly onto a QIAshredder spin column (Qiagen). The samples were centrifuged for 2 min at full 10.000 rpm. The supernatant was carefully transferred to a new microcentrifuge tube. 350 μ l of 70 % ethanol was added to the lysate, and mixed well by pipetting. The sample, including any precipitate, was transferred to an RNeasy MinElute spin column (Qiagen). The sample was centrifuged for 15 s at 10.000 rpm in a microcentrifuge (Fresco 17 microcentrifuge, Thermo Scientific). Next, 350 μ l Buffer RW1 was added to the RNeasy MinElute spin column. The sample was again centrifuged for 1 min at 10.000 rpm and 10 μ l DNase I stock solution was added to 70 μ l Buffer RDD. The DNase I incubation mix (80 μ l) was added to the RNeasy MinElute spin column membrane, and placed on the benchtop at room temperature for 15 min. Next 350 μ l Buffer RW1 was added to the RNeasy MinElute spin column and centrifuged for 15 s at 10.000 rpm. 500 μ l Buffer RPE was added to the spin column and centrifuged for 15 s at 10.000 rpm. Next, 500 μ l of 80 % ethanol was added. The RNA was eluted by adding 12 μ l RNase-free water directly to the center of the spin column membrane and centrifuging for 1 min at full speed.

2.15 cDNA synthesis

Reverse Transcription (RT) was performed using the RevertAid First Strand cDNA Synthesis Kit (Thermo Scientific) according to the manufacturer's manual. In brief the following reagents were added into a sterile, nuclease-free tube on ice in the indicated order:

cDNA synthesis mixture (total volume: 20 μ l)

Template RNA/total RNA:	200 ng
primer: oligo (dT) 18 primer	1 μ l
random hexamer primer	1 μ l
water, nuclease-free / add volume to	12 μ l
5 x Reaction buffer	4 μ l
RiboLock RNase Inhibitor (20 u/ μ l)	1 μ l
10 mM dNTP Mix	2 μ l
RevertAid M-MuLV Reverse Transcriptase (200 u/ μ l)	1 μ l

The sample was mixed gently, centrifuged and incubated for 5 min at 25 °C followed by 60 min at 42 °C. The reaction was terminated by heating at 70 °C for 5 min. The cDNA was used directly for qPCR or stored at - 80 °C for long-term storage.

2.16 quantitative PCR (qPCR)

qPCR was performed on a LightCycler 480 System (Roche) using KAPA SYBR FAST (Peqlab). Standard curves for each amplified transcript were generated to obtain the PCR efficiency. C_T values were determined by the LightCycler® Software 480 (Roche) using the following protocol:

program name	cycles	analysis mode
pre-Incubation	1	none
amplification	45	quantification
melting curve	1	melting curves

target (°C)	acquisition mode	hold (hh:mm:ss)	ramp rate (°C/s)	acquisitions (per °C)
pre-incubation				
95	none	00:05:00	4.8	–
amplification				
95	none	00:00:10	4.8	–
primer dependent	none	00:00:10	2.5	–
72	single	00:00:15	4.8	–
melting curve				
95	none	00:00:05		–
65	none	00:01:00		–
98	continuous	–	–	5 – 10

Table 2. Parameters for RT-qPCR.

Expression levels of each sample were detected in duplicate reactions. Three different biological samples were analyzed in duplicates and normalized to the expression of the housekeeping gene aminolevulinic acid synthase (ALAS). Relative quantification was determined by the method described by Pfaffl (2002). The data were presented as mean \pm SEM.

2.17 Retina preparation

The mice were euthanized and to track the orientation of the retina until cryosectioning a temporal mark was placed on the eyeball using a glowing needle. The eyes were removed and pierced at the ora serrata using a cannula (21G, Sterican, B. Braun) and prefixed using 4% PFA (paraformaldehyde) for 5 min on ice. Next, the cornea was opened using a micro-eye spring scissor (Mini Vanas, blade 3 mm, Frohnhäuser) under a dissecting/stereoscopic microscope (Stemi 2000, Zeiss). The burnt-in mark placed on the ora serrata was restored by placing a small incision into the retina. Subsequently, cornea, lens and vitreous body were dislodged. Subsequently, the eyecup was fixed for 45 min in 4 % PFA on ice. Next, the eyecup was washed thrice in 0.1 M PB and dehydrated overnight in 30 % sucrose for cryopreservation. Finally, the eyecup was embedded in tissue freezing medium (Electron Microscopy Sciences), frozen on dry ice and stored at - 80 °C until use.

0,1 M PB

Na ₂ HPO ₄ x 2 H ₂ O	28.48 g
NaH ₂ PO ₄ x H ₂ O	5.52 g
H ₂ O	ad 2 l

pH 7.4, stored at 4 °C.

4% PFA (in PB)

Paraformaldehyd (Merck)	6 g
0.1 M PB	ad 150 ml

dissolved at 60 °C and sterile filtered using a 25mm syringe filter (VWR). Aliquots were stored at – 20 °C.

30% sucrose solution (in PB)

sucrose	30 g
0.1 M PB	70 ml
0.1 M PB	ad 100 ml

sterile filtered using a 25mm syringe filter (VWR) and stored at - 20 °C.

2.18 Retinal cryosections

Retinal cryosections were prepared using the embedded eyecups in tissue freezing medium. Using a kryostat (Leica CM3050 S, Leica Biosystems) the embedded tissue was sliced to 10 µm cryosections and mounted on glass object slides (SuperFrost Plus, Menzel). The cryosections were dried at room temperature and stored at - 20 °C.

2.19 Immunohistochemistry

Coronal retinal cryosections (12 µm) from 2 and 3 week old C57-BL6/N mice were rehydrated in sterile 0.1 M phosphate buffered (PB) and fixed for 10min with 4 % paraformaldehyde (PFA) in 0.1 M PB, pH 7.4. Cryosections were treated with 2N HCl in

0.1 M PB for 20 min and incubated for 1.50 h at room temperature (RT) or overnight at 4 °C with primary antibodies in 5 % chemiblocker (Millipore) and 0.3 % Triton X-100 in sterile 0.1 M PB. The cryosections were subsequently washed 3 times with 0.1 M PB.

The following primary antibodies were used (catalogue number and working dilutions in brackets):

polyclonal rabbit anti-5hmC (Active Motif, #39769, 1:1000)

monoclonal mouse anti-5mC (Diagenode, #BI-MECY-0100; 1:1000).

For 5hmC depletion experiment the anti-hmC staining signal was competed out by 2mM hmC-DNA oligonucleotides.

The following secondary antibodies were used (catalogue number and working dilutions in brackets):

Alexa488 anti-rabbit (1:800, Cell Signaling Technologies)

Cy3 anti-mouse (1:400, Jackson ImmunoResearch)

Cell nuclei were counterstained with Hoechst 33342 (5 µg/mL, Invitrogen) and sections were mounted with aqueous mounting medium (PermaFluor, Beckman-Coulter). Tissues were analyzed using a Zeiss Axioscope epifluorescence microscope equipped with a HBO 100 mercury arc lamp, appropriate filters equipped with an MRc ccd camera (Zeiss). Laser scanning confocal micrographs were collected using a Leica SP8 microscope (Leica).

2.20 Proximity ligation assay

Proximity ligation assay (PLA) was performed using Duolink In Situ Orange Starter Kit Mouse/Rabbit (Sigma-Aldrich) according to the manufacturer's manual (Figure 13). HEK293T cells or retinal slices were fixed and permeabilized as described in the immunofluorescence studies. Subsequently, the samples were incubated with the supplied blocking solution for 10 min (retinal slices) or 30 min (cells) at room temperature. After washing, the cells were incubated with mouse and rabbit primary antibodies over night at

4 °C. Next, the samples were washed three times in 0.1 M phosphate buffer and incubated with the PLUS and MINUS PLA probes in a humid chamber for one hour at 37 °C. Subsequently, samples were washed two times in Buffer A (supplied). Ligation was performed at 37 °C for 30 min followed by washing in Buffer A. Amplification was performed for 100 min at 37 °C. After washing with Buffer B the samples were stained with Hoechst, washed again and mounted using PermaFluor Aqueous Mounting Medium (Thermo Scientific). Fluorescence signal intensity was normalized to background fluorescence levels of control PLA stainings incubated without primary antibody. The average of signals/nuclei in at least 20 cells from at least two independent experiments was reported in the graphics.

We used the following primary antibodies (working dilutions in brackets):

mouse monoclonal anti-5hmC (Active Motif, #40000, 1:1,000)

mouse monoclonal anti-5mC (Diagenode, #BI-MECY-0100; 1:1000)

rabbit polyclonal anti-REST (#095, kindly provided by Gail Mandel, Oregon Health & Science University, 1:500)

rabbit polyclonal anti-H3K36me3 (Active Motif, # 61102, 1:1000).

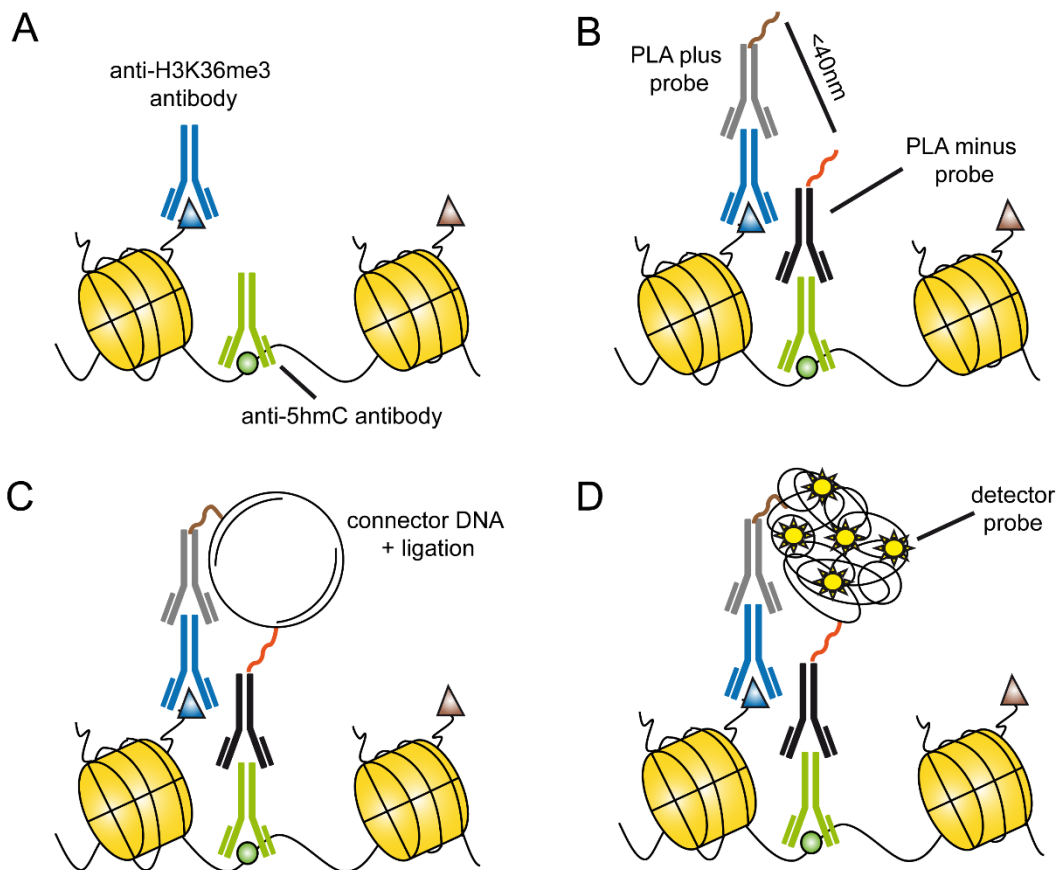


Figure 13. Schematic workflow of PLA experiment.

(A) The cryosections are incubated with two primary antibodies from different species (e.g. anti-5hmC and anti-H3K36me3). (B) Plus and minus PLA probes (secondary antibodies) are added. The attached DNA strands can interact by subsequent hybridization of two connector DNA oligonucleotides, if the secondary antibodies are in close proximity ($<40\text{ nm}$) (C) The two oligonucleotides are ligated enzymatically and amplified by a polymerase in a rolling circle amplification reaction. (D) The amplified DNA circles are hybridized with detector probes.

2.21 Nuclear extract preparation

Cell lysis of retina tissue samples was performed according to the Sigma Aldrich protocol for detergent free nuclear protein extraction (<http://www.sigmaaldrich.com/technical-documents/protocols/biology/nuclear-protein-extraction.html>). In brief, for each experiment 50 - 150 mg retinal tissue was lysed. The following procedure was optimized for extraction of nuclear proteins from 100 mg of tissue. A fresh solution of 0.1 M DTT with ultrapure sterile water, a hypotonic lysis buffer and an extraction buffer was prepared:

lysis buffer (hypotonic)

HEPES, pH 7.9	10 mM
MgCl ₂	1.5 mM
KCl	10 mM

14 µl of 0.1 M DTT solution and 14 µl of the Protease Inhibitor Cocktail (PIC; Active Motif) were added to 1.4 ml of lysis buffer.

extraction buffer

HEPES, pH 7.9	20 mM
MgCl ₂	1.5 mM
NaCl	0.42 M
EDTA	0.2 mM
glycerol	25 % (v/v)

1.5 µL of 0.1 M DTT solution and 1.5 µl of the protease inhibitor cocktail were added to 147 µl of the extraction buffer.

The tissue was rinsed twice with 0.1 M PB buffer and the supernatant was discarded. The tissue was resuspended in 1 ml lysis buffer and homogenized using mortar and pestle until more than 90 % of the cells were broken and nuclei were visualized under the microscope. The disrupted cells were centrifuged for 20 min at 10.000 x g in a microcentrifuge (Fresco 17 microcentrifuge, Thermo Scientific) and the supernatant was transferred to a fresh tube. This fraction was the cytoplasmic fraction. The crude nuclei pellet was resuspended in 140 µl extraction buffer. The samples were shaken gently for 30 min and subsequently centrifuged for 5 min at 21.000 x g. Samples were stored at – 80 °C for long-term storage.

To assess the protein concentration of the lysates, a Bradford protein assay (Thermo Scientific) was performed according to the manufacturer's instructions. Nuclear extracts for label-free quantification (LFQ) were additionally treated with 25 U benzonase for 30 min on ice. Protein samples for mass spectrometric analysis were reduced by adding 100 mM tris-2-carboxyethyl)phosphine (TCEP) (Sigma) and by incubating on a shaker (Thermo-mixer Compact, Eppendorf) at 650 rpm for 1 h at 60 °C and subsequently alkylated with 200 mM iodoacetamide (Sigma) in the dark for 30 min at 25 °C. Protein samples were

digested with 0.5 μg trypsin (Promega) for 16 h at 37 °C. The reaction was stopped using 1 mM phenylmethylsulphonylfluoride (Sigma). StageTips (Thermo Scientific) were used to purify LFQ samples as described in (Kulak et al., 2014).

2.22 Co-immunoprecipitation (Co-IP)

Immunoprecipitations were performed using Protein G Dynabeads (Invitrogen) according to manufacturer's manual. Briefly, nuclear protein extracts were prepared without the use of detergents as described in chapter 2.21. 100 μl beads were added in a 1.5 ml Eppendorf tube together with a primary antibody.

The following primary antibodies were used (source, catalogue number and working dilutions in brackets):

rabbit polyclonal anti-TET3 (Abiocode, #AC-R1092-1 1:25)

polyclonal rabbit anti-REST (#095, kindly provided by Gail Mandel, Oregon Health & Science University, 1:25)

rabbit polyclonal anti-GFP (Clonetechn, #632377; 1:20)

Next, the volume was adjusted to 500 μl using 0.1 M PBS and incubated for 30 min at 4 °C under rotation. 25 μl of BS3 solution (Life Technologies) (5.7 mg BS3 in 100 μl ddH₂O) was added to each sample and incubated for 30 min at RT under constant rotation. The excess crosslinker was inactivated by adding 25 μl 1M Tris buffer pH 7.5 and incubating for 15 min at RT under rotation. After short centrifugation the tubes were placed on a magnet rack for precipitation and the supernatant was discarded. The beads were washed twice with 300 μl 1 M PBS solution. Subsequently, 500 μg protein lysate was added to the beads and incubated for 60 min at 4 °C under rotation. The supernatant was discarded and the beads were washed 5 times with 300 μl 1M PBS solution. Proteins were eluted twice from beads using 30 μl citrate solution (0.1 M citrate, pH 2-3 (pH 2.2 used). Protein concentration of the samples before and after immune precipitation was measured using a Bradford protein assay. From each sample 50 μg protein were digested using trypsin and labeled with TMT 2-plex reagents to quantify changes in the protein composition of the samples. After labeling, the volume of the peptide samples was reduced to 5

μl in a vacuum centrifuge and filled up with 50 μl H_2O containing 0.1 % formic acid. Samples were subsequently purified using reverse phase sulfonate (SDB-RPS) stage tips and processed according to (Kulak et al., 2014).

2.23 Protein isolation for GFP-immunoprecipitation

Retinal explant cultures from 11-day-old mice were transduced with LV-CMV-TET3 Δ CXXC-eGFP or LV-CMV-eGFP and harvested after 12 days in vitro. Immunoprecipitation of nuclear extracts were performed using a GFP-Trap (Chromotek) under detergent free conditions. GFP Trap beads were equilibrated in dilution buffer. 30 μl of the bead slurry was resuspended in 500 μl ice cold dilution buffer. Nuclear protein lysates (see chapter 2.13) were added to the equilibrated GFP-Trap and incubated with gentle end-over-end mixing for 2 h at 4 °C. Samples were centrifuged at 2.000 x g for 2 min at 4 °C in a microcentrifuge (Fresco 17, Thermo Scientific) and the supernatant was stored as negative control. The pellet was washed twice with 500 μl ice cold wash buffer and proteins were eluted by adding 50 μl 0.1 M glycine pH 2.5 (incubation time: 2 min) followed by neutralization with 5 μl 1 M Tris-base.

dilution buffer

10 mM Tris/Cl pH 7.5
150 mM NaCl
0.5 mM EDTA

wash buffer

10 mM Tris/Cl pH 7.5
150 mM NaCl
0.5 mM EDTA

2.24 TMT-labeling for protein quantification

For the TMT-based quantification, peptide labeling with the TMT 2-plex reagents (Thermo Scientific) was performed after tryptic digestion according to the manufacturer's instructions. TMT 2-plex reagents (126 and 127) were used to label the samples.

When the sample was labeled with TMT 126 the control sample was labeled with the TMT 127 reagent and vice versa. Subsequent to the labeling, both sample and control, were combined. This way each experiment was performed twice as a so-called label swap experiment. Organic solvent was removed by vacuum centrifugation and the sample was finally reconstituted in 1 % formic acid for mass spectrometric analysis. TMT labelling and LC-MS analysis was conducted by Dr. David Eisen (Carell group, LMU Munich).

2.25 Acid extraction of histones

To examine histone modifications of histone 3 (H3), we followed a protocol from Shechter et al. (Shechter et al., 2007). 100 mg of cells (retinal cells or HEK293T cells) were lysed in 1 ml hypotonic buffer.

hypotonic buffer

10 mM Tris-HCl pH 8.0

1 mM KCl

1.5 mM MgCl₂ / 1 mM DTT

Subsequently, samples were incubated for 30 min under rotation at 4 °C to promote hypotonic swelling of cells and lysis by mechanical shearing during rotation. The intact nuclei were centrifuged at 10.000 x g (Fresco 17, Thermo Scientific) for 10 min at 4 °C. The supernatant was discarded and the nuclei were resuspended in 400 µl 0.4 N H₂SO₄ and incubated under rotation for 30 min. It is important that nuclei were fully resuspended with no clumps left in solution. Thus, the solution was vortexed until clumps were dissolved. The nuclear debris was removed by centrifugation at 16.000 x g for 10 min at 4 °C using a table top centrifuge (Fresco 17, Thermo Scientific). The supernatant containing histones was transferred to a new 1.5 ml Eppendorf tube (Eppendorf). Next, 132 µl trichloroacetic acid (TCA) was added drop-wise to the sample and inverted several times. The samples were incubated for 30 min on ice to precipitate histones. Histones were pelleted by 16.000 x g for 10 min at 4 °C and washed with 400 µl acetone without disturbing the pellet to remove remaining acid from the solution. Acetone was used to remove acid from the solution without dissolving the protein pellet. The sample was spun for 5 min at 16.000 x g at 4 °C in a table top centrifuge. Next, 400 µl acetone were added again and

the samples were centrifuged for 5 min at 16.000 x g at 4 °C. The supernatant is carefully removed by pipetting and the histone pellet was air-dried for 20 min at room temperature. The pellets were solubilized using 100 µl of ddH₂O and 6 µl of Laemmli DTT (6x Laemmli DTT) was added. Subsequently, the samples were heat denatured at 95°C for 5 min and stored at - 20 °C until use.

6x Laemmli DTT

4x Tris-HCl/SDS pH 6.8	7 ml
Glycerol	3 ml
SDS	1 g
bromphenol blue	1.2 mg
DTT	930 mg
ddH ₂ O	ad 10 ml

2.26 Quantification of histone modifications

For the quantification of the total levels of H3K36me3 in retinal cells the TMT 2-plex reagents (Thermo Scientific) was used. For the quantification of H3K36me3 in HEK293T cells the TMT 6-plex reagents (126, 127, 128 and 129, Thermo Scientific) were used to label the samples. The samples obtained from chapter 2.24 were loaded on a 10 % SDS PAGE and separated at 100V in a electrophorese chamber (Protean 3, Biorad). The gel was stained in a coomassie (Applichem) solution for 1 h and destained overnight in coomassie destaining solution.

stacking gel buffer

Tris-HCl	0.5 M
SDS	0.4 %
pH	6.8

separating gel buffer

Tris-HCl	1.5 M
SDS	0.4 %
pH	8.8

stacking gel

10 % separating gel

30 % acrylamide/		30 % acrylamide/	
0.8 % bisacrylamide	0.65 ml	0.8 % bisacrylamide	5.0 ml
stacking gel buffer	1.25 ml	separating gel buffer	3.75 ml
ddH ₂ O	3.05 ml	ddH ₂ O	6.25 ml
20 % ammonium persulfate	25 µl	20 % ammonium persulfate	30 µl
tetramethylethylenediamine	5 µl	tetramethylethylenediamine	10 µl

coomassie staining solution

Coomassie blue R250	1 g
methanol	45 %
acetic acid 100 %	10 %
ddH ₂ O	ad 1000 ml

coomassie destaining solution

methanol	10 %
acetic acid 100 %	10 %
ddH ₂ O	ad 1000 ml

Next, the visible protein band of histone H3 was cut out. The protein was in-gel alkylated and tryptically digested (Shevchenko et al., 2006). Trypsin activity was stopped using 1 mM PMSF (Sigma) and the peptides were TMT-labeled according to manufacturer's protocol (Thermo Scientific). Post-labeled samples of each experiment were pooled together and analyzed via LC-MS/MS. The relative reporter ion intensities of the trimethylated H3K36 peptide (SAPATGGVK(me3)KPHR) were normalized to the relative quantities of the whole protein. Finally, the fold change of the trimethylated peptides was calculated in relation to each control sample.

2.27 Bioinformatics

Sequence reads (read length = 100) of 5hmC containing DNA fragments were mapped onto the reference mouse genome (NCBI Build UCSC mm9) using the Bowtie (v0.12.7) algorithm. Peak-calling was performed using MACS Version 1.4 (<http://liulab.dfci.harvard.edu/MACS/>). Unique and monoclonal reads were used for further analysis. Minimum criteria for peaks was 4 reads and peaks had to overlap within the replicates. Overlapping peaks in all samples were defined as conserved peaks. If peaks only overlapped

at postnatal week 2, they were considered as lost peaks. If peaks only overlapped at postnatal week 3, they were considered as gained peaks. Refseq genes were downloaded from the UCSC mm9 annotation database (UCSC Genome Browser, Santa Cruz, CA). Gene ontology analyses on differentially hydroxymethylated regions were performed using Ingenuity (IPA, Ingenuity Systems, www.ingenuity.com).

The MaxQuant software (version 1.5.0.25) was used for LFQ. Quantification was performed with four biological replicates of the retinal tissue samples and biological triplicates of the transfected HEK293T cells. In the overexpressing HEK293T experiments HEK293T cells transfected with GFP served as control. The Andromeda search engine was used in combination with uniprot databases (mus musculus for the retinal full proteome analysis and homo sapiens for the overexpression analysis respectively). A maximum of two missed cleavage sites was allowed. The main search peptide tolerance was set to 10 ppm. Carbamidomethyl (C) was set as static modification. Variable modifications were Acetyl (Protein N-term) and Oxidation (M). Data of the cytoplasm and nucleus samples from the transfected HEK293T cells were analyzed as two different fractions of one experiment. The fast LFQ algorithm was applied with default settings. LFQ data was analyzed with the Perseus software (version 1.5.0.9). The LFQ intensities were log transformed and only proteins identified in at least three of the retinal tissue samples or in at least two of the transfected HEK293T lysates were retained. LFQ Proteomics and MaxQuant Analysis was performed by Andrea Künzel (Carell group, LMU Munich).

2.28 Statistics

All values are given as mean \pm standard error of the mean (S.E.M) or mean \pm standard deviation (SD) and n is the number of experiments. An unpaired Student's t-test was performed for the comparison between two groups. Values of $p < 0.05$ were considered as significant. Fisher's exact-test was applied to analyze significance of contingency tables.

3. Results

3.1 Transcriptional changes during retinal maturation

First, transcriptional changes during retinal maturation were investigated. Retinal protein levels of 2-week-old mouse retina (eye opening) and 3-week-old mouse retina (mature state) were isolated and quantified using label-free quantification (LFQ) (Figure 14A). The volcano plot shows all the proteins identified with this approach. Proteins that showed significantly lower expression at week 3 compared to week 2 are marked in black, whereas upregulated proteins are marked in blue. Proteins with no significant change in expression are marked in grey (Figure 14A). Interestingly, gene ontology (GO) analysis using the Database for Annotation, Visualization and Integrated Discovery (DAVID) (<http://david.abcc.ncifcrf.gov/>) reveals that a significant amount of upregulated proteins were involved in synaptic functions, detection of light stimulus and phototransduction (Figure 14B), suggesting that major transcriptional changes occur during retinal maturation.

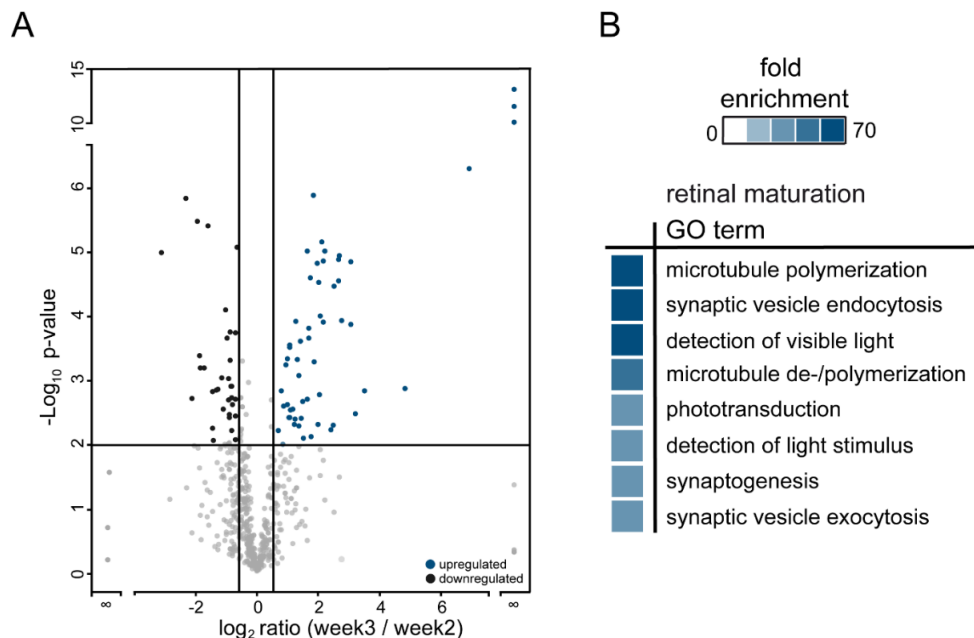


Figure 14. Transcriptional changes during retinal maturation.

(A) Volcano plot of protein expression ratios between week 2 and week 3 in the mouse retina as a function of statistical significance (Student t-test p value ≤ 0.01). Proteins with no detectable signal in one of the subsets were assigned a ratio of infinity. (B) Gene ontology (GO) analysis of upregulated proteins during retinal maturation (from eye opening at week 2 to terminal maturation of the retina at week 3) identified by label free quantification (LFQ) proteomics.

3.2 Epigenetic changes during retinal maturation

To study whether these transcriptional changes during retinal maturation are due to differential DNA modification, global levels of 5-methylcytosine (5mC) and its oxidative derivatives 5-hydroxymethylcytosine (5hmC), 5-formylcytosine (5fC) and 5-carboxycytosine (5caC) were quantified using high performance liquid chromatography coupled to tandem mass spectrometry (HPLC-MS/MS). 5mC levels remained stable during retinal maturation (p -value > 0.05 , t-test) (Figure 15A). In contrast, the levels of 5hmC were significantly accumulating from week 2 to week 3 suggesting that 5hmC might be an important DNA modification during retinal maturation (p -value < 0.01 , t-test) (Figure 15B). Interestingly, the levels of 5fC dropped significantly during the respective time points (p -value < 0.001 , t-test) (Figure 15C). Notably, 5caC was not detectable in both stages of retinal maturation, suggesting that either 5caC is a short-lived oxidative intermediate or not generated during retinal maturation.

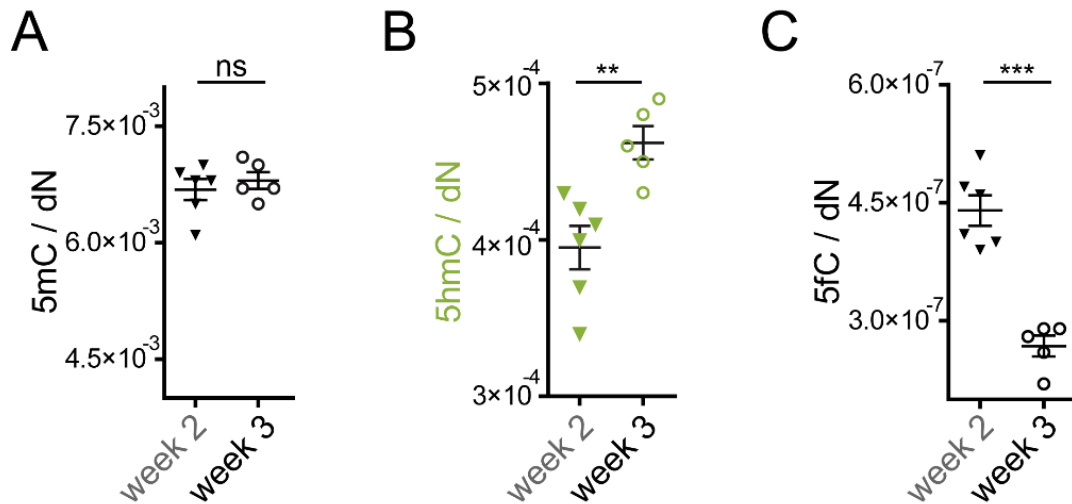


Figure 15. Cytosine derivative levels during retinal maturation.

Scatterplots of HPLC-MS/MS quantification of global (A) 5-methylcytosine (5mC), (B) 5-hydroxymethylcytosine (5hmC) and (C) 5-formylcytosine (5fC) in the mouse retina at week 2 and 3 reveal an age-dependent increase in 5hmC levels, stable 5mC levels and decreasing 5fC levels. Summary data are mean \pm SEM. ** $p < 0.01$, *** $p < 0.001$ (Student's t-test).

3.3 Dynamics of 5hmC localization

To study the localization of 5hmC during retinal maturation, a 5hmC-specific antibody was used for immunohistochemical studies on retinal cryosections. At eye opening (week 2), the strongest 5hmC signal was observed in retinal ganglion cells that are present in the ganglion cell layer (GCL). Moreover, high 5hmC levels were present in the inner nuclear layer (INL) that is composed of the nuclei of amacrine cells, bipolar cells and horizontal cells. In contrast, the nuclei of rod and cone photoreceptor cells that exist in the outer nuclear layer (ONL) and are responsible for the detection of light stimuli were only faintly stained or immuno-negative (Figure 16A).

In comparison to eye opening a stronger 5hmC immunosignal was observed in the ganglion cell layer and the inner nuclear layers of mature retina (week 3) (Figure 16B). Notably, cone and rod photoreceptors were also positive for 5hmC in the mature retina (Figure 16B), revealing dynamic 5hmC accumulation in the nuclei of photoreceptors during terminal photoreceptor differentiation. To confirm the specificity of the 5hmC antibody the immunosignal was quantitatively depleted using 2.5 μ M 5hmC-containing DNA oligonucleotides (inlay in Figure 16B).

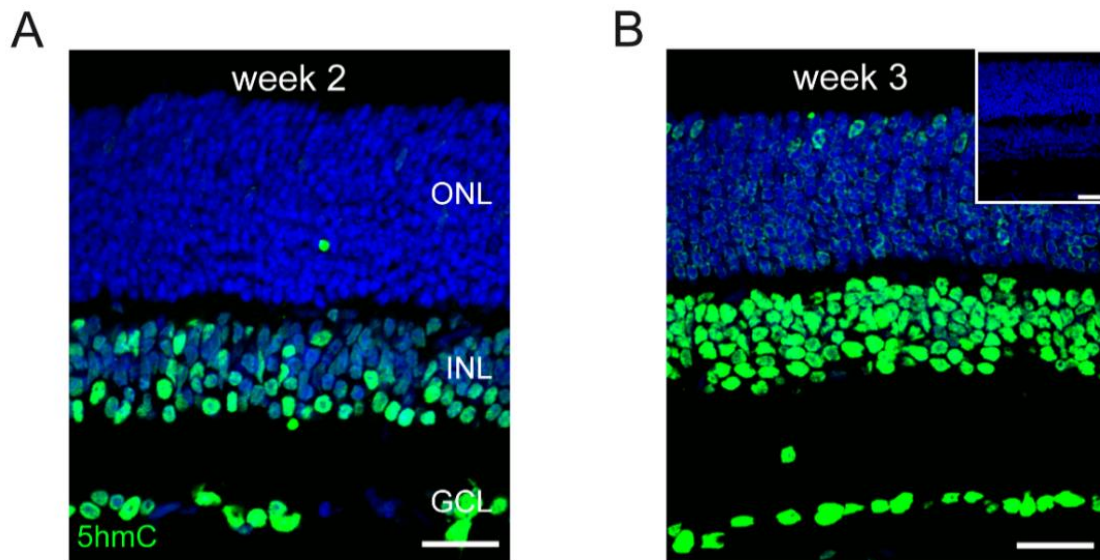


Figure 16. Immunosignal of 5hmC during retinal maturation.

(A-B) Confocal scans from mouse retinal slices at week 2 (A) and week 3 (B) immunolabeled for 5hmC (green). There is a marked increase in 5hmC signal in nuclei of all retinal layers from week 2 to 3, in particular in photoreceptors (outer nuclear layer, ONL). The inlay image in (B) is from a depletion experiment proving the specificity of the anti-5hmC antibody. Scale bar marks 25 μ m. In collaboration with Dr. Susanne Koch.

3.4 Subnuclear localization of 5hmC

In conventional nuclei, present in most eukaryotic cells, heterochromatin (inactive chromatin) is located at the nuclear periphery and euchromatin (active chromatin) is present towards the nuclear interior. Interestingly it was shown that the nuclei of rods in nocturnal retinas *e.g.* mouse retina remodel from a conventional nucleus to a unique inverted nuclear architecture, in which heterochromatin is localized in the nuclear center and euchromatin is present in the nuclear border during retinal maturation (Figures 17A) (Solovei et al. 2009).

To gain insights in the potential epigenetic functions of 5hmC the subnuclear localization of 5hmC was studied during retinal maturation by costaining with heterochromatin associated 5mC. Notably, 5hmC was predominantly present in euchromatic regions in conventional nuclei as well as inverted rod nuclei. In contrast, 5mC was concentrated in pericentromeric heterochromatin (Figures 17B). This suggests that 5hmC could be implicated in transcriptional activation of previously methylated and therefore transcriptionally repressed genes.

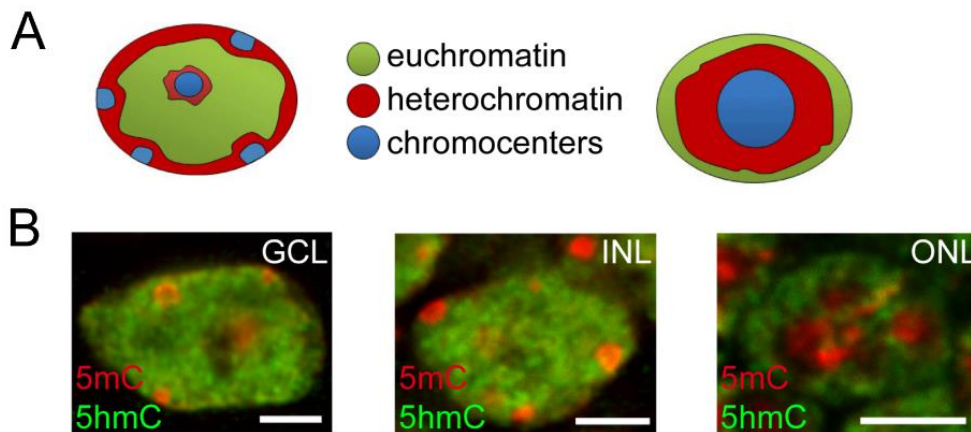


Figure 17. Subnuclear localization of 5mC and 5hmC.

(A) Schematic view of conventional and inverted nuclei depicting heterochromatin and euchromatin regions. (B) High magnification images of conventional nuclei within the ganglion cell layer (GCL) or the inner nuclear layer (INL) and a rod nucleus with inverted nuclear architecture (Solovei et al., 2009) co-immunolabeled with 5hmC (green) and 5mC (red). In all cases 5hmC is mainly found in euchromatin whereas 5mC is localized in heterochromatic regions. Scale bar in B marks 3 μm .

3.5 [methyl- $^{13}\text{CD}_3$]-L-methionine feeding

Due to the fact that 5hmC is not co-localizing with its predecessor 5mC, two possibilities are imaginable. First pre-existing 5mC present in heterochromatin could be oxidized by Tet enzymes to *de novo* 5hmC leading to chromatin remodeling by recruitment of chromatin remodeling enzymes or repulsion of heterochromatin associated proteins that interact with 5mC. Alternatively, *de novo* 5hmC could be generated from *de novo* methylation that occurs in euchromatic regions. To test those two hypotheses, the dynamics of 5hmC and 5mC generation during retinal maturation were investigated. Therefore, an isotope tracing experiment was performed by culturing retinal explants from 11-day-old mice in [methyl- $^{13}\text{CD}_3$]-L-methionine containing medium. The labeled methyl group donor [$^{13}\text{CD}_3$]-L-methionine is utilized by DNA methyltransferases for 5mC formation giving rise to labeled 5mC (5- $^{13}\text{CD}_3$ -mC) and 5hmC (5- $^{13}\text{CD}_2$ -hmC) (Pfaffeneder et al., 2014). After culturing for three, six and nine days the retinal cultures were harvested, the DNA was isolated and labeled 5mC and 5hmC was quantified using HPLC-MS/MS. Confirming the presence of *de novo* methylation in non-dividing retinal cells 5- $^{13}\text{CD}_3$ -mC was detected at linearly increasing levels (slope: 0.531, $R^2=0.999$) reaching a value of 3.9 % of total 5mC after nine days of [$^{13}\text{CD}_3$]-methionine feeding (Figure 18A). [$^{13}\text{CD}_2$]-labeled 5hmC was also detected (Figure 18B). However, the level of 5- $^{13}\text{CD}_2$ -hmC was low with only up to 1.6 % after nine days (slope: 0.208, $R^2=0.997$). Notably, the amount of labeled 5- $^{13}\text{CD}_2$ -hmC derived from nascent (labeled) 5mC accounted for 14-15 % of total *de novo* 5hmC whereas the unlabeled 5hmC generated from pre-existing (unlabeled) 5mC corresponded to 85-86 % of total *de novo* 5hmC. Thus, the majority of *de novo* 5hmC was generated from pre-existing and hence unlabeled 5mC (Figure 18C).

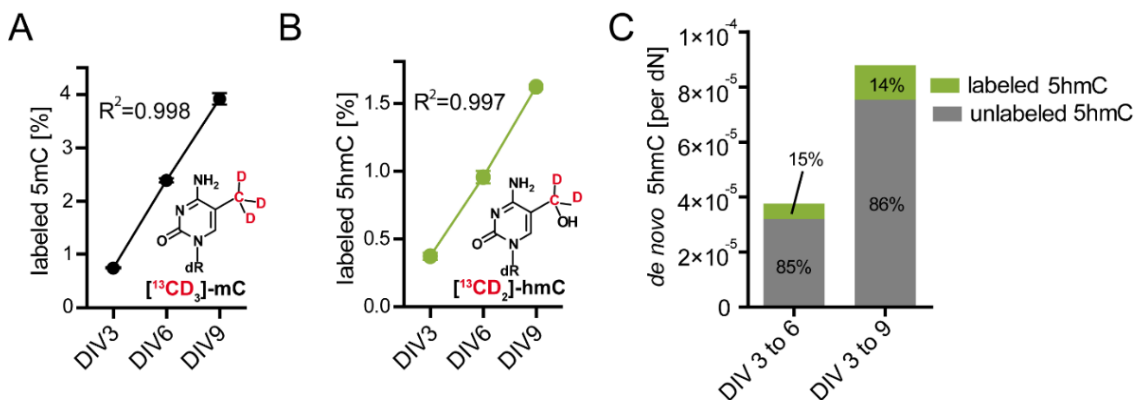


Figure 18. Isotope tracing in mouse retinal explant cultures.

Retinal explant cultures were fed with [methyl- $^{13}\text{CD}_3$]-L-methionine and harvested for HPLC-MS/MS quantification of labeled 5mC (A) and 5hmC (B) after 3, 6 and 9 days *in vitro* (DIV). (C) Stacked bar graph showing HPLC-MS/MS quantification of the absolute levels of 5hmC. Summary data in A and B are mean \pm SD.

3.6 Dnmt Expression levels

Next, the dynamics of Dnmt expression levels was studied using reverse-transcription quantitative PCR (RT-qPCR) during retinal development. Interestingly, the levels of Dnmt1 dropped significantly from postnatal day 2 (p2) to later developmental stages and were lowest during retinal maturation (p13 to p20) (Figure 19A). Dnmt3b showed low expression levels relative to ESC and the showed lowest expression during retinal maturation (Figure 19B). In contrast Dnmt3a showed increased expression levels compared to ESC and showed highest expression during retinal maturation (Figure 19C). This data suggests that Dnmt3a could be mainly involved in *de novo* methylation during retinal maturation.

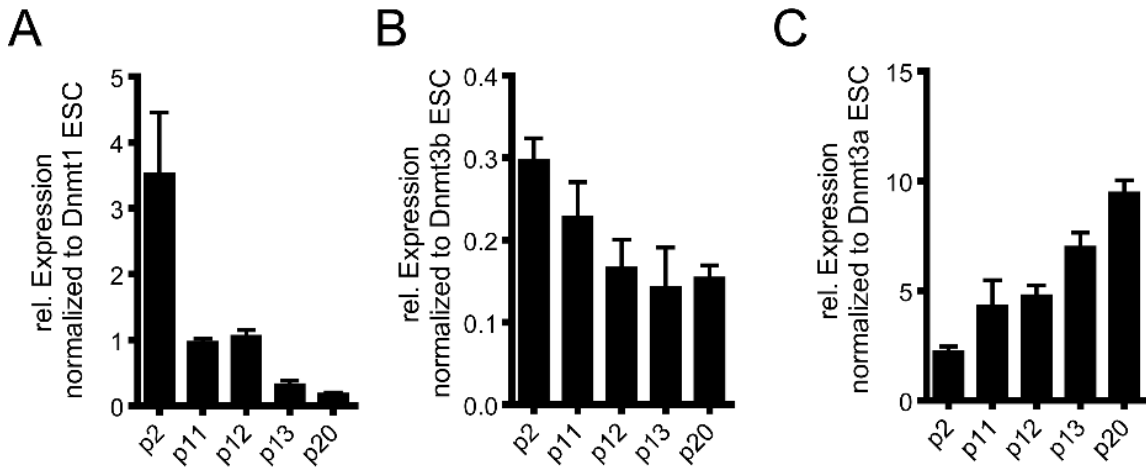


Figure 19. Time course of Dnmt expression levels.

(A-C) RT-qPCR analysis of Dnmt1 (A), Dnmt3b (B) and Dnmt3a (C) gene expression in mouse retina at postnatal day (p) 2, 11, 12, 13 and 20 normalized to corresponding mouse embryonic stem cell (ESC) levels. Summary data are mean \pm SEM.

3.7 Genomic distribution of 5hmC during retinal maturation

To further investigate the genomic localization and dynamics of 5hmC during retinal maturation an antibody-based 5hmC DNA immunoprecipitation (hMeDIP) from 2- and 3-week-old retina was performed followed by next-generation sequencing (NGS). This method allows mapping of 5hmC signal precisely to inter- or intragenic regions and detection of differential 5hmC patterns during retinal maturation.

In line with the immunohistochemical and HPLC-MS/MS quantification data higher levels of 5hmC were detected at week 3 in comparison to week 2. Furthermore, the data revealed a dynamic change of 5hmC during retinal maturation. The hMeDIP data displayed an increase of 5hmC signal, mostly in intragenic regions, especially at promoters and gene bodies (Figure 20A). Next, the genes strongly enriched with intragenic 5hmC were studied. Interestingly, 5921 intragenic regions gained 5hmC, whereas 22 times less intragenic regions were detected with lost 5hmC signal and 511 regions conserved in their 5hmC levels (Figure 20B).

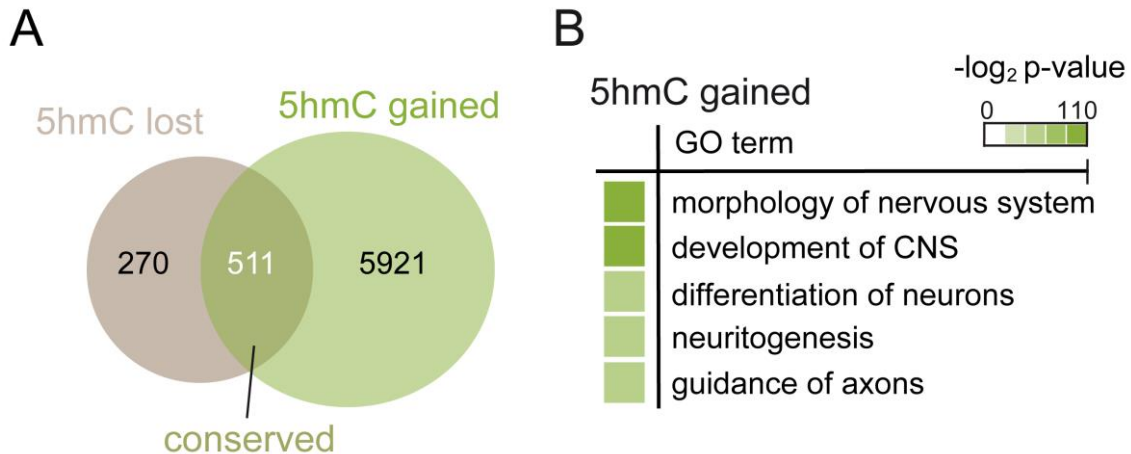


Figure 20. Differentially hydroxymethylated regions during retinal maturation.

(A) Venn diagram showing 5hmC dynamics during retinal maturation (postnatal week 3 / postnatal week 2). (B) Gene ontology analysis of genes gained that 5hmC during retinal maturation.

Gene ontology (GO) analysis revealed that genes involved in the morphology of the nervous system, CNS development, differentiation of neurons, neuritogenesis or guidance of axons are significantly enriched within the group of genes that gained 5hmC after eye opening (from week 2 to 3) (Figure 21A). Correlation of the hMeDIP data with the LFQ

protein expression data showed a positive correlation of accumulation of 5hmC in genes with increased protein expression of the corresponding genes (p value < 0.005 , t-test) (Figure 21B), suggesting a regulatory function of 5hmC in gene expression.

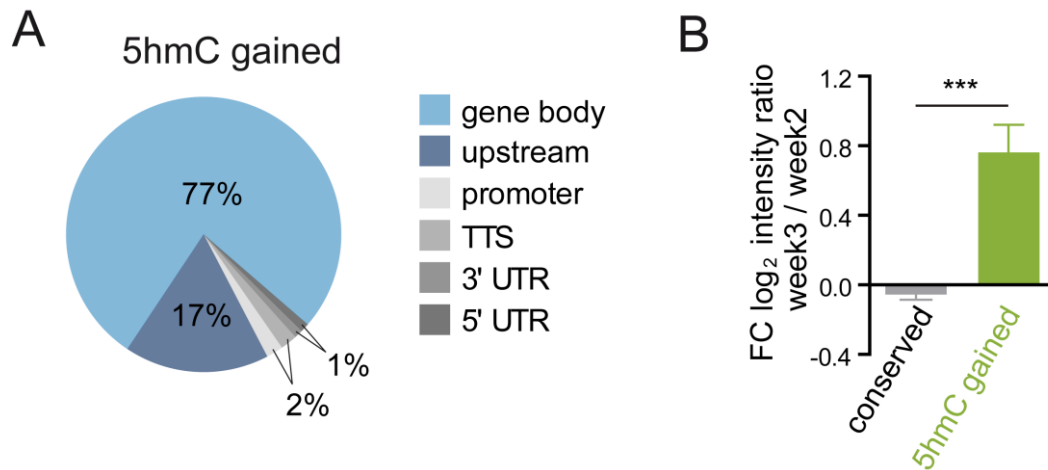


Figure 21. Genomic localization of 5hmC and its effect on gene expression.

(A) Pie chart showing intragenic distribution of 5hmC regions in mature retina. (B) Label free quantification (LFQ) of proteins encoded by genes with conserved (grey) or gained 5hmC levels (green) during retinal maturation. Summary data are mean \pm standard error of mean (SEM). *** $p < 0.001$ (Student's t-test). TSS, transcription starting site; TTS, transcription termination site; UTR, untranslated region.

3.8 Tet expression levels during retinal maturation

Next, the transcriptional levels of Tet enzymes during retinal maturation were studied using RT-qPCR. Tet3 was the major isoform in the retina at every time point and showed up to 14-18 fold higher levels of expression from postnatal day 13 (p13) to postnatal day 20 (p20) in comparison to Tet1. Importantly, the expression levels of Tet3 at eye opening (p13) and at the mature stage (p20) were comparable, ruling out that increased Tet expression causes the observed increase in 5hmC levels (Figure 22A).

A recent study showed that TET3 exists in three isoforms that differ in their N-terminal sequence; two isoforms with a CXXC DNA-binding domain and a short isoform enriched

in neuronal cells lacking the CXXC domain (Liu et al., 2013a). Using isoform-specific primer sets the short variant lacking the CXXC domain was found to be the major Tet3 isoform in the retina (Figure 22B).

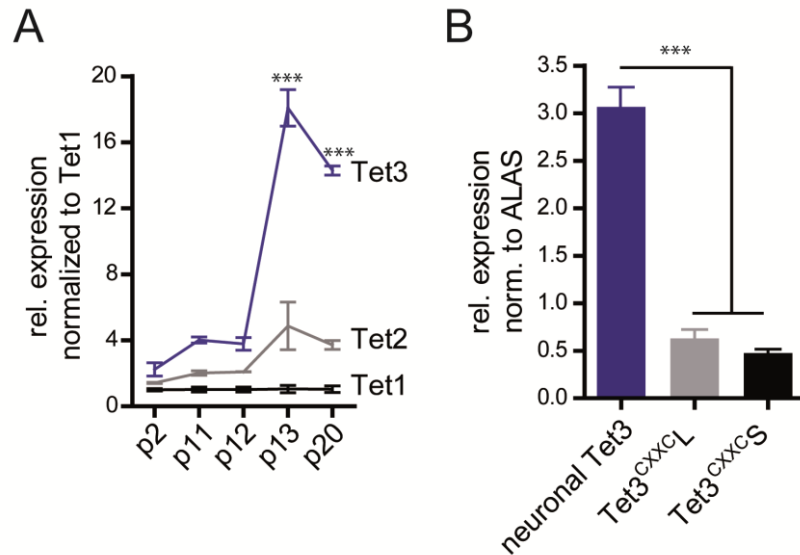


Figure 22. Tet expression levels during retinal maturation.

(A) RT-qPCR analysis of Tet1, Tet2 and Tet3 gene expression in mouse retina at postnatal day (p) 2, 11, 12, 13 and 20 normalized to corresponding Tet1 levels. Tet3 is significantly higher expressed than Tet1 and Tet2 at p13 and p20. (B) RT-qPCR analysis of Tet3 isoforms. Tet3 lacking a CXXC DNA binding domain (neuronal Tet3) is the main isoform in retina. Summary data are mean \pm SEM. *** $p < 0.001$ (1-way ANOVA).

3.9 Identification of neuronal TET3 interactors

Other than the isoforms that contained a CXXC domain this neuronal TET3 variant did not have a DNA binding affinity (Xu et al., 2012) suggesting that unknown DNA binding (transcription) factors are necessary for binding and targeting this isoform to pre-existing 5mC for targeted oxidation to 5mC (Figure 23). Therefore, interacting proteins of neuronal TET3 were identified by combining affinity purification with mass spectrometry.

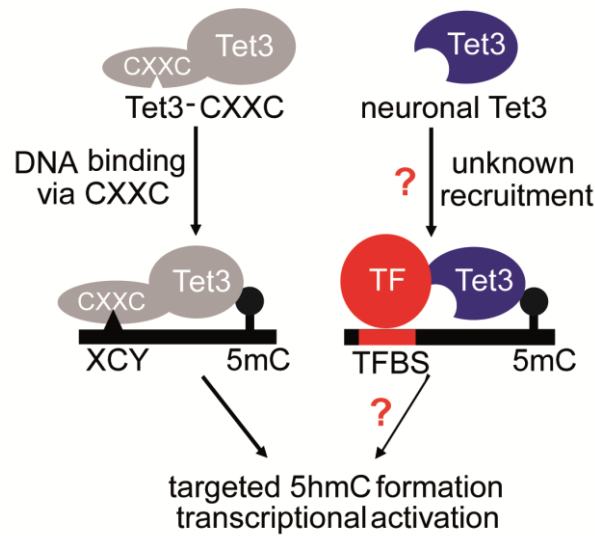


Figure 23. Schematic view of TET3 recruitment.

Cartoon illustrating putative DNA binding mechanisms of TET3 isoforms lacking (neuronal TET3) or containing a CXXC domain.

To purify interacting proteins that specifically interact with the specific TET3 isoform lacking a CXXC domain, lentiviral vectors were generated that expressed CMV-TET3 Δ CXXC-eGFP. Next, mouse retinal explant cultures were transduced with this lentiviral vector expressing an eGFP-fusion protein of the neuronal TET3. Control cultures were transduced with lentiviral vectors expressing eGFP only (LV-CMV-eGFP). After onset of expression, nuclear protein complexes were extracted, affinity-purified and subsequently labeled with TMT 2-plex reagents in forward and reverse "label swap" experiments for comparative quantification using LC-MS. 52 proteins were significantly enriched for binding to TET3 (> 1.5-fold enrichment) in forward and reverse labeling experiments (proteins in the bottom-right quadrant in Figure 24) (see also Table 6). Notably, nine of those proteins, *i.e.* CEP290, CHD4, HMGN2, MAGI2, NOLC1, PLK2, REST, SPDEF and SUZ12 are known regulators of transcription. Another six proteins are histone variants involved in chromatin modification e.g. HIST1H1C, H3F3A and H2AFJ (Figure 24).

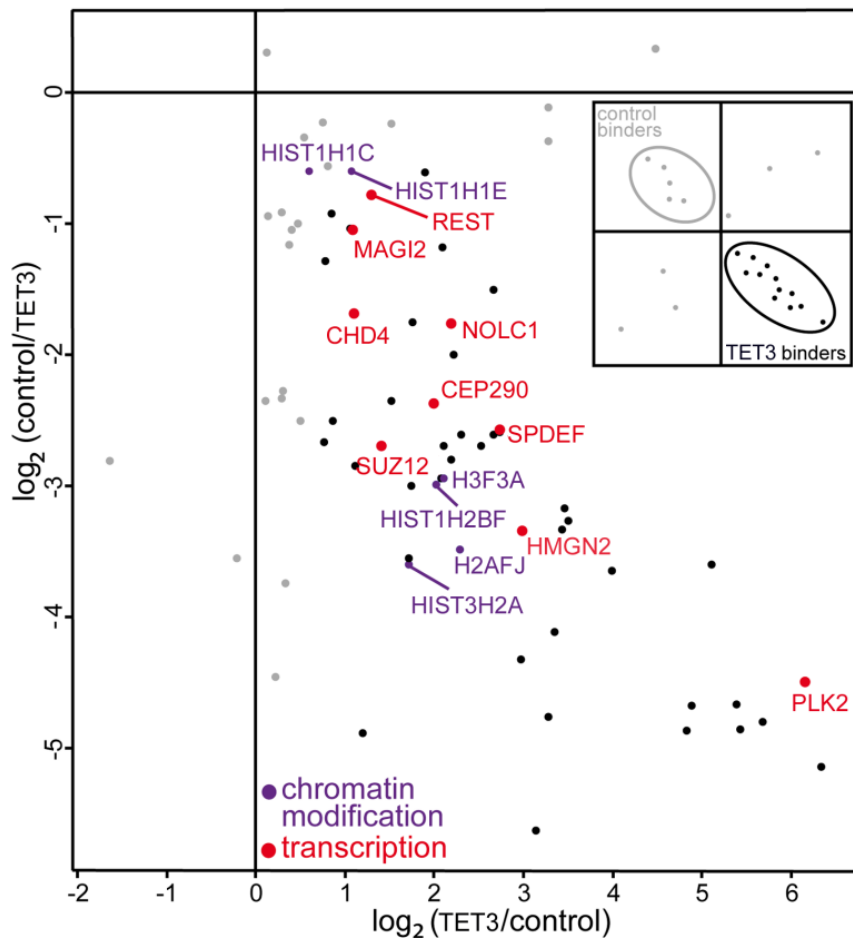


Figure 24. Neuronal TET3 interacting proteins

Scatterplot of TET3 interactors identified using lentiviral TET3-eGFP overexpression in retinal explant cultures followed by GFP-trap and LC-MS/MS.

3.10 Identification of endogenous TET3 interactors

In the experiment described in 3.9 TET3-eGFP is expected to compete for binding partners with endogenous TET3. Thus, to gain a better understanding of endogenous TET3 interaction partners, the affinity purification experiment was repeated on retinal lysates using a TET3-specific antibody. Importantly, endogenous TET3 was highly enriched in the forward and reverse experiment after antibody based purification highlighting its specificity (Figure 25A). Interestingly, three H3K36 methyltransferases (NSD2, NSD3 and SETD2) were identified as TET3 interactors displaying a significant enrichment for

binding to endogenous TET3 (>1.5 fold) (Figure 25A). Furthermore, five transcriptional regulators *i.e.* ASXL1, CTCF, MORF4L1, REST and VAX1 were identified. Notably, the TET3-interacting protein with the highest enrichment score was the transcriptional repressor REST (Figure 25A), which was also significantly enriched in the TET3-eGFP affinity purification experiment (Figure 24). Therefore, the interaction of REST and TET3 was studied further. First, the interaction of TET3 with REST was validated by performing an affinity purification using a REST-specific antibody. Importantly, endogenous REST was highly enriched in the forward and reverse experiment by the antibody (Figure 25B). In line with the previous experiments the REST antibody affinity-purified TET3 very efficiently with the overall third-highest enrichment score, but neither immunoprecipitated TET1 nor TET2 (Figure 25B).

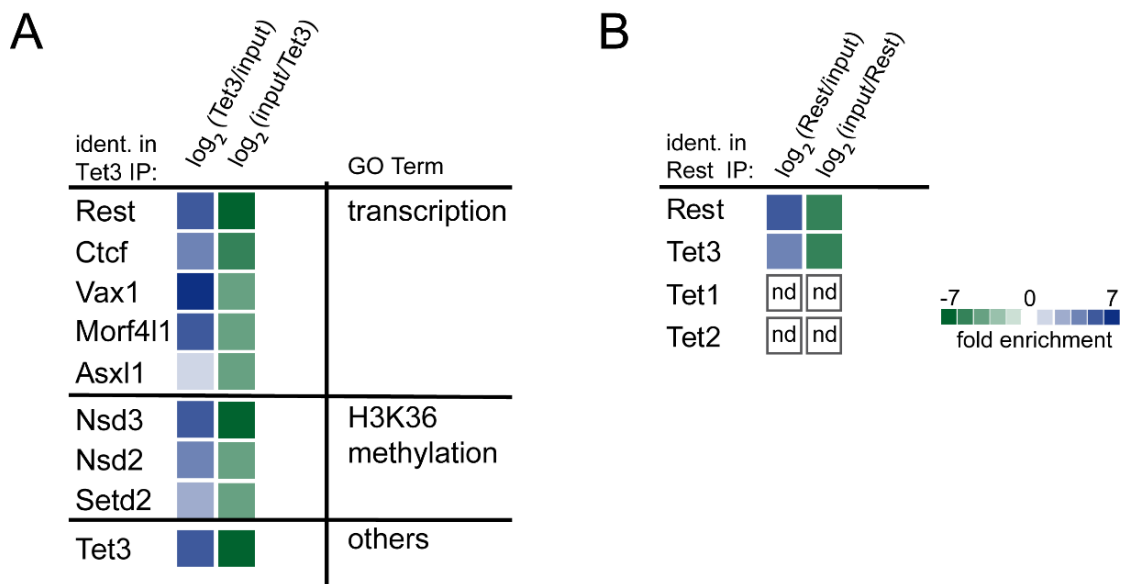


Figure 25. Endogenous TET3-interacting proteins.

(A) Heatmap of endogenous TET3 interaction partners identified by immunoprecipitation and LC-MS/MS. (B) Heatmap of endogenous REST immunopurification LC-MS/MS experiment confirming the interaction with endogenous TET3. (nd) not detected.

3.11 Functional characterization of TET3 binders

To test whether the interaction of REST with TET3 had an effect on its hydroxylase activity neuronal TET3 was overexpressed alone or together with REST in HEK293T cells. Subsequently, 5hmC levels were quantified using HPLC-MS/MS (Figure 4A). Non-transfected HEK293T cells have very low endogenous 5hmC levels and overexpression of TET3-eGFP alone resulted in increased 5hmC levels. Interestingly, co-expression of REST with neuronal TET3 led to significantly higher levels of 5hmC (Figure 26A). To validate that REST regulates TET3 hydroxylase activity a siRNA mediated REST knockdown approach was used. First knockdown efficiency of siRNA against REST was studied using RT-qPCR. Both siRNAs against REST showed a significant decrease in REST gene expression levels compared to the siRNA control (p-value < 0.01, t-test) (Figure 26B). The siRNA *REST* #1 was used for subsequent studies. Next, a siRNA mediated knockdown of endogenous REST combined with neuronal TET3 overexpression was performed in HEK293T cells. In line with the previous finding, a knockdown of REST lead to decreased 5hmC levels in comparison to control siRNA treatment (Figure 26C). In conclusion, REST is sufficient and necessary to control TET3 hydroxylase activity.

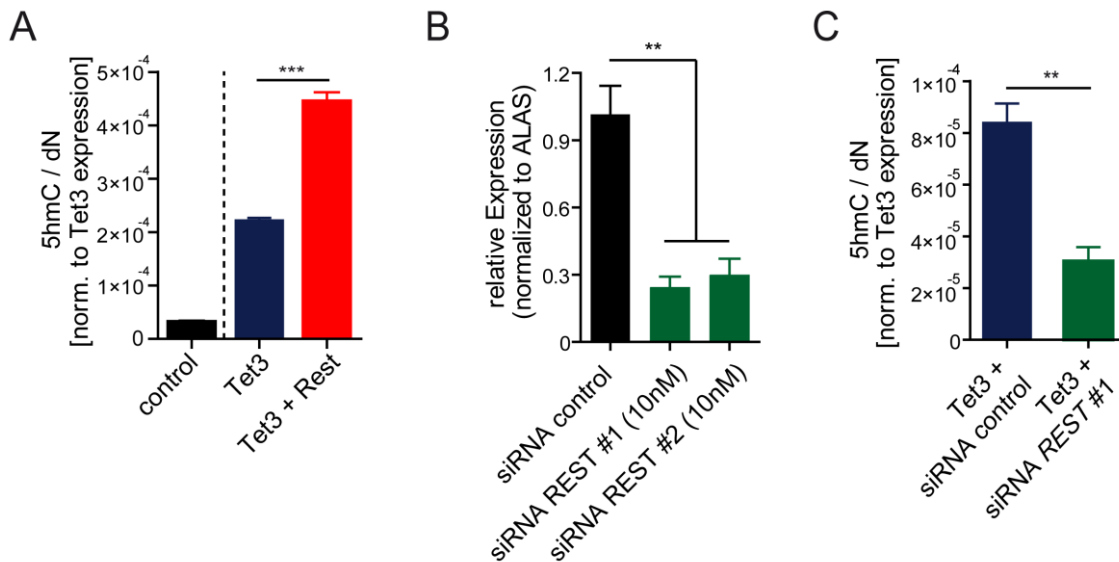


Figure 26. Functional analysis of the interaction of REST and neuronal TET3

HPLC-MS/MS quantification of global 5-hydroxymethylcytosine (5hmC) levels after overexpression (OE) of TET3-eGFP or REST and TET3-eGFP. (B) Both siRNAs efficiently reduced REST expression levels in HEK293T cells. Summary data are mean \pm SEM. * p<0.05, ** p < 0.01, *** p < 0.001 (Student's t-test). (C) HPLC-MS/MS quantification of global 5hmC levels

after overexpression (OE) of TET3-eGFP in the presence of siRNA directed against human *REST* or a scrambled siRNA control (ctrl).

3.12 TET3 induced changes in gene expression

REST is a transcriptional repressor that binds to specific RE-1 binding sites present in regulatory regions of its target genes (Kraner et al., 1992). Binding of REST results in transcriptional repression of the corresponding genes (Chong et al., 1995; Schoenherr and Anderson, 1995). Thus, it is possible that TET3 mediated 5mC oxidation might affect gene expression of REST target genes. Thus, neuronal TET3 was overexpressed in HEK293T cells that endogenously contain REST (Dietrich et al., 2012) to investigate global protein level changes using LFQ proteomics (Figures 27A-C). 308 of the identified proteins were known REST targets (Lu et al., 2014). Importantly, the protein levels of those 308 REST targets were significantly elevated in the TET3 overexpression compared to the eGFP control experiment (Figure 27A). Importantly, 11 REST targets were significantly enriched in the group of 40 TET3-induced proteins ($p = 1.6 \times 10^{-6}$, Fischer's exact-test) (Figure 27B). Overexpression of TET3-eGFP resulted in significant upregulation of 26 previously non-expressed proteins (proteins with infinite \log_2 ratios in Figure 21C), and 6 of them were known REST target genes (*LARS*, *MYH9*, *DDX39A*, *MCM4*, *RAB35* and *RBBP7*) (Figure 27C).

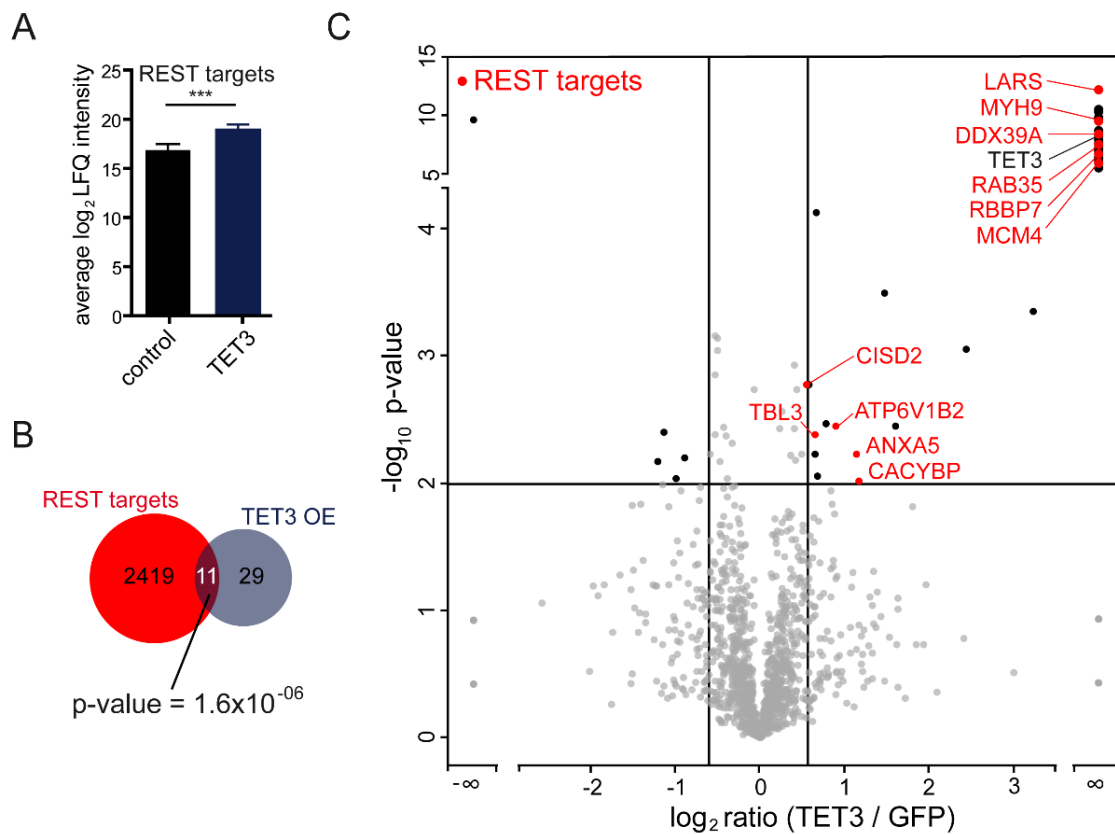


Figure 27. Neuronal TET3 induced expression changes in HEK293T cells

(A) Identification of global REST target gene expression using LFQ after eGFP (control) or TET3-eGFP overexpression in HEK293T cells. REST target genes are significantly higher expressed after TET3 OE. (B) Venn diagram showing the significant overlap (Fishers exact-test; p-value = 1.6×10^{-6}) of proteins enriched after TET3 OE and REST target genes in HEK293T cells. (C) Volcano plot of protein expression ratios between TET3eGFP and eGFP overexpression experiments in HEK293T cells as a function of statistical significance (standard t-test p value ≤ 0.01). Proteins with no statistically significant difference in expression between subsets are grey. Proteins with no detectable signal in one of the subsets were assigned a ratio of infinity. REST target genes are highlighted in red. *** p < 0.001 (Student's t-test).

3.13 siRNA knockdown of REST and TET3 overexpression

Next, the presence of REST on TET3-mediated induction of REST-target genes was investigated. Therefore, TET3-eGFP was overexpressed in the presence of REST-specific siRNA or scrambled control siRNA and the transcript levels of three selected REST-target genes (*LARS*, *MCM4* and *MYH9*) were analyzed by comparing to the housekeeping gene *ALAS* using RT-qPCR. Interestingly, the TET3-mediated induction of expression of

those genes is significantly lower after knockdown of endogenous REST (Figure 28A-C).

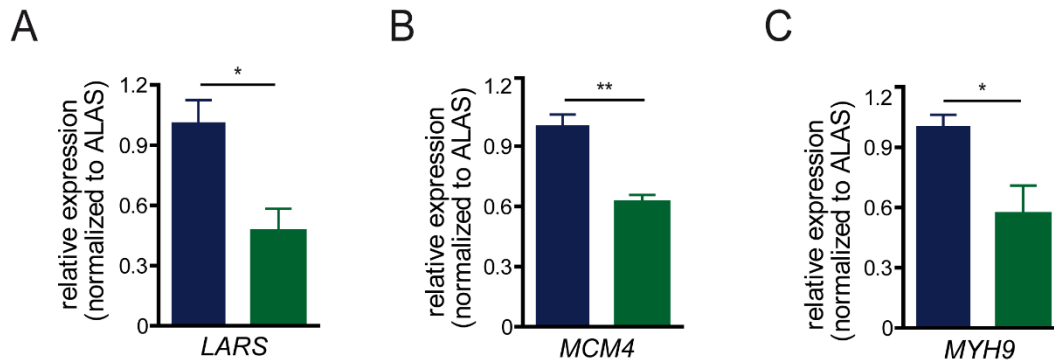


Figure 28. Gene expression of three TET3-induced REST-target genes

Quantification of three TET3-induced REST-target genes in HEK293T cells using RT-qPCR after overexpression (OE) of TET3-eGFP in the presence of siRNA directed against human REST (green) or a scrambled siRNA control (ctrl) (blue). Summary in (A-C and F) data are mean \pm standard error of mean (SEM). * $p < 0.05$, ** $p < 0.01$ (Student's t-test).

3.14 5hmC and REST co-localize in euchromatin

The previous results suggest that REST directs TET3 to repressed target genes resulting in hydroxymethylation of 5mC. This goes along with de-repression and transcriptional activation of the respective genes. Transcriptionally inactive genes are largely found in heterochromatin, whereas actively transcribed genes are present in euchromatin. As shown in Figure 17B 5mC is enriched in heterochromatin whereas 5hmC is present in euchromatin. To test for the co-localization of REST with 5mC and 5hmC in nuclei of retinal neurons an *in situ* proximity ligation assay (PLA) was performed by combining a REST-specific antibody with 5mC or 5hmC-specific antibodies. PLA gives only a positive signal when 5mC or 5hmC and REST are in close proximity ($< 40\text{nm}$) (Soderberg et al., 2006). First, a positive PLA signal was detected for both antibody combinations (Figure 29A). The PLA signal of REST with 5mC was present in heterochromatin (Figure 29, *left image*), whereas the signal of REST with 5hmC was detected exclusively in euchromatin (Figure 29, *right image*). This suggests that REST-binding sites show distinct sub-nuclear localization depending on the oxidation status of adjacent genomic cytosines.

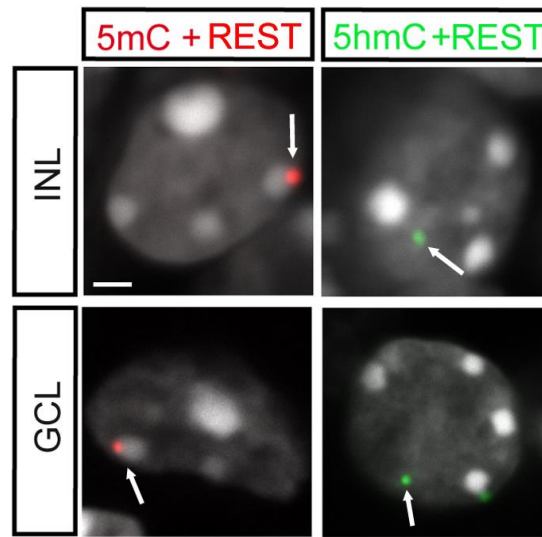


Figure 29. PLA staining of 5mC / 5hmC and REST.

(A) Proximity ligation assay (PLA) signal for 5mC and REST (upper panel) is localized in heterochromatin. In contrast, the PLA signal for 5hmC and REST is localized in euchromatin (lower panel). Scale bar marks 1 μ m.

Interestingly, the levels of PLA signal for REST/5hmC and REST/5mC varied significantly between week 2 and week 3 (Figure 30A-B). In particular, the REST/5hmC PLA signal correlated positively with the 5hmC levels increasing from week 2 to week 3 (Figure 30A). In contrast, the PLA signal for REST/5mC showed an inverse behavior during the same period of time (Figure 30B). Together, these results suggest a functional correlation between REST binding sites and proximal epigenetic DNA marks that might affect chromatin state and gene expression. Next, the subset of genes that gained 5hmC marks from week 2 to week 3 (see Figure 20) were screened for known REST target genes (Lu et al., 2014). In support of a positive effect of REST on genomic 5hmC levels in the retina, a significant enrichment of REST-target genes within the group of genes that gained 5hmC during retinal maturation was observed ($p = 1.8 \times 10^{-7}$, Fischer's exact-test) (Figure 30C).

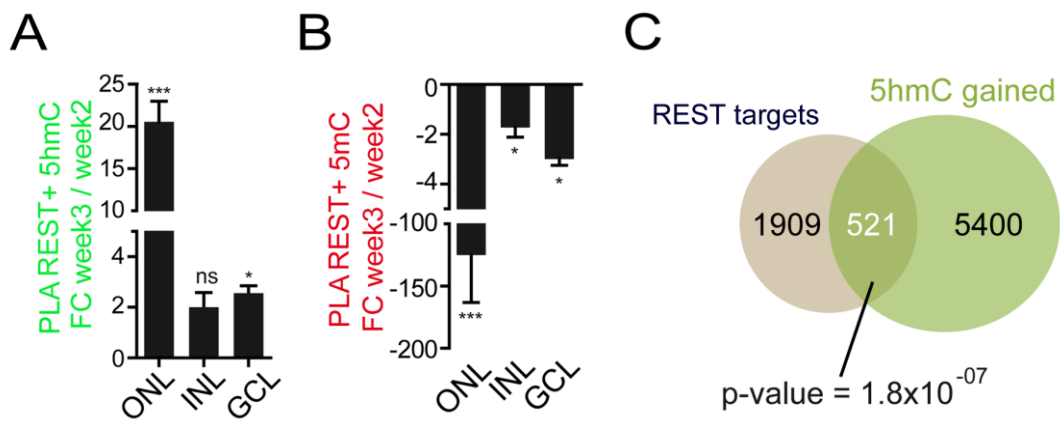


Figure 30. Accumulation of 5hmC is associated with chromatin remodeling

(A-B) Quantification data of the 5mC/REST (B) and 5hmC/REST (C) PLA experiments shown in Figure 29. (C) Venn diagram showing the significant overlap (Fishers exact-test; p-value = 1.8×10^{-7}) of REST target genes and 5hmC gained genes during retinal maturation. * p < 0.05, *** p < 0.001 (Student's t-test).

3.15 5hmC co-localizes with the active histone mark H3K36me3

Transcriptional activation of previously silenced genes requires chromatin remodeling, *e.g.* a switch from a heterochromatic to a euchromatic state (Voss and Hager, 2014). It was suggested that REST mediated chromatin remodeling involves changes of the activating histone mark lysine 36 trimethylation of the nucleosomal histone H3 (H3K36me3) an epigenetic mark commonly associated with transcription of active chromatin (Bernstein et al., 2005; Heintzman et al., 2007; Kouzarides, 2007). To test for REST mediated chromatin remodeling the PLA signal of 5hmC with the active histone mark H3K36me3 was investigated during retinal maturation (Figure 31).

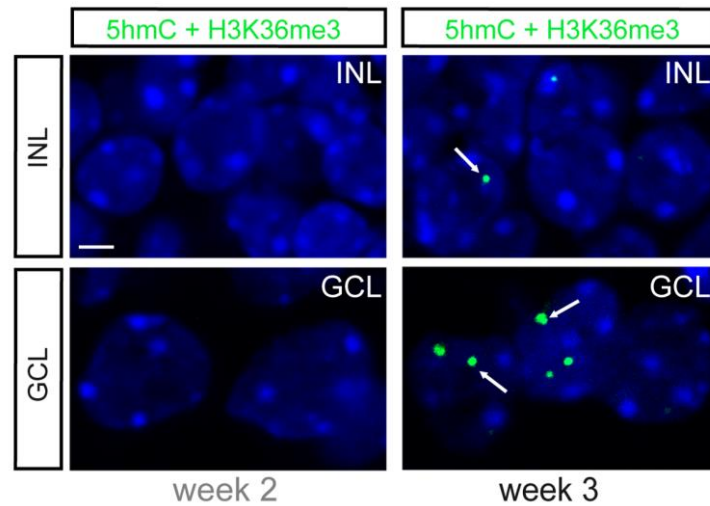


Figure 31. PLA staining of 5hmC and H3K36me3.

PLA signal for 5hmC and H3K36me3 in nuclei of the inner nuclear layer (INL; upper panel) and the ganglion cell layer (GCL; lower panel) at week 2 (left) and week 3 (right). Scale bar marks 5 μ m.

As shown in Figure 32 we observed a significant increase of the PLA signal of 5hmC with the H3K36me3 co-localization in nuclei of 3-week-old retina in comparison to week 2 retina. Thus, from week 2 to 3 the chromatin structure in retinal nuclei changes towards co-localization of 5hmC with the H3K36me3.

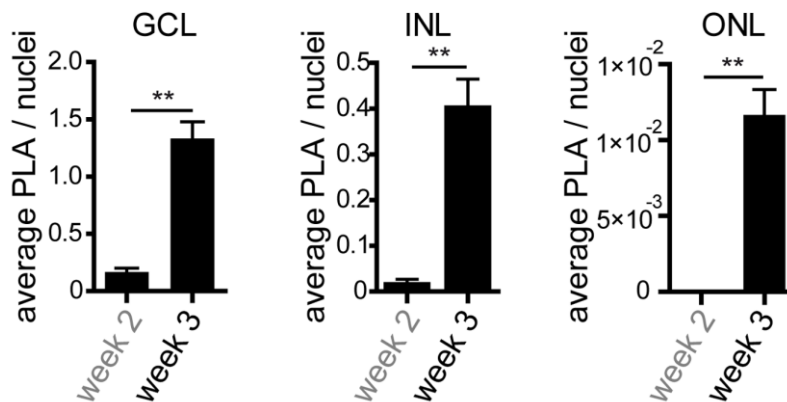


Figure 32. Quantification of PLA signal (5hmC/ H3K36me3).

(B) Quantification data of the 5hmC/H3K36me3 PLA experiments shown in Figure 31. Summary data are mean \pm standard error of mean (SEM). ** $p < 0.01$ (Student's t-test).

3.16 TET3 stimulates NSD3 for H3K36 trimethylation

Interestingly, three of the identified endogenous TET3 interacting proteins were the post-SET domain containing histone-lysine N-methyltransferases NSD3, NSD2 and SETD2 (Figure 25A). These histone writers are involved in the (tri-) methylation of nucleosomal histone H3 at lysine 36 (H3K36).

To further investigate the functional consequences of the interaction between TET3 and H3K36me3 methyltransferases a PLA experiment with HEK293T cells transfected with TET3 and/or the H3K36me3 methyltransferase was performed. The PLA signal studied was a product of the two enzymes 5hmC and H3K36me3, respectively. NSD3 overexpression did not result in any detectable PLA signal (Figure 33A-B), which is in line with the very low levels of 5hmC in HEK293T cells. TET3 overexpressing cells showed a low amount of PLA signals suggesting that 5hmC is not formed in close proximity to H3K36me3 (Figures 33A-B). In contrast, co-expression of TET3 and NSD3 resulted in a synergism and significantly increased the 5hmC/H3K36me3 PLA signal (Figures 33A-B). Next, the global changes in H3K36 trimethylation were studied by acidic histone extraction, H3 purification and subsequent quantification of K36me3 using isobaric labeling and MS (Figure 33C). The quantification data revealed a 40-fold increase of the levels of H3K36me3 in the HEK293T cells co-overexpressing TET3 and NSD3 compared to non-transfected cells (Figure 33D). Overexpression of TET3 or NSD3 alone provided only an about 2-fold increase of the H3K36me3 activation mark (Figure 33D). In conclusion, TET3 has a synergistic effect on the lysine methyltransferase activity of NSD3.

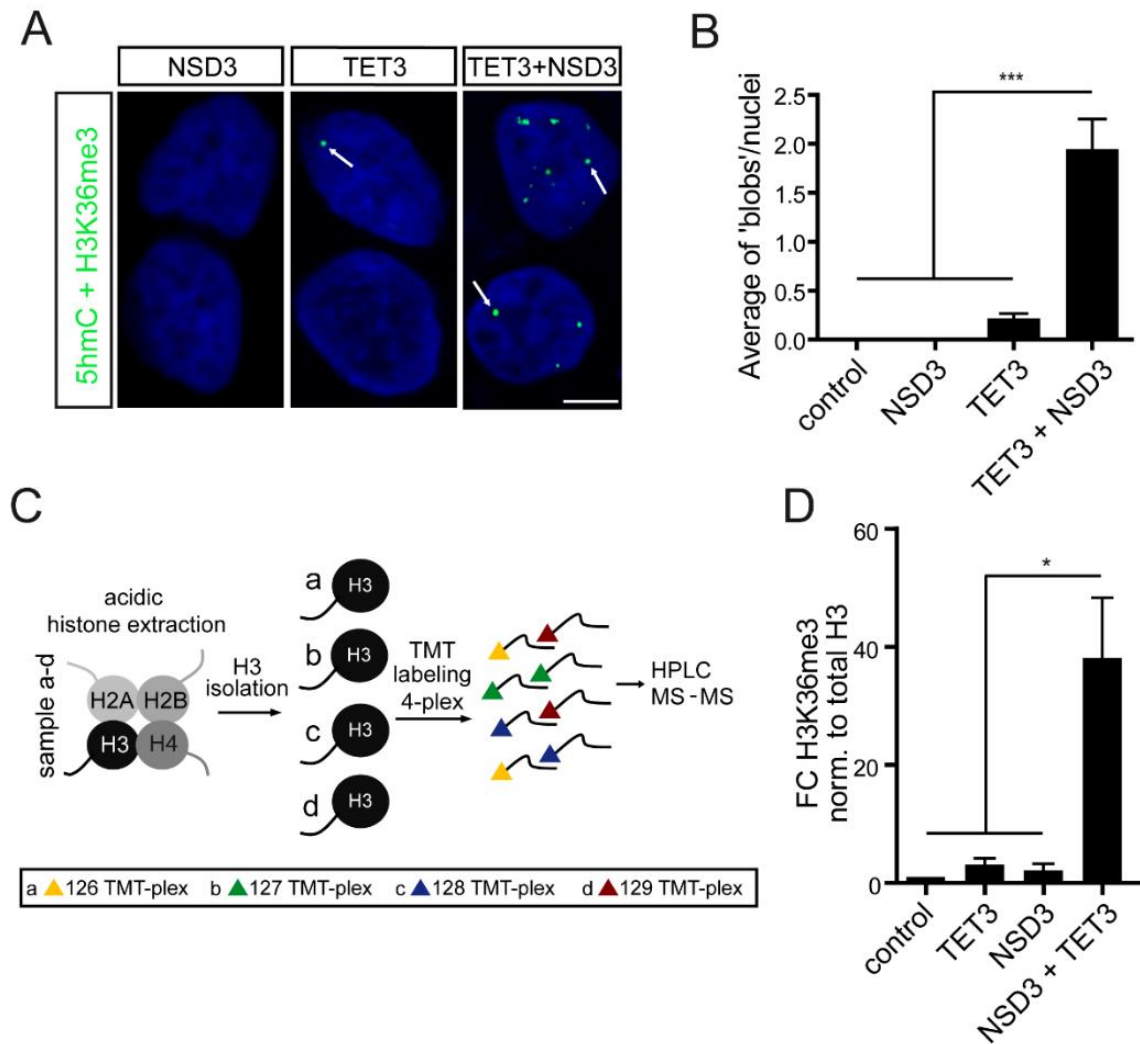


Figure 33. Effect of TET3-mediated hydroxylation on chromatin structure.

(A) PLA signal for 5hmC and H3K36me3 in HEK293T cells overexpressing TET3-eGFP (left panel) and TET3 + NSD3 (right panel). (B) Quantification data of the 5hmC/H3K36me3 PLA experiments shown in (A). (C) Scheme of TMT4 - plex isobaric labeling and LC-MS quantification of H3 modifications. (D) Isobaric labeling LC-MS quantification of H3K36me3 in HEK293T cells overexpressing TET3, NSD3 or TET3 and NSD3 compared to non-transfected cells. Summary data are mean \pm standard error of mean (SEM) in (B and D). * $p < 0.05$, *** $p < 0.001$ (1-way ANOVA). Scale bar in (A) marks 5 μ m.

3.17 Effects of TET3 overexpression in retinal explants

To analyze if TET3 overexpression has an effect on global gene expression in the retina we transduced retinal explant cultures with lentiviral vectors expressing TET3-eGFP. Compared to retinal explant cultures overexpressing eGFP only, we identified 981 proteins that were upregulated after TET3-eGFP overexpression. The TET3-eGFP overexpression strongly affects gene expression in the retina resulting in upregulation of proteins involved in several neurological functions (Figure 34A). Correlation analysis again revealed that known REST targets were significantly enriched in the subset of TET3-upregulated proteins ($p = 2.1 \times 10^{-10}$, Fischer's exact-test) (Figure 34B).

To test whether TET3 has also a positive effect on lysine methyltransferase activity in the retina we transduced retinal explant cultures with TET3-eGFP or eGFP using lentiviral vectors and determined the levels of H3K36me3 using the same methodology. Overexpression of TET3-eGFP was able to elevate the levels of H3K36me3 by a factor of 3.8 suggesting that TET3-mediated hydroxylation of 5mC in retinal cells results in activation of NSD3 or similar enzymes to induce H3K36 trimethylation (Figure 34C). The data indicates that this involves at least in part REST-assisted, TET3-mediated oxidation of genomic 5mC and subsequent gene expression.

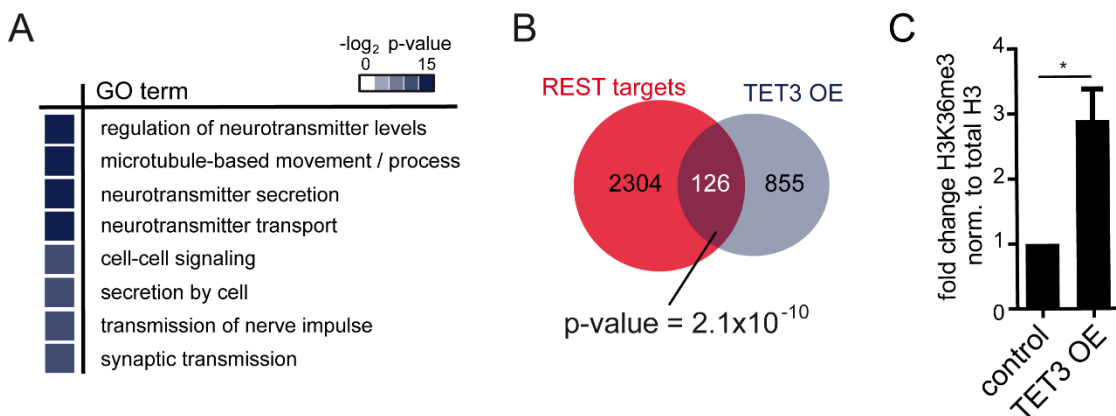


Figure 34. TET3 overexpression leads to activation of neuronal genes

(A) Gene ontology analysis reveals strong enrichment of neuronal proteins within the subset of proteins induced after TET3 OE in mouse retinal explants. (B) Venn diagram showing the significant overlap (Fishers exact-test; p -value = 2.1×10^{-10}) of proteins enriched after TET3 OE and REST target genes. (C) Isobaric labeling LC-MS quantification of H3K36me3 in mouse retina after TET3-eGFP or eGFP (control) overexpression. Summary data are mean \pm standard error of mean (SEM). * $p < 0.05$ (Student's t-test).

4. Discussion

4.1 Active DNA demethylation during retinal maturation

It was suggested that 5hmC functions as an intermediate in a TET enzyme catalyzed active DNA demethylation process (Guo et al., 2011). In this study, it was shown that 5mC is oxidized by TET enzymes to 5hmC during terminal retinal maturation suggesting active DNA demethylation. However, 5hmC predominantly accumulated in the DNA during retinal maturation and was not a short-lived metabolic by-product of oxidative active DNA demethylation. These findings were in line with previous studies in neuronal tissue that showed 5hmC accumulation during neurogenesis and ageing (Szulwach et al., 2011). Confirming the stability of 5hmC in retinal neurons, the metabolic feeding experiments revealed that *de novo* 5hmC stably increased in retinal explants. Moreover, *de novo* 5fC or 5caC formation was not detected in the feeding experiments with [methyl-¹³CD₃]-methionine, suggesting that 5hmC is not further oxidized during terminal differentiation. Nevertheless, it cannot be ruled out that 5hmC is slowly oxidized or even directly removed to cytosine to a low degree or 5hmC removal occurs over a longer time period.

Interestingly, the further oxidized cytosine derivative 5fC showed an inverse pattern of 5hmC and its levels decreased during retinal maturation. Furthermore, 5caC levels were below detection limit. Suggesting that 5fC and 5caC are short-lived DNA intermediates during retinal maturation involved in active DNA demethylation. A recent study showed that 5fC and 5caC are generated during DNA demethylation by TET1 in distinct promoters for active gene transcription in ES cells (Neri et al., 2015). Furthermore, it is known that 5fC and 5caC levels negatively correlate with TDG levels, indicating TDG-mediated excision of 5fC/ 5caC and subsequent BER. Assuming TET1 is mainly in charge of 5fC formation, it is conceivable that 5fC removal outweighs its formation due to the fairly low TET1 levels in retinal neurons. Nevertheless, it would be interesting to map 5fC enriched genomic loci to distinguish whether it is an active DNA demethylation product or maybe a distinct epigenetic signal itself during retinal maturation.

4.2 Epigenetic role of 5hmC

This study shows that approximately 1.7 % of all cytosines are hydroxymethylated, corresponding to around nine million 5hmC bases in mouse retina. This suggests that 5hmC has important functions in retinal neurons. However, the role of 5hmC in the DNA of mammalian tissue is still unknown. The data indicates that 5hmC patterns in neuronal cells are dissimilar to those in ES cells which are associated with high levels of TET1 and TET2 and low levels of TET3 (Xu et al., 2011). According to TAB sequencing data for ES cells, 5hmC is abundant at enhancers (p300 sites) and underrepresented in gene bodies (Yu et al., 2012). In contrast, cortical NPCs and neurons are characterized by low levels of 5hmC at p300 sites and by enrichment of 5hmC in gene bodies. In line with these studies, high levels of 5hmC in gene bodies and a strong increase of 5hmC levels during retinal maturation in retinal and neuronal genes are detected, suggesting a tissue and stage-specific role of 5hmC. Furthermore, deposition of 5hmC is associated with increased gene expression. However, the exact purpose of 5hmC formation remains elusive. It is imaginable that 5hmC removes the repressive effects on transcription mediated by 5mC. Another option could be that 5hmC destabilizes the DNA structure, thereby facilitating the opening of the double helix by the transcription machinery (Lopez et al., 2012; Pfeifer et al., 2013; Wanunu et al., 2011). Moreover, a recent study has shown that 5hmC can recruit specific binding proteins (readers) in a tissue specific manner (Spruijt et al., 2013; Takai et al., 2014). It cannot be excluded that such 5hmC readers contribute to the observed TET3-mediated transcriptional activation during retinal maturation. It is possible that 5hmC repels 5mC readers that mediate transcriptional repression. Furthermore, 5hmC could recruit other chromatin remodeling proteins that are important for transcriptional activation. To further unravel the role of 5hmC in, it is important to investigate 5hmC readers in retinal neurons (Figure 35).

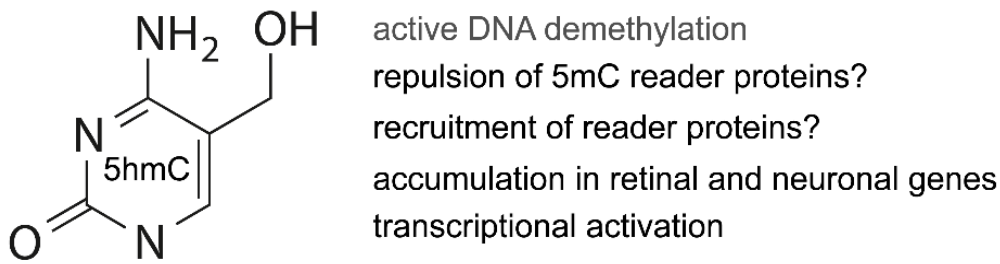


Figure 35. Potential role of 5hmC in retinal neurons.

5hmC is a rather stable epigenetic DNA base in retinal neurons. Furthermore, it is associated with transcriptional activation. It is possible that 5hmC recruits specific reader proteins or removes the repressive function of 5mC by repulsion of 5mC readers.

4.3 TET-mediated 5hmC formation

The data reveals that 5hmC accumulates especially in gene bodies of neuronal and retinal genes and is associated with increased gene transcription during retinal maturation. These findings support previous studies that showed that accumulation of 5hmC is related to neuronal genes and associated with active transcription in neurons (Hahn et al., 2013; Mellen et al., 2012). Additionally, TET3 lacking a CXXC DNA binding domain was shown to be the main TET isoform in mouse retina. Furthermore, a comprehensive analysis of interacting proteins was performed revealing that TET3 interacts with the transcriptional regulator REST but not with TET1 and TET2.

Interestingly, REST was shown to be a master regulator of genes involved in neuronal maturation processes (McGann et al., 2014). However, Rest is known to be a transcriptional repressor of neuronal genes in non-neuronal cells (Chen et al., 1998, Schoenherr et al., 1996). Moreover, REST was described to act as a repressor in cell commitment of retinal ganglion cells by preventing premature expression in retinal progenitor cells (Mao et al., 2011). This repressive function of REST is mediated by interaction with other proteins such as mSin3a or CoRest1 to form REST repressor complexes (Huang et al., 1999; McGann et al., 2014; Naruse et al., 1999). In the REST-specific affinity purification from nuclear lysates of mouse retina, none of the known REST repressive complexes were identified. However, studies suggest that REST also plays a role in proper function of neuronal cells (Lu et al., 2014; Lunyak and Rosenfeld, 2005). For example, it was shown that REST functions as an activator of neuronal genes during neuronal maturation in the

presence of a small double stranded non-coding RNA corresponding to the NRSE/RE1 REST binding sequence (Kuwabara et al., 2004). These findings suggest that REST's mechanisms of action highly depend on interaction partners. In line with this hypothesis, the present study shows that REST binds and recruits TET3 for 5hmC formation in retinal neurons that subsequently results in induction of gene expression. In particular, REST regulates TET3 hydroxylase activity and REST target genes accumulate 5hmC during retinal maturation. Furthermore, overexpression of TET3 activates REST target genes.

In support of these findings, a recent study showed that deletion of REST in mouse embryonic stem cells (ESCs) lead to significant loss of genomic 5hmC levels in regulatory regions (Feldmann et al., 2013).

Based on the 5hmC-mapping data approx. 9 % (521 out of 5921) of the genes that gained 5hmC during retinal maturation were known REST target genes. Thus, although REST contributes significantly ($p = 1.8 \times 10^{-7}$, Fischer's exact-test) to context-specific 5hmC generation additional factors should exist for TET3 recruitment. In line with this, several other transcriptional regulators interacting with TET3 such as ASXL1, CTCF, MORF4L1, SUZ12 and VAX1 were identified. It is tempting to speculate that these transcription regulators could influence TET3 hydroxylase activity in a similar way as REST. For instance, it was shown that the insulator CTCF interacts with Tet enzymes and that depletion of CTCF in mouse ESCs and adipocytes leads to a significant loss of 5hmC in transcriptional enhancers (Dubois-Chevalier et al., 2015; Feldmann et al., 2013). However, CTCF does not discriminate between the Tet isoforms, since it binds to TET1 and TET2 (Dubois-Chevalier et al., 2015) as well as to TET3 (present study).

In conclusion, REST and most probably additional DNA-binding transcriptional regulators recruit TET3 to neuronal genes during retinal maturation to oxidize 5mC to 5hmC and activate their transcription.

Transcriptional activation requires chromatin remodeling and DNA accessibility for the transcriptional machinery. Previous studies have shown translocation of genomic regions from 5mC-rich heterochromatin to 5hmC-rich euchromatin (Hahn et al., 2013; Mellen et al., 2012; Yamaguchi et al., 2013). This study reveals that TET3 interacts with several H3K36 methyltransferases i.e. NSD2, NSD3 and SETD2. Furthermore, it was shown that TET3 stimulates the activity of NSD3 to generate the activating histone mark H3K36me3 in close proximity to 5hmC.

It is likely, that TET3 is also able to stimulate the activity of NSD2 and SETD2. Interestingly previous studies have shown that TET2 and TET3 regulate O_GlycNAcylation and H3K4 methylation by interacting with OGT and the SET1/COMPASS complex in ESC (Chen et al., 2013; Deplus et al., 2013). Suggesting that different mechanisms of TET mediated transcriptional activation exist in a cell type-dependent manner.

The data reveals that the transcriptional repressor REST can facilitate the recruitment of TET3 to 5mC-containing transcriptionally inactive genes (Figure 21). This transcriptional regulator-induced and context-specific recruitment is followed by TET3-mediated oxidation of 5mC to 5hmC. Subsequently, H3K36 methyltransferases induce chromatin remodeling to facilitate active transcription (Figure 26). The findings favour a model that involves highly dynamic transcription factor-dependent DNA hydroxymethylation that supports retinal network maturation by context-specific gene activation. Accordingly, the metabolic feeding experiments showed that the majority of nascent 5hmC marks are generated from pre-existing 5mC supporting the idea of TET3-induced chromatin remodeling.

5. Summary

The 2-oxoglutarate and Fe (II)-dependent ten-eleven translocation (TET) enzymes can oxidize 5-methylcytosine (5mC) to 5-hydroxymethylcytosine (5hmC), 5-formylcytosine (5fC) and 5-carboxycytosine (5caC). Thus, it was hypothesized that this could be a pathway for active DNA demethylation. However, several studies have shown that 5hmC levels accumulate especially in neurons suggesting a role as an epigenetic mark. Nevertheless, the mechanism controlling TET activity and the role of 5hmC are poorly understood. In particular, it is not known how the neuronal TET3 isoform lacking a DNA binding domain is targeted to the DNA.

In this study, the role of 5hmC during retinal maturation by genome-wide mapping of 5hmC in immature (postnatal week 2) and mature mouse retina (postnatal week 3) was studied and correlated with expression data. Furthermore, interaction partners of neuronal TET3, the main isoform in retinal neurons, were identified.

5hmC accumulates during retinal maturation especially in retinal and neuronal genes. Furthermore, the accumulation of 5hmC is associated with increased transcription. Among the identified proteins the transcriptional repressor REST was identified as a highly enriched TET3-specific interactor. Interestingly, REST was able to enhance TET3 hydroxylase activity. Furthermore, increased 5hmC levels were detected in REST target genes during retinal maturation and overexpression of TET3 activated transcription of REST-target genes. Moreover, NSD3 and two other histone methyltransferases were found to interact with TET3 that are able to mediate H3K36 trimethylation. Finally, it was shown that TET3 is able to enhance NSD3-mediated H3K36 trimethylation to promote transcriptional activation.

In conclusion, the data suggests that 5hmC is a stable epigenetic base in retinal neurons that is involved in transcriptional activation. Furthermore, it was shown that 5hmC is generated by TET3 that is recruited to the DNA by transcriptional regulators such as REST in a context-specific manner (Figure 36).

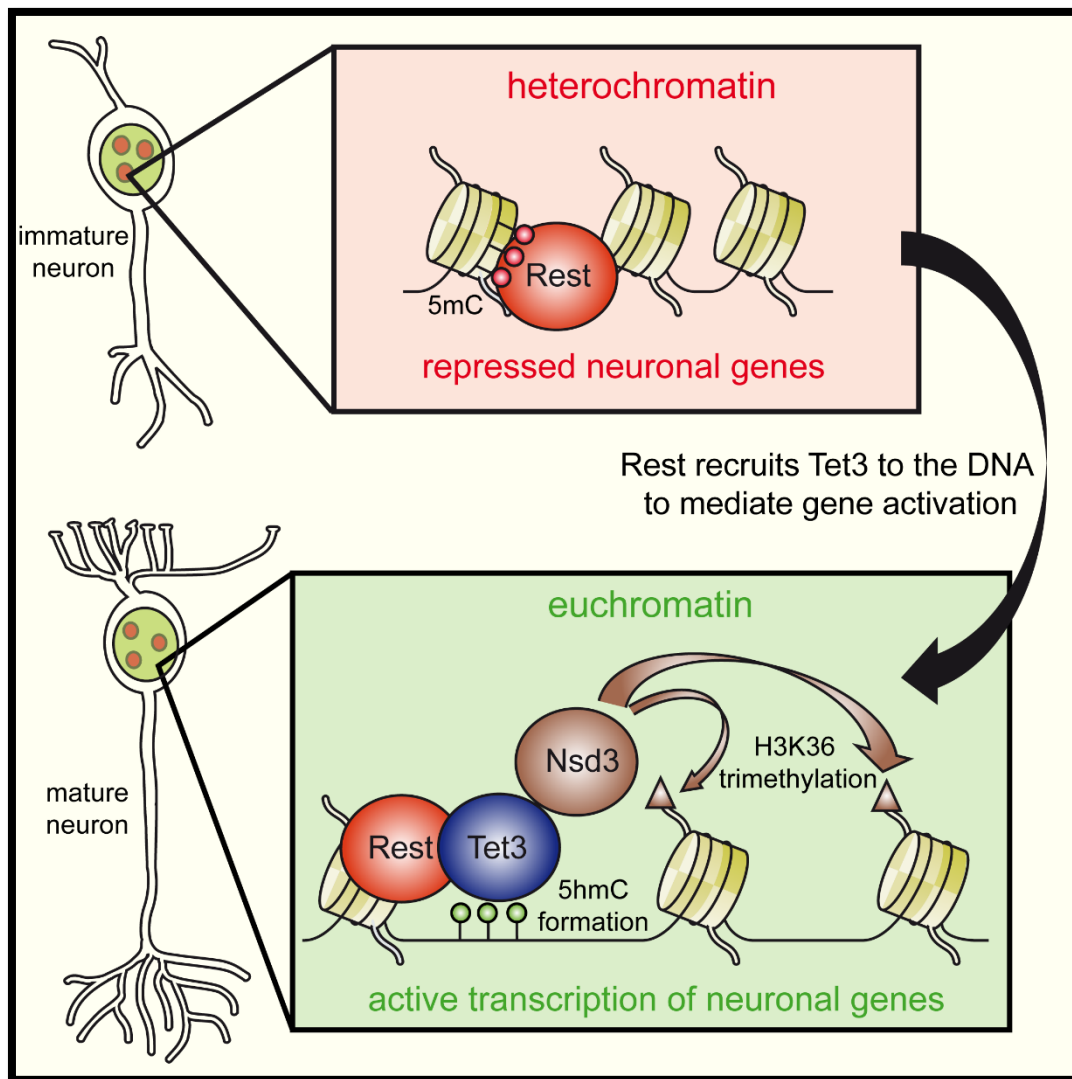


Figure 36. Model for neuronal TET3 mediated transcriptional activation.

TET3 is recruited to the DNA by transcriptional regulators like REST for context-specific 5mC hydroxylation. Subsequently, TET3 mediates H3K36 trimethylation by recruitment of histone writers such as NSD3.

Zusammenfassung

Die Fe^{2+} - und Ketoglutarat abhängigen ten-eleven translocation (TET) Enzyme können 5-Methylcytosin (5mC) zu 5-Hydroxymethylcytosin (5hmC), 5-Formylcytosin (5fC) und 5-Carboxycytosin (5caC) zu oxidieren. Es wurde vermutet, dass es sich bei diesem Oxidationsprozess, um einen möglichen Mechanismus zur aktiven DNA Demethylierung handeln könnte. Jedoch weisen einige Studien darauf hin, dass 5hmC in Neuronen akkumuliert und selbst als epigenetischer Faktor fungiert. Die Regulierung der TET Enzyme, sowie die exakte Rolle von 5hmC ist aber bisher unklar. Insbesondere die Rekrutierung der neuronal TET3 Isoform, die keine DNA Bindedomäne enthält, an die DNA zur Generierung von 5hmC ist nicht bekannt.

In dieser Arbeit wird die Rolle von 5hmC während der retinalen Entwicklung untersucht durch genomweite Analyse von 5hmC in noch unausgereiften (postnatale Woche 2), sowie ausdifferenzierten Mäuseretina (postnatale Woche 3) und anschließend wurden diese Daten mit Expressionsdaten korreliert. Desweiteren wurden Interaktionspartner des neuronalen TET3, der Hauptisoform in retinalen Neuronen, untersucht.

Wir konnten feststellen, dass 5hmC während der retinalen Entwicklung insbesondere in retinalen und neuronalen Genen akkumuliert. Diese Akkumulation korrelierte positiv mit erhöhter Transkription der entsprechenden Gene. Desweiteren fanden wir heraus, dass neuronales TET3 unter anderem mit dem Transkriptionsregulator REST interagiert. Interessanterweise war REST im Stande die Hydroxylaseaktivität von TET3 zu erhöhen. Zudem fanden wir erhöhte 5hmC Levels in REST Zielgenen und Überexpression von TET3 führte zur erhöhten Transkription von REST Zielgenen. Wir fanden auch NSD3 und zwei weitere Histonmethyltransferases, als Interaktoren von TET3 und konnten zeigen dass TET3 die H3K36 Trimethylierung von NSD3 erhöht.

Zusammenfassend, weisen unsere Daten darauf hin, dass 5hmC eine stabile epigenetische Base in retinalen Neuronen ist und eine wichtige Rolle spielt in transkriptioneller Aktivierung. Desweiteren zeigen wir, dass 5hmC von TET3 etabliert wird, das durch Transkriptionsregulatoren, wie REST an die DNA rekrutiert wird zur kontext-spezifischen Hydroxymethylierung. Abschließend zeigen wir, dass TET3 die NSD3 gesteuerte H3K36 Trimethylierung stimuliert um aktive Transkription zu steigern.

Tables

6.1 Primers

primer	sequence
mTET1_fwd	TGAAGCTCAAACATCAACA
mTET1_rev	GTACCTCCATCACAGTCAC
mTET2_fwd	AGCGGAGCCCAAGAAAGCCA
mTET2_rev	CGAAAGCTGCGGTTGTGCTGT
mTET3_fwd	CCTGCGGTGCCTCCTTCTCC
mTET3_rev	TCCGGAGCACCTCCTCCTCC
mAlas1_fwd	TCGCCGATGCCATTCTTATC
mAlas1_rev	GGCCCCAACTTCCATCATCT

Table 3. Primers used for RT-qPCR in mouse retina.

primer	sequence
Neurog2_fwd	CACCGGCAGTAACTAACCTG
Neurog2_rev	AAGTTAGCAGATCTCGGGGTC
Olig2_fwd	TCCTCCACGGGGCCCTCG
Olig2_rev	CTCAGTCCCCGCTGACAAGTGC
Ddx20_fwd	GGACAGCAACAAATGGTG
Ddx20_rev	ATTAAGACTGGCCTGAGC
Gm525_fwd	CCAGGACAGTAACTTCTG
Gm525_rev	AGCCTGACCTGACCCAAG
Opn1sw_fwd	TGTCTCTCTCTTTTACAC
Opn1sw_rev	GCATTTACAGCATCCC
Rora_fwd	GTTACTTTAAAAACGCTCTC
Rora_rev	TTTTAGTGTGTGCGAGAG
Otx2_fwd	CGTTTCCTCTACACACAC
Otx2_rev	AGTCATCCCAAATACAGTG

Table 4. Primers used for hMeDIP qPCR validation.

primer	sequence
REST_fwd	CTTTGTCCTTACTCAAGTTCTCAG
REST_rev	ACCTGTCTTGCATGGCGGGTTA
LARS_fwd	CGTCGTTCCCTTCATCACCCTG
LARS_rev	AGGCTGTCCATCTTTCGGAGAG
MCM4_fwd	CTTGCTTCAGCCTTGGCTCCAA
MCM4_rev	GTCGCCACACAGCAAGATGTTG
MYH9_fwd	ATCCTGGAGGACCAGAACTGCA
MYH9_rev	GGCGAGGCTCTTAGATTTCTCC

Table 5. Primers used for RT-qPCR in HEK293T cells.

6.2 Lists of identified interaction partners

gene name	Description	# peptides	log ₂ (IP/control)	log ₂ (control/IP)
4930595M18Rik	Protein 4930595M18Rik	14	0.78	-1.29
4932431P20Rik	Protein 4932431P20Rik	65	2.30	-2.61
Ahsa2	Activator of 90 kDa heat shock protein ATPase homolog 2 (Fragment)	14	0.77	-2.67
Akd1	Protein Akd1 (Fragment)	6	0.85	-0.93
Angpt1	Angiopietin-1	30	5.39	-4.67
Bace1	Beta-secretase 1 (Fragment)	76	5.43	-4.86
BC005561	Protein BC005561	30	3.46	-3.17
Cdc14b	Dual specificity protein phosphatase CDC14B	4	3.27	-4.77
Cep290	Centromal protein of 290 kDa	23	1.99	-2.38
Chd4	Chromodomain-helicase-DNA-binding protein 4	29	1.11	-1.69
Ckmt2	Creatine kinase S-type, mitochondrial	5	0.86	-2.51
Col12a1	Collagen alpha-1(XII) chain	10	2.02	-2.99
Col5a2	Collagen alpha-2(V) chain	12	1.90	-0.62
Dlg4	Disks large homolog 4 (Fragment)	4	5.68	-4.80
Dmd	Dystrophin	25	3.50	-3.27
Dnajc14	DnaJ homolog subfamily C member 14	4	2.08	-1.18
Dopey1	Isoform 5 of Protein dopey-1	17	1.74	-3.00
Dsg3	Isoform 2 of Desmoglein-3	6	3.99	-3.65
Fsip2	Fibrous sheath-interacting protein 2	22	2.66	-1.51
Gigyf2	PERQ amino acid-rich with GYF domain-containing protein 2	24	2.18	-1.76
Gm3760	Protein D830030K20Rik (Fragment)	68	3.35	-4.12
Gm7221	Protein Gm7221	5	3.43	-3.34
H2afj	Histone H2A.J	8	1.72	-3.55
H3f3a	Histone H3	9	2.19	-2.80
Hist1h1c	Histone H1.2	59	0.60	-0.61
Hist1h1e	Histone H1.4	41	1.08	-0.61
Hist1h2bf	Histone H2B type 1-F/J/L	11	2.07	-2.95
Hist2h2bb	Histone H2B type 2-B	11	2.10	-2.95
Hist3h2a	Histone H2A type 3	8	1.72	-3.60

Hmgn2	Non-histone chromosomal protein HMG-17	6	2.98	-3.35
Jakmip2	MCG4624, isoform CRA_c	4	2.10	-2.70
Kif20b	Isoform 2 of Kinesin-like protein KIF20B	10	2.97	-4.33
Magi2	Isoform 4 of Membrane-associated guanylate kinase, WW and PDZ domain-containing protein 2	9	1.09	-1.05
Manf	Armet protein	9	3.15	-5.63
Neb	Protein Neb	40	2.53	-2.70
Nhs1	Isoform 3 of NHS-like protein 1	22	1.20	-4.89
Nolc1	Protein Nolc1	15	2.21	-2.01
Pacrgl	PACRG-like protein	5	1.06	-1.04
Pitpnm3	Isoform 2 of Membrane-associated phosphatidylinositol transfer protein 3	4	1.75	-1.76
Plk2	Serine/threonine-protein kinase PLK2	4	6.16	-4.50
Ptcd1	Pentatricopeptide repeat-containing protein 1, mitochondrial	221	4.83	-4.87
Rest	RE1-silencing transcription factor	7	1.30	-0.78
Rpl7a-ps10	MCG18601	16	5.11	-3.60
Scn2a1	Protein Scn2a1	5	1.52	-2.35
Spdef	SAM pointed domain-containing Ets transcription factor (Fragment)	4	2.67	-2.61
Suz12	Polycomb protein Suz12	5	2.10	-2.70
Syne1	Isoform 4 of Nesprin-1	104	4.88	-4.68
Ttn	Titin	104	2.73	-2.59
Tyk2	Non-receptor tyrosine-protein kinase TYK2	63	6.34	-5.15
Vps52	Vacuolar protein sorting-associated protein 52 homolog	5	1.40	-2.70
Wdr66	Protein Wdr66	15	1.11	-2.85

Table 6. TET3 interaction partners identified after TET3 overexpression.

Lentiviral transduction of LV-CMV-TET3 Δ CXXC-eGFP in retinal explant cultures followed by GFP-trap purification and TMT-labeling in retina.

gene name	description	# peptides	log ₂ (IP/control)	log ₂ (control/IP)
Tet3	Methylcytosine dioxygenase TET3	7	5.71	-7.19
Rest	RE1-silencing transcription factor	8	6.30	-7.03
H3f3a	Histone H3	36	5.99	-6.74
Nhs1l	Isoform 3 of NHS-like protein 1	56	5.71	-6.50
	Histone-lysine N-methyltransferase			
Whsc111	NSD3	87	5.55	-6.47
Ctcf	Transcriptional repressor CTCF	59	3.45	-5.56
	Baculoviral IAP repeat-containing			
Birc6	protein 6	26	2.46	-5.35
	Uncharacterized protein C5orf42			
C5orf42	homolog	26	2.56	-4.43
	Putative Polycomb group protein			
Asx11	ASXL1	14	1.78	-4.43
	G-protein coupled receptor-associated sorting protein 1			
Gprasp1	Uncharacterized protein C3orf20	14	2.72	-4.17
	homolog			
C3orf20	homolog	12	2.24	-3.64
Kif3b	Kinesin-like protein KIF3B	22	2.49	-3.51
Setd2	Protein Setd2	26	3.34	-3.47
	Histone-lysine N-methyltransferase			
Whsc1	NSD2	32	3.60	-3.24
	Isoform 2 of Ventral anterior homeobox 1			
Vax1	obox 1	11	7.10	-3.10
Morf411	Mortality factor 4-like protein 1	57	4.92	-2.75
Postn	Isoform 4 of Periostin	15	3.31	-2.66
Postn	Periostin	8	3.31	-2.66
Mdn1	Midasin	16	2.04	-2.61
Trdn	Protein Trdn	24	1.47	-2.51
Spag5	Sperm-associated antigen 5	6	5.02	-2.41
	Isoform 3 of Lipopolysaccharide-responsive and beige-like anchor protein			
Lrba	tein	13	1.96	-2.32
Top2b	DNA topoisomerase 2-beta	50	4.31	-2.13
	Isoform 6 of E3 ubiquitin-protein			
Trim9	ligase TRIM9	5	5.50	-2.11
Hydin	Hydrocephalus-inducing protein	47	3.71	-2.07
	Isoform 3 of Uncharacterized protein KIAA1109			
Kiaa1109	tein KIAA1109	16	1.83	-2.02
Ttn	Titin	419	2.90	-1.98
Myo5a	Unconventional myosin-Va	14	1.61	-1.95
Ttn	Titin	398	2.77	-1.94
	Isoform 3 of Bifunctional protein			
Mgea5	NCOAT	7	1.25	-1.87

	ATP-binding cassette sub-family A			
Abca1	member 1	34	1.79	-1.79
Polk	DNA polymerase kappa	7	4.86	-1.72
	Leucine-rich repeat-containing protein 71			
Lrrc71	71	8	2.95	-1.72
	Isoform 4 of Tyrosine-protein kinase			
Tec	Tec	17	4.68	-1.67
Herc1	Protein Herc1	12	2.66	-1.65
	ATPase family AAA domain-containing protein 5			
Atad5	5	16	3.38	-1.61
Gm973	Protein Gm973	6	4.79	-1.61
Zmynd8	Protein Zmynd8	9	3.20	-1.61
Utrn	Protein Utrn	18	1.61	-1.59
Akd1	Protein Akd1 (Fragment)	15	2.52	-1.47
Ctnna2	Isoform 2 of Catenin alpha-2	18	1.37	-1.47
	Dihydropyrimidinase-related protein 2			
Dpysl2	2	8	2.61	-1.42
Hkdc1	Putative hexokinase HKDC1	20	2.63	-1.27
Akap13	Protein Akap13	46	4.31	-1.25
Rbm19	Probable RNA-binding protein 19	23	2.08	-1.25
Ttn	Isoform 3 of Titin	25	3.31	-1.21
	Ubiquitin carboxyl-terminal hydrolase 16			
Usp16	16	18	2.00	-1.18
Fsip2	Fibrous sheath-interacting protein 2	42	1.81	-1.17
Gpatch8	G patch domain-containing protein 8	14	2.25	-1.14
	Pre-mRNA-processing factor 40 homolog B (Fragment)			
Prpf40b	40	106	2.14	-1.14
	Tripartite motif-containing protein 67			
Trim67	67	9	1.02	-1.14
Eea1	Early endosome antigen 1	10	3.80	-1.11
	Isoform 2 of Vacuolar protein sorting-associated protein 13C			
Vps13c	13C	30	2.56	-1.02
	Actin filament-associated protein 1-like 1			
Afap111	1	7	4.25	-1.01
Dnah5	Dynein heavy chain 5, axonemal	22	2.97	-1.01

Table 7. Endogenous TET3 interaction partners.

Co-IP of endogenous TET3 followed by TMT-labeling in retina (postnatal week 3).

gene name	description	# peptides	log₂ (IP/control)	log₂ (control/IP)
2700049A03Rik	Protein 2700049A03Rik	30.00	5.14	-4.37
Arfgef3	Brefeldin A-inhibited guanine nucleotide-exchange protein 3	10.00	4.00	-1.83
Atp5b	ATP synthase subunit beta, mitochondrial	26.00	5.29	-5.09
Axdnd1	Axonemal dynein light chain domain-containing protein 1	84.00	5.92	-2.59
Cbx2	Chromobox protein homolog 2	11.00	6.53	-3.19
Col6a6	Collagen alpha-6(VI) chain	27.00	7.08	-2.98
Ctcf1	Transcriptional repressor CTCFL	22.00	8.31	-4.97
Cylc2	Protein Cylc2	24.00	3.78	-3.29
Dennd4a	Protein Dennd4a	23.00	8.03	-2.72
Dhx29	ATP-dependent RNA helicase Dhx29	51.00	5.42	-4.47
Dnahc10	Protein Dnahc10	51.00	4.22	-4.79
Dync1h1	Cytoplasmic dynein 1 heavy chain 1	33.00	7.35	-1.84
Evpl	Envoplakin	48.00	4.37	-3.78
Fam217a	Protein FAM217A	34.00	6.99	-5.24
Fsip2	Fibrous sheath-interacting protein 2	64.00	4.16	-3.58
Gcc2	GRIP and coiled-coil domain containing 2	38.00	3.79	-2.83
Gcc2	GRIP and coiled-coil domain-containing protein 2	38.00	3.79	-2.83
Gcn111	Protein Gcn111	54.00	4.13	-3.24
Gm4945	Protein Gm4945	27.00	4.77	-3.86
Gm5828	Uncharacterized protein	38.00	4.83	-3.15
Gm973	Protein Gm973	117.00	4.08	-2.09
Gnat3	Guanine nucleotide-binding protein G(t) subunit alpha-3	17.00	4.00	-3.34
Grm8	Metabotropic glutamate receptor 8	7.00	8.09	-2.34
H1f0	Histone H1.0	104.00	7.39	-4.57
H1foo	Histone H1oo	80.00	4.11	-3.81
H2afv	Histone H2A.V	51.00	4.33	-2.82
H2afz	Histone H2A.Z	45.00	4.33	-2.82
H3f3a	Histone H3	59.00	5.25	-3.29
Hist1h1b	Histone H1.5	125.00	5.71	-5.06

Hist1h1c	Histone H1.2	234.00	6.06	-4.80
Hist1h1d	Histone H1.3	266.00	4.38	-4.86
Hist1h1e	Histone H1.4	180.00	4.71	-5.26
Hist1h1t	Histone H1t	40.00	4.17	-4.33
Hist1h2aa	Histone H2A	81.00	4.89	-1.88
Hist1h2ab	Histone H2A type 1	135.00	4.72	-2.69
Hist1h2af	Histone H2A type 1-F	139.00	5.07	-1.90
Hist1h2ak	Histone H2A type 1-K	113.00	4.89	-1.88
Hist1h2ba	Histone H2B type 1-A	52.00	5.28	-4.83
Hist1h2bb	Histone H2B type 1-B	75.00	5.75	-5.23
Hist1h2bf	Histone H2B type 1-F/J/L	77.00	5.28	-5.30
Hist1h2bm	Histone H2B type 1-M	77.00	5.28	-5.30
Hist1h2bp	Histone H2B type 1-P	75.00	5.51	-5.23
Hist2h2aa1	Histone H2A type 2-A	127.00	4.89	-2.82
Hist2h2ac	Histone H2A type 2-C	101.00	5.02	-2.82
Hist2h2bb	Histone H2B type 2-B	79.00	5.28	-5.30
Hist2h2be	Histone H2B type 2-E	61.00	5.28	-5.33
Hist3h2bb	Histone H2B type 3-B	61.00	5.28	-5.33
Hk1	Hexokinase-1	21.00	7.03	-3.42
Hk1	Isoform HK1-SB of Hexokinase-1	21.00	7.03	-3.42
Hnrnpa2b1	Isoform 3 of Heterogeneous nuclear ribonucleoproteins A2/B1	23.00	5.11	-4.09
Kdm6b	Lysine-specific demethylase 6B	59.00	6.99	-5.24
Kiaa1109	Isoform 6 of Uncharacterized protein KIAA1109	27.00	6.42	-4.45
Lama1	Laminin subunit alpha-1	24.00	5.97	-2.49
Lamb1	Laminin subunit beta-1	21.00	5.15	-5.28
Map1a	Microtubule-associated protein 1A	64.00	6.95	-2.81
Naca	Nascent polypeptide-associated complex subunit alpha, muscle-specific form	54.00	5.82	-5.44
Nemf	Nuclear export mediator factor Nemf	69.00	5.34	-5.76
Nfx1	Transcriptional repressor NF-X1	27.00	8.12	-6.13
Pclo	Isoform 2 of Protein piccolo	55.00	3.90	-3.66
Pik3cg	Phosphatidylinositol 4,5-bisphosphate 3-kinase catalytic subunit gamma isoform	13.00	3.74	-2.43
Plcb1	Isoform B of 1-phosphatidylinositol 4,5-bisphosphate phosphodiesterase beta-1	29.00	6.25	-4.54

Plcb2	1-phosphatidylinositol 4,5-bisphosphate phosphodiesterase beta-2	33.00	7.72	-2.28
Pold3	DNA polymerase delta subunit 3	31.00	7.46	-3.32
Pxk	Isoform 2 of PX domain-containing protein kinase-like protein	46.00	4.11	-2.91
Rest	RE1-silencing transcription factor	53.00	8.62	-6.50
Rpl29	60S ribosomal protein L29	36.00	4.14	-3.86
Rrp15	RRP15-like protein	25.00	4.01	-5.42
Scml2	Protein Scml2	19.00	4.91	-4.52
Sh3tc1	Protein Sh3tc1 (Fragment)	32.00	5.54	-5.07
Sos2	Son of sevenless homolog 2	20.00	8.58	-3.97
Srebf1	Isoform SREBP-1C-W42 of Sterol regulatory element-binding protein 1	6.00	8.78	-4.78
Suclg2	Isoform 2 of Succinyl-CoA ligase [GDP-forming] subunit beta, mitochondrial	30.00	4.93	-3.16
Syt4	Synaptotagmin-4	22.00	7.76	-6.61
TET3	Methylcytosine dioxygenase TET3	11.00	6.46	-6.64
Tln1	Talin-1	79.00	3.90	-4.81
Tma7	Translation machinery-associated protein 7	31.00	4.47	-5.98
Tnxb	Protein Tnxb	27.00	6.05	-2.77
Top2a	DNA topoisomerase 2-alpha	42.00	4.00	-2.76
Tox4	TOX high mobility group box family member 4	40.00	4.83	-3.15
Traf3ip3	TRAF3-interacting JNK-activating modulator	25.00	4.44	-2.22
Ttn	Titin (Fragment)	87.00	4.67	-2.42
Tyk2	Non-receptor tyrosine-protein kinase TYK2	64.00	7.02	-5.29
Usp53	Inactive ubiquitin carboxyl-terminal hydrolase 53	20.00	5.80	-6.61
Uty	Histone demethylase UTY	12.00	6.93	-4.61

Table 8. Endogenous REST interaction partners.

Co-IP of endogenous REST followed by TMT-labeling in retina (postnatal week 3).

6. Appendix

7.1 List of Publications

7.1.1 Publications

- **Perera A**, Eisen D, Wagner M, Laube, S K, Künzel A F, Koch S, Steinbacher J, Schulze E, Splith V, Mittermeier N, Müller M, Biel M, Carell T, Michalakis S (2015) REST recruits neuronal TET3 for context-specific hydroxymethylation and gene induction. *Cell Reports* (*accepted*)
- Farinelli P, **Perera A**, Arango-Gonzalez B, Trifunovic D, Wagner M, Carell T, Biel M, Zrenner E, Michalakis S, Paquet-Durand F, Ekström PA. (2014) DNA methylation and differential gene regulation in photoreceptor cell death. *Cell Death Dis.* 5, 1558.
- Wagner M, Steinbacher J, **Perera A**, Kraus T F J, Michalakis S, Müller M, Kretschmar H A, Carell T. (2015) Age-dependent variation in global levels of 5-methyl-, 5-hydroxymethyl-, and 5-formylcytosine in human and mouse brain tissues. *Angew. Chem. Int. Ed.* (*Submitted*)
- **Perera A**, Wagner M, Nagel Wolfrum K, Neuhauss S, Wolfrum U, Carell T, Biel M, Michalakis S. 5hmC is a stable epigenetic base in vertebrate retina. *Manuscript in preparation.*

7.1.2 Meeting Abstracts

- Perera A**, Eisen D, Wagner M, Laube, S K, Müller, M, Biel M, Carell, T, Michalakis, S (2014) The epigenetic mark 5hmC recruits a dynamic set of readers in the retina: **Naunyn-Smiedebergs-Archives of Pharmacology** Volume: 387 Suppl. 1. 80th Annual Meeting, German Society for Experimental and Clinical Pharmacology and Toxicology, Haale/Saale. Meeting Abstract: 059.
- **Perera A**, Koch S, Biel M, Michalakis S (2014) Hyperhydroxymethylation in rd1 retinal degeneration, *Invest. Ophthalmol. Vis. Sci.* 55: E-Abstract 5000.
 - Michalakis S, **Perera A**, Eisen D, Laube S K, Wagner M, Müller M, Carell T, and Biel M (2014) Hyperhydroxymethylation in rd1 retinal degeneration, *Invest. Ophthalmol. Vis. Sci.* 55: E-Abstract 4997.
 - Michalakis S, **Perera A**, Koch S, Wagner M, Windhager L, Nagel-Wolfrum K, T Strom T, R Zimmer R, T Carell C, and Biel M (2013) Role of 5-hydroxymethylcytosine during postnatal retinal development. *Invest. Ophthalmol. Vis. Sci.* 54: E-Abstract 2618.
 - **Perera A.**, Koch S., Wagner M., Pfaffeneder T., Windhager L., Koch F., Nagel Wolfrum K., Strom T. - M., Neuhauss S., Wolfrum U., Zimmer R., Meitinger T., Carell T., Biel M., Michalakis S. (2013) Role of 5-hydroxymethylcytosine during postnatal retinal development **Naunyn-Smiedebergs-Archives of Pharmacology** Volume: 386 Suppl. 1. 79th Annual Meeting, German Society for Experimental and Clinical Pharmacology and Toxicology, Haale/Saale. Meeting Abstract: 274.

7.2 Curriculum vitae

Personal Details

Address: Nymphenburger Str.88a
80636 Munich
E-Mail: arshan.perera@cup.lmu.de

Birth of date : 23.10.1987 in Wiesbaden

Nationality: German

Education

Since 01/2013 Graduate School Life Science Munich (LSM), Deutschland
Member of the graduate school

Since 01/2012 Ludwig-Maximilians-University, Germany
PhD student

09/2010 – 10/2011 King's College London, United Kingdom
Master of Science Biopharmaceuticals

10/2007 – 08/2010 University of Ulm, Germany
Bachelor of Science Molecular Medicine

2000 - 2007 Oranienschule Wiesbaden, Germany
A levels

Awards

06/2014 Best Talk Award
Life Science Munich (LSM) Retreat, Chiemsee, Deutschland

05/2014 Arvo Travel Grant
Association for Research in Vision and Ophthalmology Meeting,
Orlando, USA

02/2014 CIPSM Award 2014
Center for integrated Protein Science Munich (CIPSM) confer-
ence, Wildbad Kreuth, Germany

05/2013 Best Poster Award
Life Science Munich (LSM) Retreat, Starnberg, Germany

Conferences (selection)

Presentations

- 04/2014 80. Annual Meeting of the German Society for experimental and clinical pharmacology and toxicology
Hanover, Germany
- 07/2013 5th LMU-Harvard Young Scientists' Forum (YSF)
Munich, Germany
- 03/2013 79. Annual Meeting of the German Society for experimental and clinical pharmacology and toxicology
Halle-Wittenberg, Germany

Poster

- 12/2014 3rd Epigenetics Meeting, Max Planck Institute of Immunobiology and Epigenetics
Fribourg, Germany
- 05/2014 Association for Research in Vision and Ophthalmology Meeting,
Orlando, USA
- 02/2014 Center for integrated Protein Science Munich (CIPSM) conference
Wildbad Kreuth, Germany

7.3 Curriculum vitae (German)

Persönliche Daten

Adresse: Nymphenburger Str.88a
80636 München
E-Mail: arshan.perera@cup.lmu.de

Geburtsdatum: 23.10.1987 in Wiesbaden

Nationalität: Deutschland

Bildungsweg

Seit 01/2013 Graduate School Life Science Munich, Deutschland
Mitglied der Graduiertenschule (LSM)

Seit 01/2012 Ludwig-Maximilians-Universität, Deutschland
Doktorand

09/2010 – 10/2011 King's College London, Großbritannien
Master of Science Biopharmazie

10/2007 – 08/2010 Universität Ulm, Deutschland
Bachelor of Science Molekulare Medizin

2000 - 2007 Oranienschule Wiesbaden, Deutschland
Abitur

Auszeichnungen

06/2014 Vortragspreis
Life Science Munich (LSM) Retreat, Chiemsee, Deutschland

05/2014 Arvo Reisestipendium
Association for Research in Vision and Ophthalmology Meeting,
Orlando, USA

02/2014 CIPSM Award 2014
Center for integrated Protein Science Munich (CIPSM) confer-
ence, Wildbad Kreuth, Deutschland

05/2013 Posterpreis
Life Science Munich (LSM) Retreat, Starnberg, Deutschland

Konferenzbeiträge und Vorträge (Auswahl)

Vorträge

- 04/2014 80. Jahrestagung der Deutschen Gesellschaft für Experimentelle
und klinische Pharmakologie und Toxikologie e.V.
Hannover, Deutschland
- 07/2013 5. LMU-Harvard Young Scientists' Forum (YSF)
München, Deutschland
- 03/2013 79. Jahrestagung der Deutschen Gesellschaft für Experimentelle
und klinische Pharmakologie und Toxikologie e.V.
Halle-Wittenberg, Deutschland

Poster

- 12/2014 3. Epigenetics Meeting, Max Planck Institute of Immunobiology
and Epigenetics
Freiburg, Deutschland
- 05/2014 Association for Research in Vision and Ophthalmology Meeting,
Orlando, USA
- 02/2014 (CIPSM) Konferenz
Wildbad Kreuth, Deutschland

7.4 References

1. Ahmad, K., and Henikoff, S. (2002). The histone variant H3.3 marks active chromatin by replication-independent nucleosome assembly. *Molecular cell* 9, 1191-1200.
2. Allen, M.D., Grummitt, C.G., Hilcenko, C., Min, S.Y., Tonkin, L.M., Johnson, C.M., Freund, S.M., Bycroft, M., and Warren, A.J. (2006). Solution structure of the nonmethyl-CpG-binding CXXC domain of the leukaemia-associated MLL histone methyltransferase. *The EMBO journal* 25, 4503-4512.
3. Allfrey, V.G., Faulkner, R., and Mirsky, A.E. (1964). Acetylation and Methylation of Histones and Their Possible Role in the Regulation of Rna Synthesis. *Proceedings of the National Academy of Sciences of the United States of America* 51, 786-794.
4. Andrews, A.J., and Luger, K. (2011). Nucleosome structure(s) and stability: variations on a theme. *Annual review of biophysics* 40, 99-117.
5. Arold, S.T., Leonard, P.G., Parkinson, G.N., and Ladbury, J.E. (2010). H-NS forms a superhelical protein scaffold for DNA condensation. *Proceedings of the National Academy of Sciences of the United States of America* 107, 15728-15732.
6. Bachman, M., Uribe-Lewis, S., Yang, X., Williams, M., Murrell, A., and Balasubramanian, S. (2014). 5-Hydroxymethylcytosine is a predominantly stable DNA modification. *Nature chemistry* 6, 1049-1055.
7. Bannister, A.J., Schneider, R., and Kouzarides, T. (2002). Histone methylation: dynamic or static? *Cell* 109, 801-806.
8. Barth, T.K., and Imhof, A. (2010). Fast signals and slow marks: the dynamics of histone modifications. *Trends in biochemical sciences* 35, 618-626.
9. Bernstein, B.E., Kamal, M., Lindblad-Toh, K., Bekiranov, S., Bailey, D.K., Huebert, D.J., McMahon, S., Karlsson, E.K., Kulbokas, E.J., 3rd, Gingeras, T.R., *et al.* (2005). Genomic maps and comparative analysis of histone modifications in human and mouse. *Cell* 120, 169-181.
10. Bernstein, B.E., Mikkelsen, T.S., Xie, X., Kamal, M., Huebert, D.J., Cuff, J., Fry, B., Meissner, A., Wernig, M., Plath, K., *et al.* (2006). A bivalent chromatin structure marks key developmental genes in embryonic stem cells. *Cell* 125, 315-326.
11. Boyes, J., and Bird, A. (1991). DNA methylation inhibits transcription indirectly via a methyl-CpG binding protein. *Cell* 64, 1123-1134.
12. Cao, R., and Zhang, Y. (2004). The functions of E(Z)/EZH2-mediated methylation of lysine 27 in histone H3. *Current opinion in genetics & development* 14, 155-164.
13. Chedin, F., Lieber, M.R., and Hsieh, C.L. (2002). The DNA methyltransferase-like protein DNMT3L stimulates de novo methylation by Dnmt3a. *Proceedings of the National Academy of Sciences of the United States of America* 99, 16916-16921.

14. Chen, C., Nott, T.J., Jin, J., and Pawson, T. (2011). Deciphering arginine methylation: Tudor tells the tale. *Nature reviews Molecular cell biology* 12, 629-642.
15. Chen, C.C., Wang, K.Y., and Shen, C.K. (2012). The mammalian de novo DNA methyltransferases DNMT3A and DNMT3B are also DNA 5-hydroxymethylcytosine dehydroxymethylases. *The Journal of biological chemistry* 287, 33116-33121.
16. Chen, Q., Chen, Y., Bian, C., Fujiki, R., and Yu, X. (2013). TET2 promotes histone O-GlcNAcylation during gene transcription. *Nature* 493, 561-564.
17. Choi, Y., Gehring, M., Johnson, L., Hannon, M., Harada, J.J., Goldberg, R.B., Jacobsen, S.E., and Fischer, R.L. (2002). DEMETER, a DNA glycosylase domain protein, is required for endosperm gene imprinting and seed viability in arabidopsis. *Cell* 110, 33-42.
18. Chong, J.A., Tapia-Ramirez, J., Kim, S., Toledo-Aral, J.J., Zheng, Y., Boutros, M.C., Altshuler, Y.M., Frohman, M.A., Kraner, S.D., and Mandel, G. (1995). REST: a mammalian silencer protein that restricts sodium channel gene expression to neurons. *Cell* 80, 949-957.
19. Colquitt, B.M., Allen, W.E., Barnea, G., and Lomvardas, S. (2013). Alteration of genic 5-hydroxymethylcytosine patterning in olfactory neurons correlates with changes in gene expression and cell identity. *Proceedings of the National Academy of Sciences of the United States of America* 110, 14682-14687.
20. Deplus, R., Delatte, B., Schwinn, M.K., Defrance, M., Mendez, J., Murphy, N., Dawson, M.A., Volkmar, M., Putmans, P., Calonne, E., *et al.* (2013). TET2 and TET3 regulate GlcNAcylation and H3K4 methylation through OGT and SET1/COMPASS. *The EMBO journal* 32, 645-655.
21. Dietrich, N., Lerdrup, M., Landt, E., Agrawal-Singh, S., Bak, M., Tommerup, N., Rappsilber, J., Sodersten, E., and Hansen, K. (2012). REST-mediated recruitment of polycomb repressor complexes in mammalian cells. *PLoS genetics* 8, e1002494.
22. Dillon, S.C., Zhang, X., Trievel, R.C., and Cheng, X. (2005). The SET-domain protein superfamily: protein lysine methyltransferases. *Genome biology* 6, 227.
23. Dubois-Chevalier, J., Oger, F., Dehondt, H., Firmin, F.F., Gheeraert, C., Staels, B., Lefebvre, P., and Eeckhoute, J. (2015). A dynamic CTCF chromatin binding landscape promotes DNA hydroxymethylation and transcriptional induction of adipocyte differentiation. *Nucleic acids research* 42, 10943-10959.
24. Egger, G., Liang, G., Aparicio, A., and Jones, P.A. (2004). Epigenetics in human disease and prospects for epigenetic therapy. *Nature* 429, 457-463.
25. Feldmann, A., Ivanek, R., Murr, R., Gaidatzis, D., Burger, L., and Schubeler, D. (2013). Transcription factor occupancy can mediate active turnover of DNA methylation at regulatory regions. *PLoS genetics* 9, e1003994.
26. Figueroa-Romero, C., Hur, J., Bender, D.E., Delaney, C.E., Cataldo, M.D., Smith, A.L., Yung, R., Ruden, D.M., Callaghan, B.C., and Feldman, E.L. (2012).

- Identification of epigenetically altered genes in sporadic amyotrophic lateral sclerosis. *PloS one* 7, e52672.
27. Globisch, D., Münzel, M., Müller, M., Michalakis, S., Wagner, M., Koch, S., Brückl, T., Biel, M., and Carell, T. (2010). Tissue distribution of 5-hydroxymethylcytosine and search for active demethylation intermediates. *PloS one* 5, e15367.
 28. Gong, Z., Morales-Ruiz, T., Ariza, R.R., Roldan-Arjona, T., David, L., and Zhu, J.K. (2002). ROS1, a repressor of transcriptional gene silencing in Arabidopsis, encodes a DNA glycosylase/lyase. *Cell* 111, 803-814.
 29. Gregory-Evans, C.Y., Wallace, V.A., and Gregory-Evans, K. (2013). Gene networks: dissecting pathways in retinal development and disease. *Progress in retinal and eye research* 33, 40-66.
 30. Gu, P., Xu, X., Le Menuet, D., Chung, A.C., and Cooney, A.J. (2011). Differential recruitment of methyl CpG-binding domain factors and DNA methyltransferases by the orphan receptor germ cell nuclear factor initiates the repression and silencing of Oct4. *Stem cells* 29, 1041-1051.
 31. Guo, J.U., Su, Y., Zhong, C., Ming, G.L., and Song, H. (2011). Hydroxylation of 5-methylcytosine by TET1 promotes active DNA demethylation in the adult brain. *Cell* 145, 423-434.
 32. Hahn, M.A., Qiu, R., Wu, X., Li, A.X., Zhang, H., Wang, J., Jui, J., Jin, S.G., Jiang, Y., Pfeifer, G.P., *et al.* (2013). Dynamics of 5-hydroxymethylcytosine and chromatin marks in Mammalian neurogenesis. *Cell reports* 3, 291-300.
 33. Hashimoto, H., Liu, Y., Upadhyay, A.K., Chang, Y., Howerton, S.B., Vertino, P.M., Zhang, X., and Cheng, X. (2012). Recognition and potential mechanisms for replication and erasure of cytosine hydroxymethylation. *Nucleic acids research* 40, 4841-4849.
 34. He, Y.F., Li, B.Z., Li, Z., Liu, P., Wang, Y., Tang, Q., Ding, J., Jia, Y., Chen, Z., Li, L., *et al.* (2011). Tet-mediated formation of 5-carboxylcytosine and its excision by TDG in mammalian DNA. *Science* 333, 1303-1307.
 35. Heavner, W., and Pevny, L. (2012). Eye development and retinogenesis. *Cold Spring Harbor perspectives in biology* 4.
 36. Heintzman, N.D., Stuart, R.K., Hon, G., Fu, Y., Ching, C.W., Hawkins, R.D., Barrera, L.O., Van Calcar, S., Qu, C., Ching, K.A., *et al.* (2007). Distinct and predictive chromatin signatures of transcriptional promoters and enhancers in the human genome. *Nature genetics* 39, 311-318.
 37. Hino, S., Sakamoto, A., Nagaoka, K., Anan, K., Wang, Y., Mimasu, S., Umehara, T., Yokoyama, S., Kosai, K., and Nakao, M. (2012). FAD-dependent lysine-specific demethylase-1 regulates cellular energy expenditure. *Nature communications* 3, 758.
 38. Hoon, M., Okawa, H., Della Santina, L., and Wong, R.O. (2014). Functional architecture of the retina: development and disease. *Progress in retinal and eye research* 42, 44-84.

39. Huang, Y., Myers, S.J., and Dingledine, R. (1999). Transcriptional repression by REST: recruitment of Sin3A and histone deacetylase to neuronal genes. *Nature neuroscience* 2, 867-872.
40. Jaenisch, R., and Bird, A. (2003). Epigenetic regulation of gene expression: how the genome integrates intrinsic and environmental signals. *Nature genetics* 33 *Suppl*, 245-254.
41. Jakovcevski, M., and Akbarian, S. (2012). Epigenetic mechanisms in neurological disease. *Nature medicine* 18, 1194-1204.
42. Jenuwein, T., and Allis, C.D. (2001). Translating the histone code. *Science* 293, 1074-1080.
43. Jiang, C., and Pugh, B.F. (2009). Nucleosome positioning and gene regulation: advances through genomics. *Nature reviews Genetics* 10, 161-172.
44. Kagiwada, S., Kurimoto, K., Hirota, T., Yamaji, M., and Saitou, M. (2013). Replication-coupled passive DNA demethylation for the erasure of genome imprints in mice. *The EMBO journal* 32, 340-353.
45. Ko, M., An, J., Bandukwala, H.S., Chavez, L., Aijo, T., Pastor, W.A., Segal, M.F., Li, H., Koh, K.P., Lahdesmaki, H., *et al.* (2013). Modulation of TET2 expression and 5-methylcytosine oxidation by the CXXC domain protein IDAX. *Nature* 497, 122-126.
46. Kohli, R.M., and Zhang, Y. (2013). TET enzymes, TDG and the dynamics of DNA demethylation. *Nature* 502, 472-479.
47. Kouzarides, T. (2007). Chromatin modifications and their function. *Cell* 128, 693-705.
48. Kraner, S.D., Chong, J.A., Tsay, H.J., and Mandel, G. (1992). Silencing the type II sodium channel gene: a model for neural-specific gene regulation. *Neuron* 9, 37-44.
49. Kriaucionis, S., and Heintz, N. (2009). The nuclear DNA base 5-hydroxymethylcytosine is present in Purkinje neurons and the brain. *Science* 324, 929-930.
50. Kuhrt, H., Gryga, M., Wolburg, H., Joffe, B., Grosche, J., Reichenbach, A., and Noori, H.R. (2012). Postnatal mammalian retinal development: quantitative data and general rules. *Progress in retinal and eye research* 31, 605-621.
51. Kulak, N.A., Pichler, G., Paron, I., Nagaraj, N., and Mann, M. (2014). Minimal, encapsulated proteomic-sample processing applied to copy-number estimation in eukaryotic cells. *Nature methods* 11, 319-324.
52. Kuwabara, T., Hsieh, J., Nakashima, K., Taira, K., and Gage, F.H. (2004). A small modulatory dsRNA specifies the fate of adult neural stem cells. *Cell* 116, 779-793.

53. Lander, E.S., Linton, L.M., Birren, B., Nusbaum, C., Zody, M.C., Baldwin, J., Devon, K., Dewar, K., Doyle, M., FitzHugh, W., *et al.* (2001). Initial sequencing and analysis of the human genome. *Nature* *409*, 860-921.
54. Liu, N., Wang, M., Deng, W., Schmidt, C.S., Qin, W., Leonhardt, H., and Spada, F. (2013a). Intrinsic and extrinsic connections of Tet3 dioxygenase with CXXC zinc finger modules. *PLoS one* *8*, e62755.
55. Liu, X., Gao, Q., Li, P., Zhao, Q., Zhang, J., Li, J., Koseki, H., and Wong, J. (2013b). UHRF1 targets DNMT1 for DNA methylation through cooperative binding of hemimethylated DNA and methylated H3K9. *Nature communications* *4*, 1563.
56. Lopez, C.M., Lloyd, A.J., Leonard, K., and Wilkinson, M.J. (2012). Differential effect of three base modifications on DNA thermostability revealed by high resolution melting. *Analytical chemistry* *84*, 7336-7342.
57. Lu, T., Aron, L., Zullo, J., Pan, Y., Kim, H., Chen, Y., Yang, T.H., Kim, H.M., Drake, D., Liu, X.S., *et al.* (2014). REST and stress resistance in ageing and Alzheimer's disease. *Nature* *507*, 448-454.
58. Luger, K., Mader, A.W., Richmond, R.K., Sargent, D.F., and Richmond, T.J. (1997). Crystal structure of the nucleosome core particle at 2.8 Å resolution. *Nature* *389*, 251-260.
59. Lunyak, V.V., and Rosenfeld, M.G. (2005). No rest for REST: REST/NRSF regulation of neurogenesis. *Cell* *121*, 499-501.
60. Maiti, A., and Drohat, A.C. (2011). Thymine DNA glycosylase can rapidly excise 5-formylcytosine and 5-carboxylcytosine: potential implications for active demethylation of CpG sites. *The Journal of biological chemistry* *286*, 35334-35338.
61. McGann, J.C., Oyer, J.A., Garg, S., Yao, H., Liu, J., Feng, X., Liao, L., Yates, J.R., and Mandel, G. (2014). Polycomb- and REST-associated histone deacetylases are independent pathways toward a mature neuronal phenotype. *eLife* *3*.
62. Mellen, M., Ayata, P., Dewell, S., Kriaucionis, S., and Heintz, N. (2012). MeCP2 binds to 5hmC enriched within active genes and accessible chromatin in the nervous system. *Cell* *151*, 1417-1430.
63. Mikkelsen, T.S., Ku, M., Jaffe, D.B., Issac, B., Lieberman, E., Giannoukos, G., Alvarez, P., Brockman, W., Kim, T.K., Koche, R.P., *et al.* (2007). Genome-wide maps of chromatin state in pluripotent and lineage-committed cells. *Nature* *448*, 553-560.
64. Mistrik, P., Mader, R., Michalakis, S., Weidinger, M., Pfeifer, A., and Biel, M. (2005). The murine HCN3 gene encodes a hyperpolarization-activated cation channel with slow kinetics and unique response to cyclic nucleotides. *The Journal of biological chemistry* *280*, 27056-27061.
65. Mohn, F., Weber, M., Schubeler, D., and Roloff, T.C. (2009). Methylated DNA immunoprecipitation (MeDIP). *Methods in molecular biology* *507*, 55-64.

66. Münzel, M., Globisch, D., Bruckl, T., Wagner, M., Welzmler, V., Michalakis, S., Müller, M., Biel, M., and Carell, T. (2010). Quantification of the sixth DNA base hydroxymethylcytosine in the brain. *Angewandte Chemie* 49, 5375-5377.
67. Murray, K. (1964). The Occurrence of Epsilon-N-Methyl Lysine in Histones. *Biochemistry* 3, 10-15.
68. Musselman, C.A., Lalonde, M.E., Cote, J., and Kutateladze, T.G. (2012). Perceiving the epigenetic landscape through histone readers. *Nature structural & molecular biology* 19, 1218-1227.
69. Naruse, Y., Aoki, T., Kojima, T., and Mori, N. (1999). Neural restrictive silencer factor recruits mSin3 and histone deacetylase complex to repress neuron-specific target genes. *Proceedings of the National Academy of Sciences of the United States of America* 96, 13691-13696.
70. Nielsen, P.R., Nietlispach, D., Mott, H.R., Callaghan, J., Bannister, A., Kouzarides, T., Murzin, A.G., Murzina, N.V., and Laue, E.D. (2002). Structure of the HP1 chromodomain bound to histone H3 methylated at lysine 9. *Nature* 416, 103-107.
71. Okano, M., Bell, D.W., Haber, D.A., and Li, E. (1999). DNA methyltransferases Dnmt3a and Dnmt3b are essential for de novo methylation and mammalian development. *Cell* 99, 247-257.
72. Okawa, H., Hoon, M., Yoshimatsu, T., Della Santina, L., and Wong, R.O. (2014). Illuminating the Multifaceted Roles of Neurotransmission in Shaping Neuronal Circuitry. *Neuron* 83, 1303-1318.
73. Olins, A.L., and Olins, D.E. (1974). Spheroid chromatin units (v bodies). *Science* 183, 330-332.
74. Pacaud, R., Sery, Q., Oliver, L., Vallette, F.M., Tost, J., and Cartron, P.F. (2014). DNMT3L interacts with transcription factors to target DNMT3L/DNMT3B to specific DNA sequences: role of the DNMT3L/DNMT3B/p65-NFkappaB complex in the (de-)methylation of TRAF1. *Biochimie* 104, 36-49.
75. Pastor, W.A., Aravind, L., and Rao, A. (2013). TETonic shift: biological roles of TET proteins in DNA demethylation and transcription. *Nature reviews Molecular cell biology* 14, 341-356.
76. Pfaffeneder, T., Spada, F., Wagner, M., Brandmayr, C., Laube, S.K., Eisen, D., Truss, M., Steinbacher, J., Hackner, B., Kotljarova, O., *et al.* (2014). Tet oxidizes thymine to 5-hydroxymethyluracil in mouse embryonic stem cell DNA. *Nature chemical biology* 10, 574-581.
77. Pfaffl, M.W., Horgan, G.W., and Dempfle, L. (2002). Relative expression software tool (REST) for group-wise comparison and statistical analysis of relative expression results in real-time PCR. *Nucleic acids research* 30, e36.
78. Pfeifer, G.P., Kadam, S., and Jin, S.G. (2013). 5-hydroxymethylcytosine and its potential roles in development and cancer. *Epigenetics & chromatin* 6, 10.

79. Portela, A., and Esteller, M. (2010). Epigenetic modifications and human disease. *Nature biotechnology* 28, 1057-1068.
80. Razin, A. (1998). CpG methylation, chromatin structure and gene silencing—a three-way connection. *The EMBO journal* 17, 4905-4908.
81. Reidel, B., Orisme, W., Goldmann, T., Smith, W.C., and Wolfrum, U. (2006). Photoreceptor vitality in organotypic cultures of mature vertebrate retinas validated by light-dependent molecular movements. *Vision research* 46, 4464-4471.
82. Richmond, T.J., and Davey, C.A. (2003). The structure of DNA in the nucleosome core. *Nature* 423, 145-150.
83. Ruthenburg, A.J., Allis, C.D., and Wysocka, J. (2007). Methylation of lysine 4 on histone H3: intricacy of writing and reading a single epigenetic mark. *Molecular cell* 25, 15-30.
84. Schiesser, S., Pfaffeneder, T., Sadeghian, K., Hackner, B., Steigenberger, B., Schroder, A.S., Steinbacher, J., Kashiwazaki, G., Hofner, G., Wanner, K.T., *et al.* (2013). Deamination, oxidation, and C-C bond cleavage reactivity of 5-hydroxymethylcytosine, 5-formylcytosine, and 5-carboxycytosine. *Journal of the American Chemical Society* 135, 14593-14599.
85. Schmidt, C.K., and Jackson, S.P. (2013). On your mark, get SET(D2), go! H3K36me3 primes DNA mismatch repair. *Cell* 153, 513-515.
86. Schoenherr, C.J., and Anderson, D.J. (1995). The neuron-restrictive silencer factor (NRSF): a coordinate repressor of multiple neuron-specific genes. *Science* 267, 1360-1363.
87. Shechter, D., Dormann, H.L., Allis, C.D., and Hake, S.B. (2007). Extraction, purification and analysis of histones. *Nature protocols* 2, 1445-1457.
88. Shi, Y., Lan, F., Matson, C., Mulligan, P., Whetstine, J.R., Cole, P.A., Casero, R.A., and Shi, Y. (2004). Histone demethylation mediated by the nuclear amine oxidase homolog LSD1. *Cell* 119, 941-953.
89. Soderberg, O., Gullberg, M., Jarvius, M., Ridderstrale, K., Leuchowius, K.J., Jarvius, J., Wester, K., Hydbring, P., Bahram, F., Larsson, L.G., *et al.* (2006). Direct observation of individual endogenous protein complexes in situ by proximity ligation. *Nature methods* 3, 995-1000.
90. Solovei, I., Kreysing, M., Lanctot, C., Kosem, S., Peichl, L., Cremer, T., Guck, J., and Joffe, B. (2009). Nuclear architecture of rod photoreceptor cells adapts to vision in mammalian evolution. *Cell* 137, 356-368.
91. Spruijt, C.G., Gnerlich, F., Smits, A.H., Pfaffeneder, T., Jansen, P.W., Bauer, C., Munzel, M., Wagner, M., Muller, M., Khan, F., *et al.* (2013). Dynamic readers for 5-(hydroxy)methylcytosine and its oxidized derivatives. *Cell* 152, 1146-1159.
92. Surani, M.A. (2001). Reprogramming of genome function through epigenetic inheritance. *Nature* 414, 122-128.

93. Szulwach, K.E., Li, X., Li, Y., Song, C.X., Wu, H., Dai, Q., Irier, H., Upadhyay, A.K., Gearing, M., Levey, A.I., *et al.* (2011). 5-hmC-mediated epigenetic dynamics during postnatal neurodevelopment and aging. *Nature neuroscience* *14*, 1607-1616.
94. Tahiliani, M., Koh, K.P., Shen, Y., Pastor, W.A., Bandukwala, H., Brudno, Y., Agarwal, S., Iyer, L.M., Liu, D.R., Aravind, L., *et al.* (2009). Conversion of 5-methylcytosine to 5-hydroxymethylcytosine in mammalian DNA by MLL partner TET1. *Science* *324*, 930-935.
95. Takai, H., Masuda, K., Sato, T., Sakaguchi, Y., Suzuki, T., Suzuki, T., Koyama-Nasu, R., Nasu-Nishimura, Y., Katou, Y., Ogawa, H., *et al.* (2014). 5-Hydroxymethylcytosine plays a critical role in glioblastomagenesis by recruiting the CHTOP-methylosome complex. *Cell reports* *9*, 48-60.
96. Tan, C.P., and Nakielny, S. (2006). Control of the DNA methylation system component MBD2 by protein arginine methylation. *Molecular and cellular biology* *26*, 7224-7235.
97. Tsukada, Y., Fang, J., Erdjument-Bromage, H., Warren, M.E., Borchers, C.H., Tempst, P., and Zhang, Y. (2006). Histone demethylation by a family of JmjC domain-containing proteins. *Nature* *439*, 811-816.
98. Turner, B.M. (2000). Histone acetylation and an epigenetic code. *BioEssays : news and reviews in molecular, cellular and developmental biology* *22*, 836-845.
99. van Holde, K., and Zlatanova, J. (1996). What determines the folding of the chromatin fiber? *Proceedings of the National Academy of Sciences of the United States of America* *93*, 10548-10555.
100. Verdin, E., and Ott, M. (2015). 50 years of protein acetylation: from gene regulation to epigenetics, metabolism and beyond. *Nature reviews Molecular cell biology* *16*, 258-264.
101. Voss, T.C., and Hager, G.L. (2014). Dynamic regulation of transcriptional states by chromatin and transcription factors. *Nature reviews Genetics* *15*, 69-81.
102. Waddington, C.H. (2012). The epigenotype. *1942. International journal of epidemiology* *41*, 10-13.
103. Wanunu, M., Cohen-Karni, D., Johnson, R.R., Fields, L., Benner, J., Peterman, N., Zheng, Y., Klein, M.L., and Drndic, M. (2011). Discrimination of methylcytosine from hydroxymethylcytosine in DNA molecules. *Journal of the American Chemical Society* *133*, 486-492.
104. Wijesinghe, P., and Bhagwat, A.S. (2012). Efficient deamination of 5-methylcytosines in DNA by human APOBEC3A, but not by AID or APOBEC3G. *Nucleic acids research* *40*, 9206-9217.
105. Wysocka, J., Swigut, T., Milne, T.A., Dou, Y., Zhang, X., Burlingame, A.L., Roeder, R.G., Brivanlou, A.H., and Allis, C.D. (2005). WDR5 associates with histone H3 methylated at K4 and is essential for H3 K4 methylation and vertebrate development. *Cell* *121*, 859-872.

106. Xiang, M. (2013). Intrinsic control of mammalian retinogenesis. *Cellular and molecular life sciences : CMLS* 70, 2519-2532.
107. Xu, Y., Wu, F., Tan, L., Kong, L., Xiong, L., Deng, J., Barbera, A.J., Zheng, L., Zhang, H., Huang, S., *et al.* (2011). Genome-wide regulation of 5hmC, 5mC, and gene expression by Tet1 hydroxylase in mouse embryonic stem cells. *Molecular cell* 42, 451-464.
108. Xu, Y., Xu, C., Kato, A., Tempel, W., Abreu, J.G., Bian, C., Hu, Y., Hu, D., Zhao, B., Cerovina, T., *et al.* (2012). Tet3 CXXC domain and dioxygenase activity cooperatively regulate key genes for *Xenopus* eye and neural development. *Cell* 151, 1200-1213.
109. Yamaguchi, S., Hong, K., Liu, R., Inoue, A., Shen, L., Zhang, K., and Zhang, Y. (2013). Dynamics of 5-methylcytosine and 5-hydroxymethylcytosine during germ cell reprogramming. *Cell research* 23, 329-339.
110. Yildirim, O., Li, R., Hung, J.H., Chen, P.B., Dong, X., Ee, L.S., Weng, Z., Rando, O.J., and Fazio, T.G. (2011). Mbd3/NURD complex regulates expression of 5-hydroxymethylcytosine marked genes in embryonic stem cells. *Cell* 147, 1498-1510.
111. Yu, M., Hon, G.C., Szulwach, K.E., Song, C.X., Zhang, L., Kim, A., Li, X., Dai, Q., Shen, Y., Park, B., *et al.* (2012). Base-resolution analysis of 5-hydroxymethylcytosine in the mammalian genome. *Cell* 149, 1368-1380.
112. Zeng, L., Zhang, Q., Li, S., Plotnikov, A.N., Walsh, M.J., and Zhou, M.M. (2010). Mechanism and regulation of acetylated histone binding by the tandem PHD finger of DPF3b. *Nature* 466, 258-262.
113. Zhou, V.W., Goren, A., and Bernstein, B.E. (2011). Charting histone modifications and the functional organization of mammalian genomes. *Nature reviews Genetics* 12, 7-18.

7.5 Acknowledgments

First and foremost, I would like to thank and dedicate this work to my family, who always believed in me and was always there whenever I needed them. I owe you everything.

I would also like to express my gratitude to Prof Dr Biel for giving me the opportunity to work in his group and for his helpful advices. Moreover, I would like to thank my supervisor PD Dr Michalakis for offering me this interesting project.

I would also like to thank Prof Dr Carell and Dr Markus Müller for their scientific input and numerous discussions that greatly influenced this project. Further, I want to thank Dr David Eisen, Mirko Wagner, Jessica Steinbacher and Andrea Künzel for their great efforts in this project. I am thankful to have had such a fruitful collaboration.

My gratitude is also extended to Elisabeth Schulze. You were one of the first friendly faces to greet me when I began this doctoral program and you have always been a tremendous help no matter the task or circumstance. You are a great colleague and more importantly a true friend. For this, I cannot thank you enough. Furthermore, I want to thank Samira Perera and Joshua Lüdke for proof reading my thesis and your continuous help during the last couple of years.